TI89 010989

NUREG/CR--5275

FLAME Facility

The Effect of Obstacles and Transverse Venting on Flame Acceleration and Transition to Detonation for Hydrogen–Air Mixtures at Large Scale

Manuscript Completed: March 1989
Date Published: April 1989

Prepared by
M. P. Sherman, S. R. Tieszen, W. B. Benedick

Sandia National Laboratories
Albuquerque, NM 87185

Prepared for
Division of Systems Research
Office of Nuclear Regulatory Research
U.S. Nuclear Regulatory Commission
Washington, DC 20555
NRC FIN A1246

We dedicate this report to our coauthor, colleague, and friend, William "Bill" Benedick (1926-1989). All who worked with him were impressed with the breadth and depth of his knowledge. There was no one with whom it was more pleasant to work. He will be greatly missed by those who knew him at Sandia and around the world.

ABSTRACT

This report describes research on flame acceleration and deflagration-to-detonation transition (DDT) for hydrogen-air mixtures carried out in the FLAME facility, and describes its relevance to nuclear reactor safety. Flame acceleration and DDT can generate high peak pressures that may cause failure of containment. FLAME is a large rectangular channel 30.5 m long, 2.44 m high, and 1.83 m wide. It is closed on the ignition end and open on the far end. The three test variables were hydrogen mole fraction (12 - 30%), degree of transverse venting (by moving steel top plates - 0%, 13%, and 50%), and the absence or presence of certain obstacles in the channel (zero or 33% blockage ratio). The most important variable was the hydrogen mole fraction. The presence of the obstacles tested greatly increased the flame speeds, overpressures, and tendency for DDT compared to similar tests without obstacles. Different obstacle configurations could have greater or lesser effects on flame acceleration and DDT. Large degrees of transverse venting reduced the flame speeds, overpressures, and possibility of DDT. For small degrees of transverse venting (13% top venting), the flame speeds and overpressures were higher than for no transverse venting with reactive mixtures ($> 18\%$ H_2), but they were lower with leaner mixtures. The effect of the turbulence generated by the flow out the vents on increasing flame speed can be larger than the effect of venting gas out of the channel and hence reducing the overpressure. With no obstacles and 50% top venting, the flame speeds and overpressures were low, and there was no DDT. For all other cases, DDT was observed above some threshold hydrogen concentration. DDT was obtained at 15% H_2 with obstacles and no transverse venting.

CONTENTS

LIST OF FIGURES

LIST OF FIGURES
(continued)

LIST OF FIGURES
(continued)

ACKNOWLEDGMENTS

The authors would like to acknowledge the contributions of Dr. J. Fisk. He designed the FLAME facility and played a large role in carrying out the earlier tests. Dr. Fisk has written sections on the structural design of FLAME and on details of the site for this report. These specialized sections were not included in the report but remain on file. The FLAME facility was constructed by the Cardenas Construction Company, Albuquerque, NM. The initial computer programs for operating the data acquisition system were developed by O. Lindquist of Santa Fe Energy Research Corporation, Santa Fe, NM. Dr. J. Barry, while a graduate student on a mentorship, developed the second generation data acquisition computer programs and otherwise assisted in the research. S. Winters operated and further developed the DAASY data acquisition system. I. Lenz was in charge of the high-speed cinematography. Dr. M. Carcassi from the University of Pisa played an important role in the data reduction while at Sandia as a Visiting Scientist. He has been working on modelling the FLAME tests. The advice of Professors J. H. S. Lee and R. Knystautas of McGill University was highly valuable in this research. The authors would like to thank the NRC Contract Managers J. Larkins and P. Worthington. We wish to thank M. Berman, supervisor of Division 6427, for obtaining the support for this research, and for continuing technical advice. The authors also appreciate the technical support of C. Daniel, D. Montgomery, M. Oliver, D. Beeker, D. Weigand, and B. Heideman.

EXECUTIVE SUMMARY

The purpose of this report is to describe research on flame acceleration and deflagration-to-detonation transition (DDT) of hydrogen-air mixtures carried out in the FLAME facility, and to explain its relevance to nuclear reactor safety. In addition to the quasi-static pressures generated by the slow combustion of hydrogen in containments during hypothetical severe accidents, rapid combustion, i.e. accelerated flames and detonations, can generate strong pressure waves, which might threaten containment and lead to a release of radioactivity.

FLAME is a large (30.5-m long) rectangular channel designed and built for the U.S. Nuclear Regulatory Commission. It was built as a half-scale model of the upper plenum volume in ice condenser pressurized water reactor (PWR) containments. The effects of three variables known to be important in small-scale tests and in a relatively small number of large-scale tests were investigated: hydrogen concentration, obstacles in the path of the combustion front, and the degree of transverse venting. The results of this research help define the threat from flame acceleration and detonation in ice condenser and other containments. A methodology of estimating the likelihood of DDT based on FLAME and other results was developed.

During hypothetical severe nuclear accidents, large quantities of hydrogen can be generated by the oxidation of the zirconium fuel cladding and from other mechanisms. As the hydrogen escapes into containment, it may continuously burn. The combustion in such a "diffusion flame" is limited by the rate of laminar or turbulent mixing of hydrogen and oxygen. The pressure rise will be small, but there can be severe thermal loads on structures near the flame. If the hydrogen does not immediately burn, a premixed volume of hydrogen, oxygen, and other diluent gases will form. These can burn as a deflagration or detonation, with much higher pressure rises than for a diffusion flame.

Deflagrations (flames) are combustion fronts traveling at subsonic speeds relative to the unburned combustible gas. Ordinary deflagrations travel at speeds much less than sonic. For these deflagrations the pressure will be nearly uniform throughout containment, and the peak pressure will be bounded by the adiabatic isochoric (constant volume) complete combustion pressure (AICC pressure). The AICC pressure can be computed to high accuracy by thermodynamic calculations. At most, the AICC pressure for hydrogen-air, or hydrogen-air-steam mixtures is eight times the precombustion pressure. If the deflagration speed is accelerated to more than about 100 m/s, shock waves will be generated, and the peak instantaneous pressure can be higher

than the AICC pressure. If the deflagration is fast enough, a transition to a detonation may occur. Detonations are combustion fronts traveling at supersonic speed relative to the unburned gas. For detonations the peak reflected pressures will be considerably above the AICC pressure, up to 35 times the precombustion pressure. For highly accelerated flames or detonations, dynamic loads will be imposed on the containment in addition to more slowly changing quasi-static loads.

In our FLAME experiments, the hydrogen mole fraction was varied between 12% and 30% hydrogen. At 12% hydrogen there was negligible flame acceleration, regardless of the degree of transverse venting or the presence of obstacles. The most reactive hydrogen-air mixtures are near stoichiometric (two hydrogen molecules per one oxygen molecule), i.e. about 30% hydrogen. The flame speeds and overpressures varied by over two orders of magnitude over the range of hydrogen mole fractions tested: velocities of from less than 10 m/s to 1800 m/s and overpressures of from less than a few kPa to over 2000 kPa. The reactivity of the mixture as determined by the hydrogen concentration, was the most important variable.

The presence of obstacles in the path of the expanding flame is known to promote flame acceleration in small-scale experiments by enlarging the burning surface and increasing the local burning rate. The FLAME channel was built with provision for attaching obstacles to the walls and floor. We carried out tests with no obstacles in the channel (other than two mixing fans and thermocouple rakes), with baffles that obstructed 1/3 of the channel cross section, and with half-scale models of the air handlers in the ice condenser upper plenum region. It should be remembered that our observations of the effects of obstacles were based on a limited set of obstacle configurations. Other obstacle configurations would give different quantitative results. The presence of obstacles causes a dramatic increase in flame speed and overpressure and a lowering of the minimum hydrogen mole fraction for DDT. For example, with a large degree of transverse venting (50% top venting) and no obstacles, DDT was not observed at 28% hydrogen, and the maxiumum speed of the flame down the channel was 126 m/s. With obstacles, DDT was observed at 20% hydrogen. With obstacles present, the distinction between detonation and highly accelerated flames blurs. Even without a detonation, deflagrations are accelerated to speeds of 500 - 700 m/s, and high pressure pulses are observed. A DDT was observed at 15% hydrogen in a test with obstacles and no top venting. This is below the old value of lean "detonation limit" of 18% hydrogen, still sometimes quoted in the combustion literature.

The effect of venting is complex, being tied to combustible mixture reactivity, chamber geometry, and scale. In small-scale experiments, the presence of venting transverse to the path of

the deflagration inhibits flame acceleration. FLAME was built with the top covered by movable steel plates. Tests were carried out without top venting, with a large degree of top venting (50%), and a small degree of top venting (13%).

The presence of large degrees of transverse venting does inhibit flame acceleration, as in small-scale tests. Without obstacles, low flame speeds, low overpressures, and no detonations were observed even with nearly stoichiometric mixtures. With obstacles, DDT was obtained at 20% hydrogen. In these large-scale tests, the effects of small degrees of transverse venting differ from small-scale tests. There are two opposing phenomena. The loss of gas in the channel tends to reduce the pressure and hence flame acceleration. The turbulence created by flow through the vents, and possible reignition in the channel by rapid burning above the vents, tends to increase flame speed. We found that for less reactive mixtures (below 18% hydrogen) the small degree of transverse venting did inhibit flame acceleration somewhat. For more reactive mixtures, the combustion was more violent with the 13% top venting than with no top venting.

The conclusions from these tests are here summarized:

1. The reactivity of the mixture as determined by the hydrogen concentration is the most important variable. For very lean mixtures no significant flame acceleration and no transition to detonation was observed.

2. The presence of obstacles in the path of the flame greatly increases flame speeds and overpressures, and reduces the lean limit for transition to detonation.

3. Large degrees of transverse venting reduce flame speeds and overpressures.

4. Small degrees of transverse venting reduce flame speeds and overpressures for less reactive mixtures, but increase them for more reactive mixtures.

An application of the DDT results from FLAME to nuclear reactor safety is that of Sherman and Berman in which a methodology for estimating the likelihood of detonation in containment during a severe accident was presented. A short presentation of this methodology is given in Appendix B. This work was applied to hypothetical accidents at the Bellefonte nuclear power plant with a large dry containment. The methodology has been used in the NUREG-1150 containment loads expert panel evaluation for the Sequoyah nuclear power plant with

an ice condenser containment and for the Grand Gulf Mark 3 BWR plant. The results of applying the methodology ranged from the Bellefonte studies, in which detonation threats appear remote for the accidents considered, to the Sequoyah studies in which certain accident scenarios lead to predictions of local detonations in the ice condenser. In a hypothetical accident within an ice condenser containment with the return air fans not operating, a highly reactive mixture is formed in the ice condenser. Since the ice condenser has a geometry which can promote flame acceleration, the methodology developed predicts a DDT is highly likely there.

1. INTRODUCTION

1.1 Purpose of FLAME facility

The FLAME facility was designed and constructed for the U. S. Nuclear Regulatory Commission to study hydrogen combustion problems relevant to nuclear reactor safety: accelerated flames, transition to detonation, combustion in simulated reactor containment geometries, etc. The main concerns with hydrogen combustion are that the resultant overpressure may threaten containment and lead to a release of radioactivity, and that safety-related equipment may be damaged by thermal or mechanical loads, leading to a breach of containment. The possible importance of hydrogen combustion to overall risk has long been understood. [1,2] Less well understood were conditions in which potentiallly destructive detonations and highly accelerated deflagrations can occur. The experimentation in FLAME has been mainly directed to furnish data from a large-scale facility to help clarify these phenomena. We studied the effects of variation in hydrogen concentration, degree of venting transverse to the channel axis, and the presence of particular obstacle types.

1.2 History of Hydrogen Concern

During the Three Mile Island Unit 2 (TMI-2) accident, a considerable amount of hydrogen was generated due to the oxidation of zirconium by steam in the reactor core. The hydrogen was released into containment, forming a combustible mixture estimated to be about 8% hydrogen in air. [3] After nearly ten hours into the accident, a deflagration took place with a peak overpressure greater than 192 kPa (28 psig). It has been estimated that the time to burn the hydrogen in TMI-2 was 12 seconds. [3] It was an ordinary deflagration. We will use the words "flame" and "deflagration" interchangeably. A hydrogen deflagration can be considered "ordinary" if its speed is much less than the speed of sound relative to the adjacent combustible mixture. For an ordinary hydrogen deflagration in containment, the pressure will be nearly spatially uniform, and the resultant pressure loads on a containment structure will be quasi-static. Quasi-static pressure loads are those in which the characteristic time for pressure change is long compared to the natural period of the structure. Containment structure natural periods relevant to hydrogen burns are of the order of 10 to 200 milliseconds. [4,5] In contrast to the quasi-steady loads caused by an ordinary deflagration, a highly accelerated deflagration or a detonation will cause dynamic loads on structures in addition to static loads. The pressure loads at TMI-2 did not threaten the strong containment structure. However, the pressure rise would have been higher and the combustion even more rapid if the hydrogen concentration had been higher. This might occur in

smaller sized containments, if more hydrogen had been generated, or if the released hydrogen was more concentrated and not mixed throughout containment.

In the Chernobyl accident, it was reported that there were two or more explosions. [6] The first is generally believed to have been a steam explosion. The second and possibly later explosions may have been due to hydrogen combustion. At the time this report is being written, the initial conditions of the possible hydrogen combustions are not known.

1.3 Adiabatic Isochoric Complete Combustion Pressure

In the combustion of a premixed hydrogen-air or hydrogen-air-steam mixture, we can distinguish three regimes: ordinary deflagrations, highly accelerated deflagrations, and detonations. If a hydrogen-air mixture is far from stoichiometric ($\simeq$ 30% hydrogen), either very lean or very rich, its deflagration speed will be small compared to the speed of sound. The pressure in all accessible volumes will be spatially uniform. The pressure will rise to a peak in a period of seconds, and then decay as the gas cools by heat transfer to the surroundings and possibly to water sprays. The peak pressure is bounded by the Adiabatic Isochoric Complete Combustion Pressure (AICC pressure), often called the Constant Volume Explosion Pressure. The AICC pressure can be determined to high accuracy because its determination requires only thermodynamic property data of several simple chemical species which are accurately known. In particular, for hydrogen combustion one needs the heats of formation, species enthalpies, and either equilibrium constants for the dissociation reactions or free energies for the species H_2, O_2, N_2, H_2O, OH, NO, H, and O. Other species such as N, NO_2, HO_2, O_3, and H_2O_2 are present in small amounts and could be included. The AICC pressure can be accurately computed using standard computer codes [7] or estimated from graphical results. [8] For combustion of a homogeneous mixture in a fixed volume, the peak pressure can be below the AICC pressure because of incomplete burning and because of heat transfer from the hot gases to the cooler surroundings during the combustion.

1.4 Flammability Limits

The flammability limits of a combustible mixture, at a given temperature and pressure, are defined as the limiting concentrations of fuel which will propagate a deflagration indefinitely. [9-11] For a given fuel-air mixture, there will be a lean and a rich limit. The flammability limits are assumed to be independent of the method of ignition, provided it is sufficiently strong to ignite a flame. It is also independent of the size of the enclosure, provided it is much larger than the

quenching distance. The flammability limits depend on the direction of flame propagation because of buoyancy effects. The lean and rich limits span a wider range of concentration for upward than downward propagation.

Hydrogen-air-steam flammability limits have been measured by several researchers [12-21] at temperatures below 200°C and for pressures from atmospheric up to 7 atmospheres. In the combustion of premixed hydrogen-air-steam mixtures, the presence of steam acts as a diluent, reducing the combustion temperature. The effect of increasing amounts of steam on hydrogen-air-steam mixtures, is to narrow the combustible range of hydrogen-to-air between the lean and rich limits. The lean and rich limits meet with the addition of sufficient steam, and the mixture is said to be inerted by the steam. Approximately 55% steam mole fraction will inert hydrogen-air-steam mixtures, although the measured mole fraction of steam for inerting has varied between about 52% and 63%. [12-21]

Moderate degrees of turbulence have no significant effect on the flammability limits. [21] There is some information on flammability limits of hydrogen-air lean mixtures at higher temperatures [22] and of hydrogen-oxygen-nitrogen mixtures. [23] These studies show the flammability limits widen with increasing temperature. There is still a lack of higher temperature hydrogen-air-steam flammability limit data.

1.5 Combustion Completeness

None of the flammability-limit papers carried out a systematic study of the combustion completeness at just inside the flammability limits; however, several of the papers did include some measurements of post-combustion composition. [20,21] The completeness of combustion for flammable hydrogen-air and hydrogen-air-steam mixtures was investigated at large scale [24-28] and intermediate scale. [29-33] For initially quiescent lean mixtures, these studies show the combustion completeness varies from low fractions of hydrogen burned at the upward flammability limits to complete burning of hydrogen near the downward flammability limits. For mixtures which showed low combustion completeness in the quiescent case, initial turbulent motion in the chamber greatly increases the combustion completeness. Combustion completeness increases with increasing container volume.

1.6 Definitions of Burning Velocity and Flame Speed

The "burning velocity" is the normal component of velocity of a deflagration relative to the unburned gas ahead of the front. Unless the unburned gas is stationary, the speed of propagation

of a flame relative to a stationary observer will not be the burning velocity. If the burned gas is stationary, the "flame speed" will be the burning velocity multiplied by the ratio of unburned gas to burned gas densities, as shown in Figure 1.1. The volumetric rate of burning is the surface integral of the local rate of burning. If the flame front is highly convoluted, the volumetric rate of burning can be high even if the local burning rate is not high. The burning velocity is the fundamental quantity for studying the combustion front structure. It is most often reported in the combustion literature. For studies of pressure buildup, venting, transition to detonation, etc., the volumetric rate-of-burning, or some average flame speed is more useful. In this report we will use two quantities, the speed of propagation of the flame and an equivalent planar flame speed. They are defined in Section 5.

There exists a wide range of combustion front speeds beginning with laminar deflagrations, wrinkled laminar deflagrations, turbulent deflagrations, highly accelerated turbulent deflagrations, quasi-detonations, and detonations. We will briefly discuss them in the following paragraphs.

1.7 Laminar Deflagrations

The minimum burning velocity is the laminar burning velocity. There are several experimental studies of hydrogen-air laminar burning velocities, e.g., References 34 and 35, which are in reasonably good agreement with each other and with theoretical calculations of laminar burning velocity. [36] For H_2-air mixtures at room temperature, the peak laminar burning velocity is about 3 m/s for a rich mixture of about 40% H_2, 2 m/s at stoichiometric conditions ($\simeq$ 30% H_2), and progressively less for leaner mixtures. Liu and MacFarlane [37] carried out experimental measurements at higher temperatures for hydrogen-air and hydrogen-air-steam mixtures. At 250°C the peak burning velocity for H_2-air was measured to be about 9 m/s. The presence of steam reduces the laminar burning velocity. The laminar flame speed will be about six times the laminar burning velocity. For hydrogen-air mixtures at ambient conditions, it will be below 20 m/s. Compared to the speed of sound, $\simeq$ 300 m/s, this is negligible.

For lean H_2-air mixtures the laminar flame front is not stable but deforms into a cellular structure. This will increase the flame area and increase the apparent laminar flame speed somewhat.

1.8 Ordinary Turbulent Deflagrations

In practical accident situations the flame will be turbulent. With increasing turbulent intensity, turbulent flame speeds

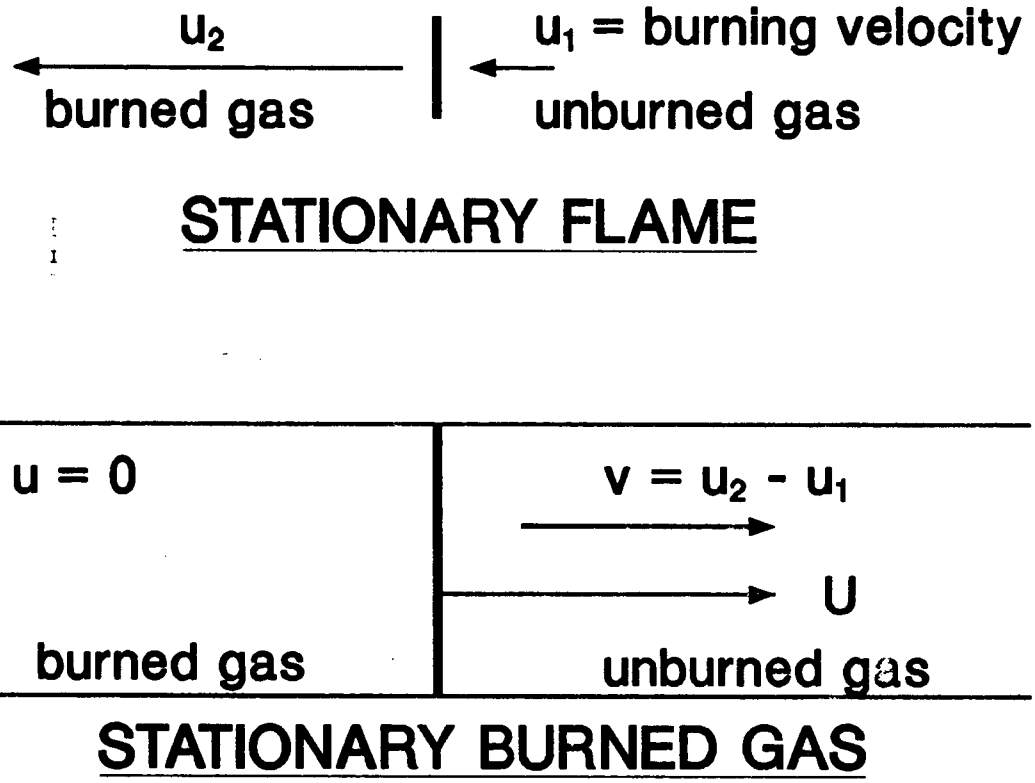

Flame speed to stationary observer, U, is

$U = u_2 = (\rho_u/\rho_b)u_1$ {$\simeq 6\ u_1$ for H_2-air}

$v = u_2 - u_1 = (\rho_u/\rho_b - 1)u_1$ = unburned gas velocity

ρ_u = unburned gas density

ρ_b = burned gas density

Figure 1.1. Burning Velocity & Flame Speed Definitions

increase, reach a maximum, decrease, and then quench. [39,40] The the ratio of maximum turbulent flame speed to laminar flame speed is largest for nearly stoichiometric mixtures. For hydrogen-air mixtures at room temperature and pressure, the maximum ratio is above 16. [40] Hence for H_2-air mixtures the turbulent burning velocity might be as high as 35 m/s, and the turbulent flame speed as high as 200 m/s for high degrees of turbulence. However, much higher effective flame speeds can occur in accidents even with moderate degrees of turbulence through the phenomenon of flame acceleration discussed in the next section.

Since many of the studies of combustion completeness and some of flammability limits included a time history of the pressure rise, one can infer flame speeds. Benedick, Cummings, and Prassinos [29,30] used an array of thermocouples to measure flame time-of-arrival, and hence flame speeds. They found upward flame speeds up to about 15 m/s for 15% hydrogen. Kumar, Tamm, and Harrison [38] measured burning velocities only up to 20 m/s in a small 2.3-m diameter sphere, even though they used highly reactive H_2-air concentrations, and passed some of the flames through a turbulence producing grid.

1.9 Flame Acceleration - Highly Accelerated Deflagrations

In contrast to "ordinary deflagrations" it is possible to have deflagrations moving at hundreds of meters per second. In such cases we say there is considerable "flame acceleration." Strong shock waves can be generated, giving highly nonuniform pressures in the volume. The local peak pressure can greatly exceed the AICC pressure during the pressure pulses. The strong shock waves preheat unburned gas, and the flows generated in the unburned gas create great turbulence. Deflagration-to-detonation transition (DDT) may be observed between the deflagration and the leading shock waves.

It is known that when flames pass through an obstacle field, the effective deflagration speed can be greatly increased. [41-44] This is due both to the increase in flame front area by flame folding and to the local increase in burning velocity by increased turbulence. In large volumes, the effect of hydrodynamic-combustion instabilities can also greatly increase flame speed. [45,46] We define highly accelerated flames as turbulent deflagrations in which the flame speeds are sufficiently high so that compressibility effects become important, i.e., the Mach number of the flame front relative to the speed of sound of the unburned gas, is not small compared to unity.

1.10 Deflagration-to-Detonation Transition

Although transition to detonation has been studied for over 50 years, [47-53] there is still considerable uncertainty whether transition will occur in practical accident situations. Transition may be more likely to occur than previously believed. [54] The "Gas Dynamic" explanation for DDT is essentially a one-dimensional explanation. The volume expansion of the hot burned gases generate shock waves moving into the unburned gas. The shock waves preheat the unburned gas, increasing the burning rate, which leads to generation of further shock waves. Some of the shock waves merge into a strong enough waves to that there is a local "explosion" that transforms into a steady detonation. Oppenheim [55] has shown that this cannot be the entire story. Transition often begins with a local explosion in region of high turbulence, even though the shock wave compression heating of the gas is not sufficient to cause a local explosion.

Analyses of postulated severe accidents in ice condenser containments predict that detonable mixtures can be formed under certain conditions. [56] The possibility of forming local detonable mixtures and undergoing transition to detonation in a large dry PWR containment, the Bellefonte nuclear power plant, has been investigated. [57] The FLAME facility has supplied experimental data which have been used to understand the possibilities of accelerated flames and detonations. In particular, its data were used in the Bellefonte study, [57] and in the NUREG-1150 Containment Loads expert panel analysis.

2. THE FLAME FACILITY

FLAME (Flame Acceleration Measurements and Experiments) is a large horizontal rectangular channel made of heavily-reinforced concrete. [58-60] The dimensions were selected to be half-scale of the upper plenum region of an ice condenser PWR containment. This section will discuss the configuration of the FLAME channel. The instrumentation used in FLAME is discussed in Section 3. The data acquisition system is discussed in Section 4.

The upper plenum of the ice condenser PWR containment is an annular region of rectangular cross section extending about 350 degrees around the containment. It contains large obstructions in the form of air handler units mounted on the walls, and considerable wall roughness due to the presence of pipes, wires, etc. FLAME was designed so that its interior width, 1.83 m (6.0 ft), and height, 2.44 m (8.0 ft) are half the corresponding dimensions of the upper plenum. It length, 30.5 m (100.0 ft) is just short of half the length of the upper plenum. FLAME also differs from the upper plenum in being straight instead of curved, and in having a solid concrete floor instead of doors which cover the ice condenser.

FLAME was designed in 1981-2 and built in 1983 at the Sandia National Laboratories Explosive Test Site 9920. A photograph of FLAME and its surroundings is shown in Figure 2.1. A map of the area is shown in Figure 2.2. The channel is oriented from the southeast to the northwest. A schematic diagram of the FLAME structure is shown in Figure 2.3. The main structure consists of a heavily reinforced concrete "U" shaped structure. Each wall has five viewports, 20.3 cm (8 inches) in diameter, and 44 penetrations consisting of 2.54-cm (1 inch) black iron pipe. The penetrations are used for the entry of instrumentation lines, hydrogen supply lines, ignition cables, and compressed air lines used to power mixing fans. The walls and floor are covered with 1105 structural embeds (bolt holes) which are used as strong attachment points for obstacles to be placed in the flow path and for attachment of devices such as the mixing fans to the walls. A photographic view of the interior of the FLAME channel with simple plywood baffles attached to the side walls is shown in Figure 2.4. The blockage ratio was 33%, i.e., obstacles blocked one-third of the cross section of the channel. A photographic view of the half-scale model of the ice condenser upper plenum region of PWR containments with ice condensers is shown in Figure 2.5 prior to test F-26. The boxes simulated the air handlers present in this region, and the angles bolted to the side walls simulated some of the wall roughness present. The blockage ratio was 11%. The photograph in Figure 2.6 was taken after test F-26 in which there was transition to detonation. The violent loads resulted in complete destruction of the plywood boxes. The

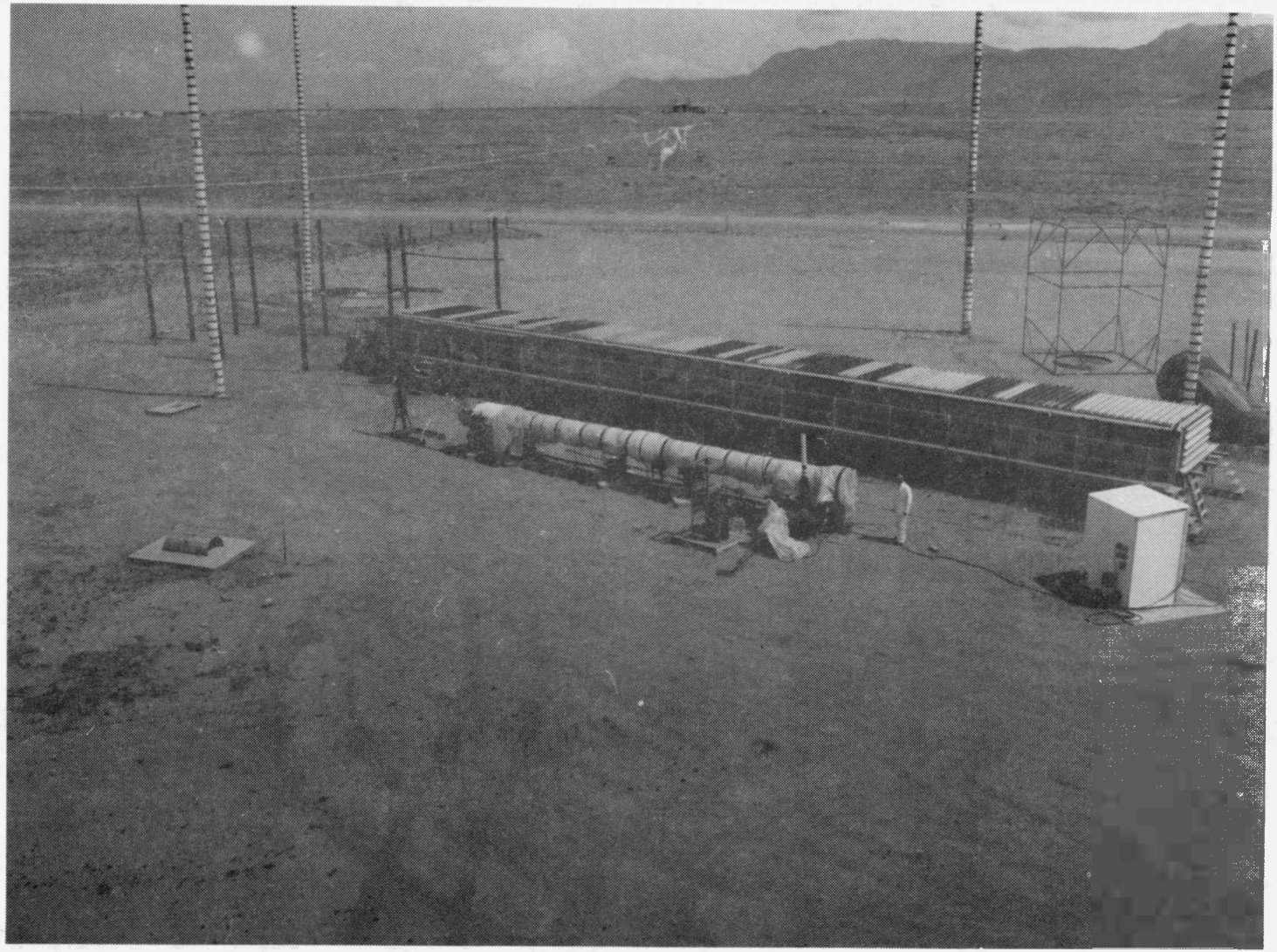

Figure 2.1. Flame Channel and Its Surroundings. Heated Detonation Tube in the foreground.

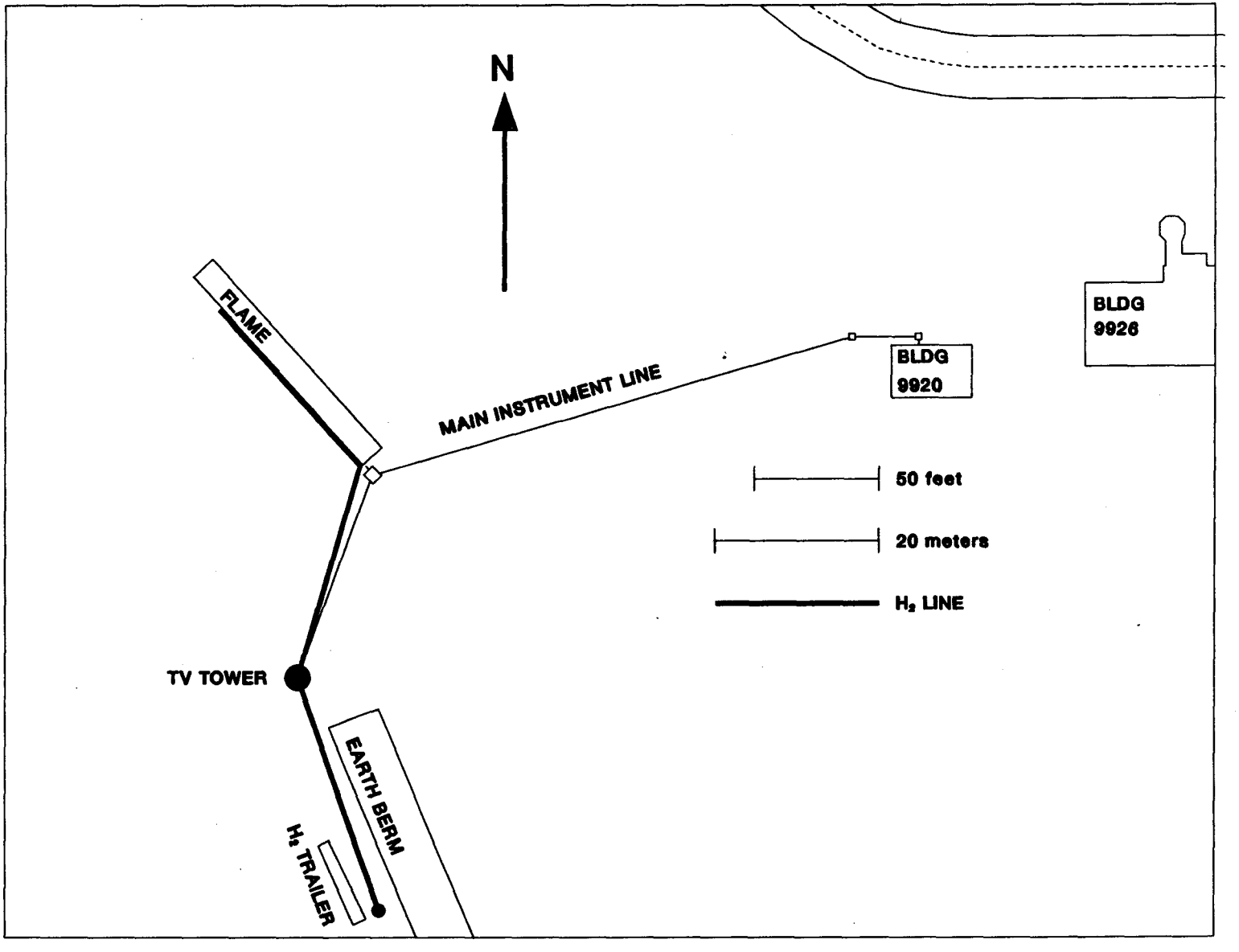

Figure 2.2. Map of Flame Facility at Site 9920, Area Y

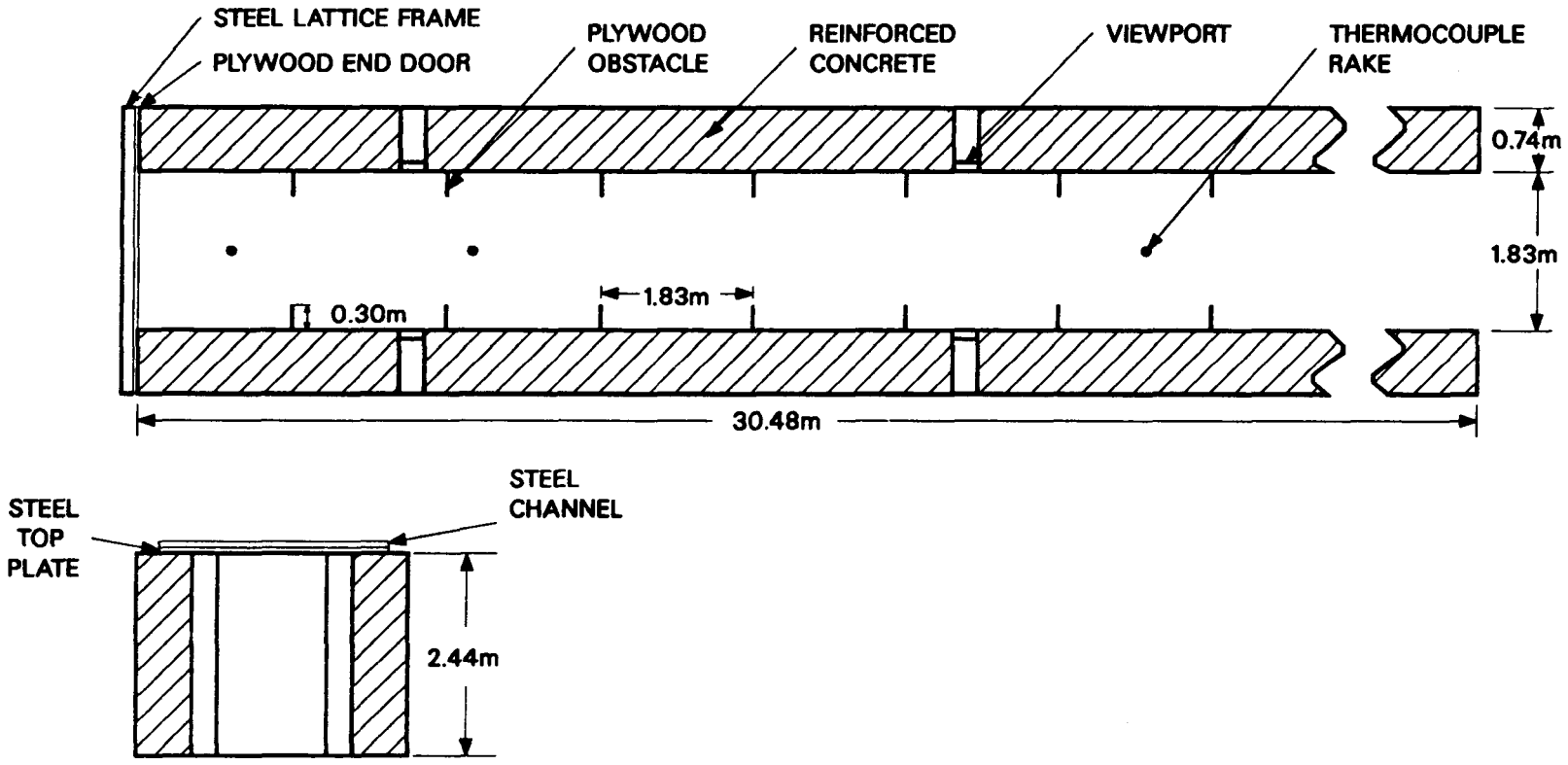

Figure 2.3. Schematic of FLAME Facility With Simple Obstacles Installed, 33% Blockage Ratio.

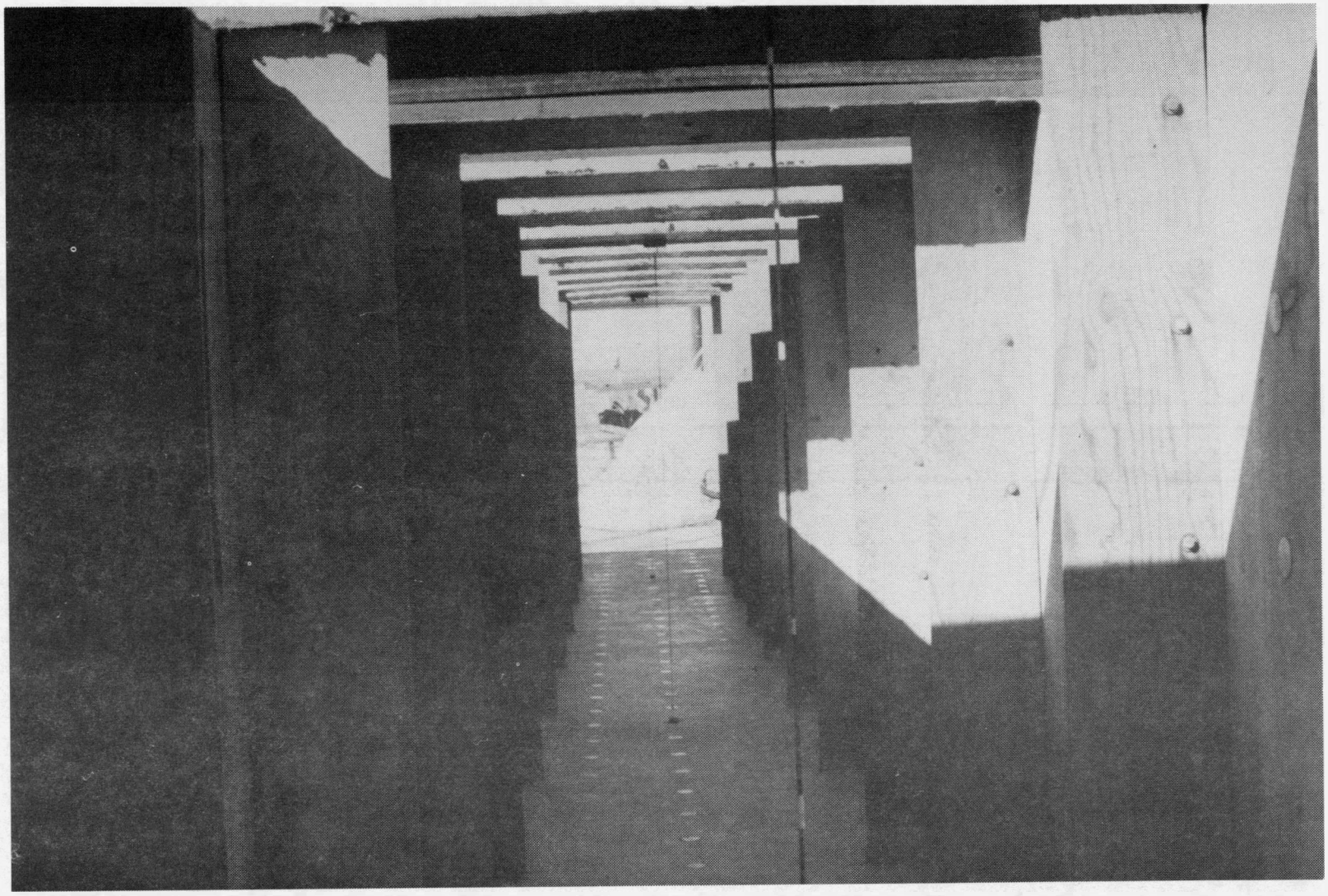

Figure 2.4. Interior of the FLAME Channel With Simple Plywood Baffles Installed. The blockage ratio is 33%. Two thermocouple rakes on the midplane are visible.

Figure 2.5. Interior of FLAME Channel With Plywood Boxes Simulating Half-Scale Model of the Ice Condenser Upper Plenum Region. Blockage ratio is 11%.

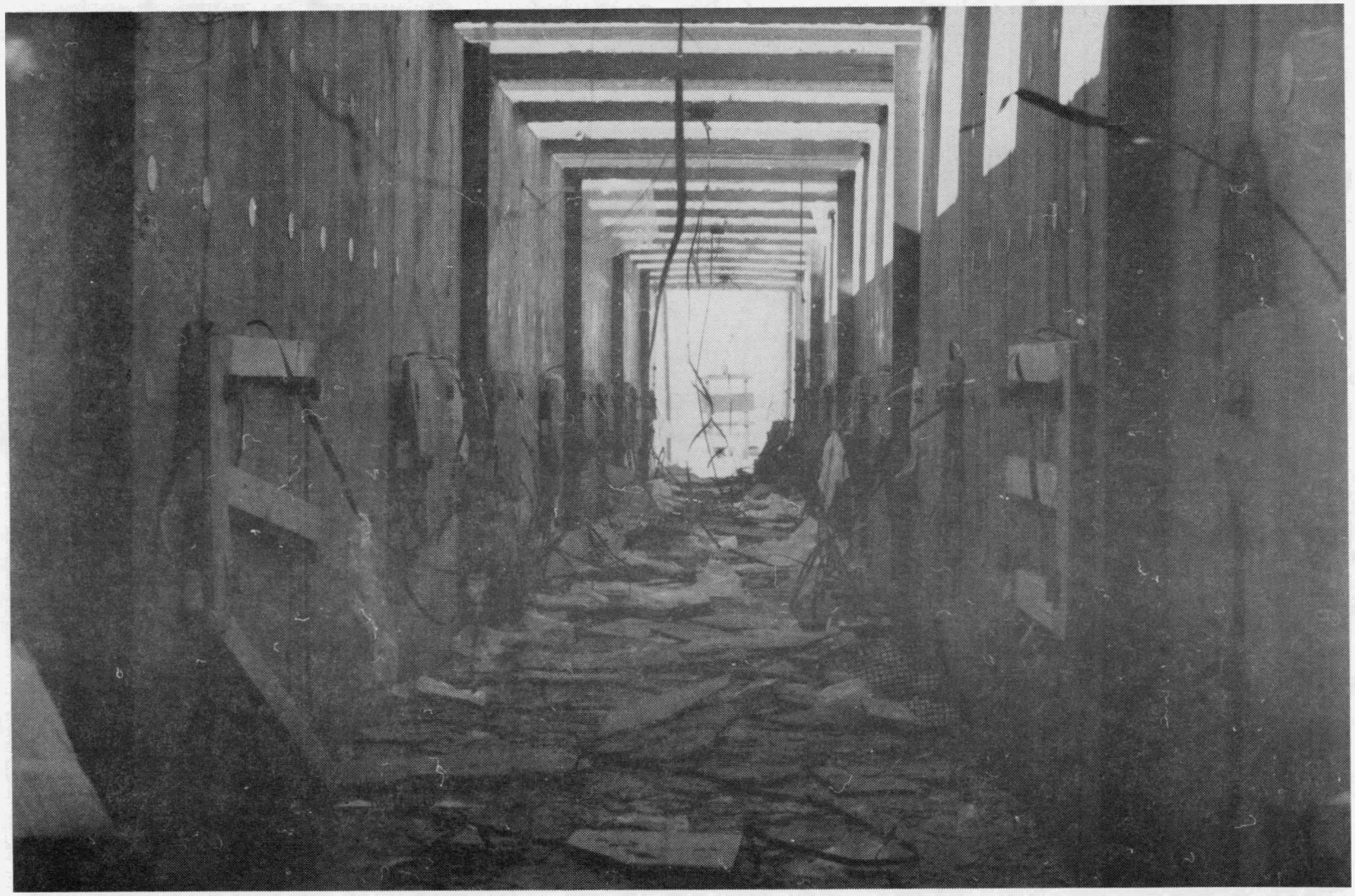

Figure 2.6. Interior of FLAME Channel After Test F-26. Detonation has destroyed boxes shown in Figure 2.5.

FLAME channel structure was designed to withstand loads resulting from detonations. To monitor some of the loads, strain gauges were bonded on some of the reinforcing bars in one of the walls.

The top of FLAME can be partly or wholly covered with up to thirty eight 5.1-cm-thick (2.0 inch) steel plates, each 0.80 m (31.5 inch) wide. Each plate is reinforced with three 20.3-cm (8 inch) channels. The plates and reinforcing channels are bolted to the top of FLAME using embeds placed every 11.4 cm (4.5 inch) along the length of the structure. Different degrees of transverse venting can be achieved by various arrangements of the top plates. Tests have been conducted with the top fully closed by the plates (0% top venting), with every other plate removed (50% top venting), and with the plates separated by one bolt hole (13% top venting). The designer of FLAME suggested that tests not be conducted with more than 50% top venting to prevent damage to the side walls. Without the top plates, the side walls would lose simple support on the top and become cantilever beams. Some of the top plates and their reinforcing channels have been permanently deformed by detonation loads. However, they still fulfill their function.

A special wheeled carriage device resting on the top of the FLAME walls has been used to move the top plates. The plates each weigh over a ton. Changing the degree of top venting usually takes two technicians several days work.

To act as a gas seal, the top of FLAME was covered with a 0.15 mm (6 mil) virgin polyethylene sheet. The sheet was taped to painted metal angles on the outer top edges of the concrete walls, and to metal angles on the ends of the channel. The polyethylene sheet does offer some small restraint to gas expansion before it melts or is torn off. Methods of tearing the sheet just prior to ignition of the gas in the channel were considered but not pursued.

The southeast (ignition) end of FLAME is closed by a rigid plate. The hydrogen-air mixture is normally ignited near the center of this plate. In the first fourteen tests the rigid plate was a 5.1-cm-thick (2 inch) steel plate, reinforced with 25.4-cm (10 inch) steel channels. The plate was bolted to the FLAME structure using 19 embeds, supported on the two vertical sides and the bottom. This plate was permanently deformed and the concrete near the top embeds was damaged as a result of loads from a detonation in test F-14, as shown in Figure 2.7. The damaged embeds were replaced, and the concrete at the channel end was repaired. To avoid damage to the FLAME structure, we replaced the steel plate with 1/2 inch (1.27 cm) plywood sheets held in place by a strong steel lattice frame as shown in Figure 2.8. The plywood panels were designed to withstand loads expected from ordinary deflagrations, but to blow out at

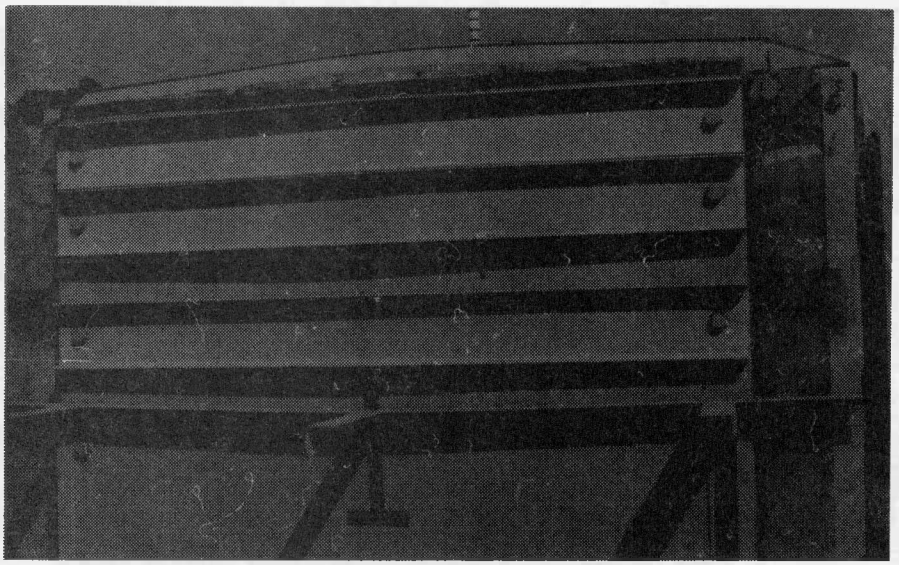

a. Exterior Showing Concrete Cracking and Bent Steel

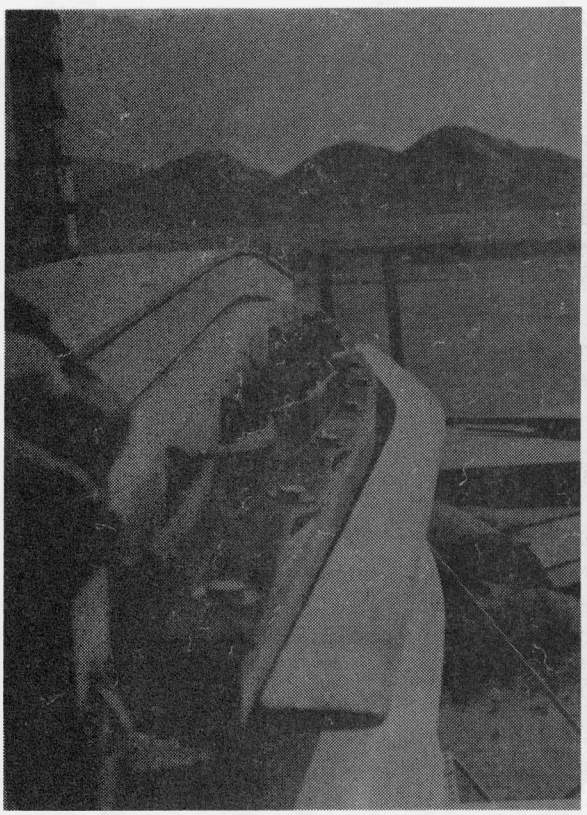

b. Closeup of the Top

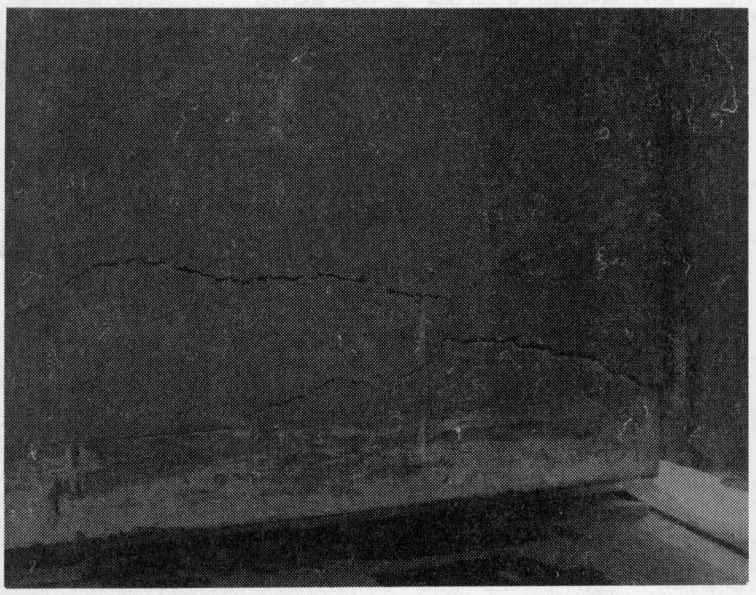

c. Interior Showing Cracked Concrete Walls

Figure 2.7 Damage to the FLAME Structure at the Ignition End After Test F-14

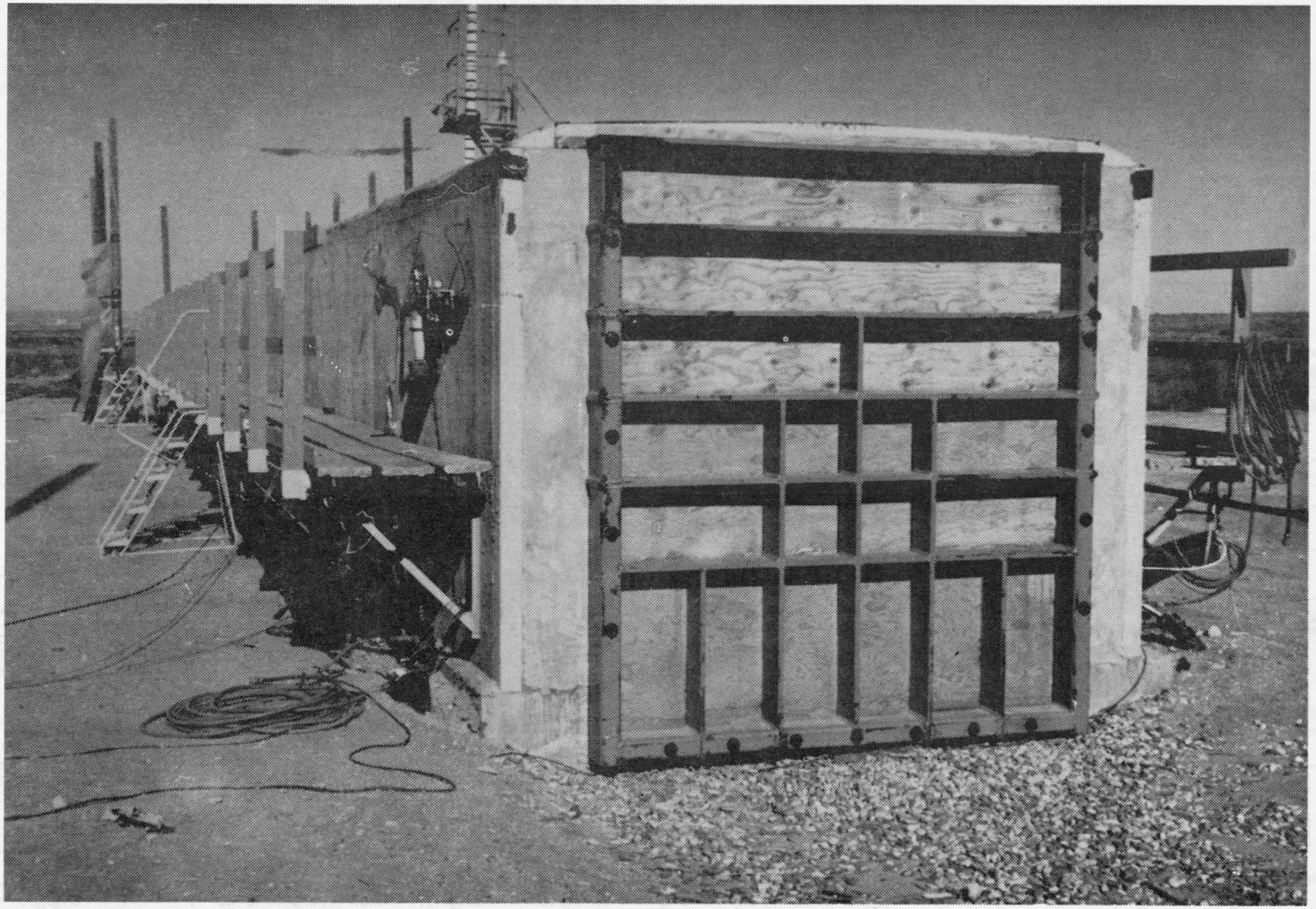

Figure 2.8. Exterior View of the Ignition End of the FLAME Channel Showing the Steel Frame and Sacrificial Plywood Sheet. These replaced a steel end door that was bent in test F-14.

overpressures of about 350 kPa (50 psig). In tests conducted since its use, this system has worked. The plywood survived tests with ordinary deflagrations, and was destroyed in tests with detonations and highly accelerated deflagrations. There has been no damage to the steel lattice frame or the concrete in 16 additional tests. The only deviation from the design is that the bursting pressure of the plywood may be below the design overpressure.

Prior to a test, the northwest end of FLAME was closed with a 0.10-mm (4 mil) polyethylene bag, as shown in Figure 2.9. The bags were cylindrical in shape, with one end open. The open end of the bag was taped to the end of FLAME to form a gas-tight seal. One small opening in the taped surface was left. Four wire-rope guide lines surrounded the bag running parallel to the channel axis. Each guide line had clips which could freely move down the length of the line. The bags were manufactured with loops made of strapping tape on its sides. The side of the bag was supported when these loops were attached to the clips on the guide lines. Just prior to a test, the bag was compressed until it was flush with the end of the channel. The remaining opening in the bag-to-channel tape seal was then closed. At a later time after all personnel had retired to safe areas, hydrogen was allowed to enter the channel. The side supports permitted the bag to expand parallel to the channel axis while largely preventing motion perpendicular to the axis. This was needed to counter loads due to buoyancy and wind. The bag lengths were designed so that the bags would be almost fully inflated when the desired amount of hydrogen had entered the channel. Hence the richer the mixture, the longer the bag used. The longest bag used was over 10 m long. For additional protection from wind, a surrounding wind break was used. After a canvas wind break was destroyed by detonation loads in test F-12, plastic sheet was used. Our procedure was to test with a wind speed of no more than 8 kmph (5 mph). The possibility of wind damage to the bag or the top sheet was the main environmental constraint on testing. In particular, testing in the spring was discouraged because strong winds often develop during the day in the spring season.

The hydrogen used in the tests is obtained from a tube-type semitrailer of 33,300-ft^3 (943-m^3) capacity. Prior to a test, one or two tubes in the trailer were prepared with the desired amount of hydrogen by filling them to a desired pressure. After all personnel retired to the concrete buildings, the hydrogen from the prepared tubes was emptied into the FLAME channel. The hydrogen entered the FLAME channel through three penetrations near the floor, one at either end of the channel, and one in the middle. The gas was mixed using two air-driven mixing fans of 2100 ft^3/min (59 m^3/min) capacity. One fan was placed near the ignition end and one near the exit, hence leaving the main section of FLAME free of their obstruction. After the gas had

Figure 2.9. Prior to a Test, the Polyethylene Bag Has Been Taped to the End of the FLAME Channel and Attached to the Guidelines. The plastic windbreak can be seen on the extreme left and right.

been mixed, five gas samples in five different locations in the channel were obtained. The gas sampling systems each consisted of a line through a wall penetration, a solenoid valve, a 50-cm^3 evacuated gas sample bottle, and a larger vacuum bottle. The solenoid valves were opened, gas samples pulled into the sample bottle, and the solenoids valves were closed. After the test, manual valves on both ends of the sample bottle were closed. The sample bottle was removed from the gas sampling system and sent to the analysis laboratory at Sandia National Laboratories. Initially, gas composition was measured by gas chromatography. Later in the testing program, mass spectroscopy was used, which was deemed more reliable. The reported hydrogen mole fractions were an average of the reported values for the five sample bottles, excluding outliers. Based on the variation in hydrogen mole fraction for the different bottles, we estimate the uncertainty in hydrogen mole fraction was below ± 1/2.

The ignition system was capable of three independent methods of ignition, a bridgewire, a spark plug, and a glow plug. All three systems have independent cabling. All tests to date have been conducted using a single point bridgewire ignition. A capacitive firing set was used to provide high-amplitude current to vaporize the bridgewire.

3. INSTRUMENTATION

3.1 Introduction

The instrumentation used in FLAME is discussed in this section. The discussion of test results in Section 6 is based on combustion front time-of-arrival measurements and on pressure measurements. Combustion front time-of-arrival has been measured by a variety of instruments: thermocouples, photodiodes, lithium-niobate gauges, and high-speed cinematograhy.

When FLAME was constructed, strain gauges were mounted on selected reinforcing bars that were buried in the concrete walls. Although some of these gauges failed soon after the concrete was poured, data were obtained from the other gauges. This data will not be covered in this report. In the effort to model the behavior of the FLAME tests, it was stated that it would be useful to measure the flow velocity in FLAME, even if only at one point, the center of the exit plane. Several efforts were made to measure flow velocity, but they were not successful because of the wide range of speeds found in the tests and the fast transient response required.

3.2 Time-of-arrival measurement

The main tool for measuring flame time-of-arrival was chromel-alumel (type K) thermocouples mounted on vertical "rakes" along the midplane of the channel, about equally spaced axially. The positions of these rakes and of the other instruments for the various tests are given in Appendix A. Two thermocouple rakes were used in the first test; four rakes were used in tests F-2 to F-12; five vertical rakes were used in the later tests. A horizontal rake near the exit was included from test F-16 to F-19. From test F-20 onward the horizontal rake was removed and several thermocouples were mounted on one of the side walls near each rake. The thermocouple wire used is 0.25 mm (0.01 inch) diameter with a roughly spherical welded junction of approximately 1.0 mm (0.04 inch) diameter. Later butt welded thermocouple junctions not much larger than the wire diameter were used.

The thermocouples gave a clear indication of flame time-of-arrival. Prior to the flame arrival, the measured temperature was either constant with some noise present or slowly rising. There was a clear break in the slope of the temperature-time curve at the flame time-of-arrival. In addition, the thermocouples indicated detonation time-of-arrival. The results from one thermocouple taken in a test with a lean hydrogen mixture and a slow flame (test F-9, 6.9% H_2) are shown in Figure 3.1. Figure. 3.1b is a sufficient enlargement of the

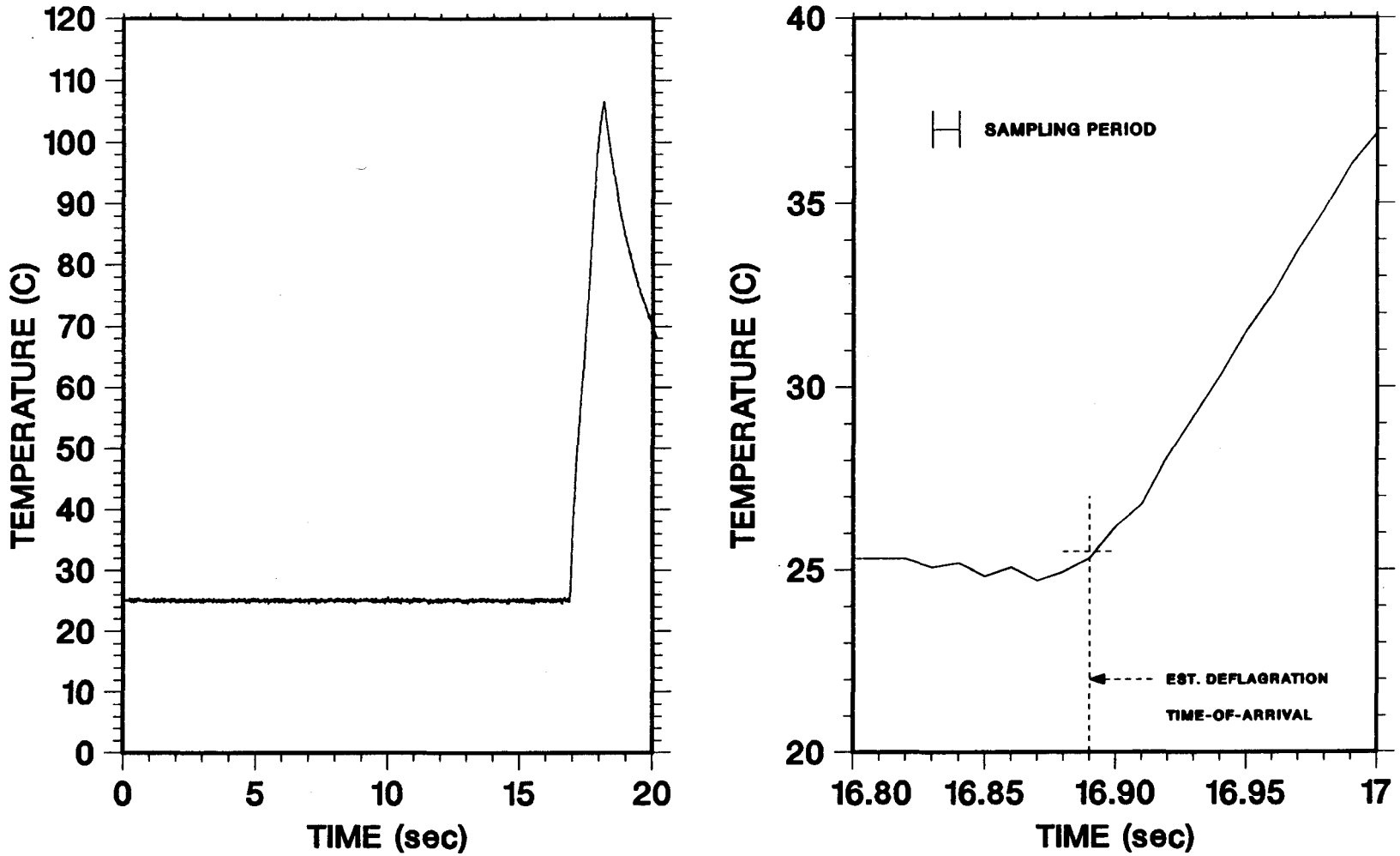

Figure 3.1. Deflagration Time-of-Arrival

time-of-arrival region in Figure 3.1a to show individual digitally recorded sample temperature measurements. As in most tests with lean burns, there was usually little noise in the thermocouple signal. The selected time for the flame time-of-arrival in Figure 3.1b is uncertain to no more than a single sample period, close to the limit that can be expected from digital recording. For the tests with higher flame speeds, the noise in the thermocouple signals was usually higher, and the uncertainty in the time-of-arrival greater than one sample interval, typically ± 3 sample intervals. For a typical sampling speed of 2 kHz, this corresponds to ± 1.5 ms. In Figure 3.2 results are shown from a thermocouple near the ignition end of a test that had a transition to detonation. Figure 3.2a shows the overall thermocouple record, while Figures 3.2b and 3.2c show enlargements of the two interesting periods. The time-of-arrival estimate of the flame is shown in Figure 3.2b and the estimate for the returning shock wave is shown in Figure 3.2c.

In tests where there was transition to detonation, it appears that the thermocouples responded to the arrival of the detonation or shock wave in two ways, as illustrated in Figure 3.2c. The slope of the temperature-time curve was steeper after the arrival, as expected by higher heat transfer rates to the thermocouple from a higher temperature faster moving gas. Even more dramatically, there is usually a strong oscillation in the signal near the time-of-arrival, often with continued increased noise levels. This oscillation cannot be response to temperature changes in the gas. We speculate that since very hot combustion gases are partly ionized, the increased noise level in higher temperature combustion and the nonthermal behavior with detonations or shock waves may be due to magneto-hydrodynamic effects. However, we have not made any study to back up this hypothesis. If the onset of this behavior is considered the detonation time-of-arrival, then the results are in good agreement with the detonation time-of-arrival of the other instrumentation to be discussed shortly: germanium photodiodes, pressure transducers and lithium-niobate gauges. This corroboration gives confidence that we are correctly measuring detonation/shock wave time-of-arrival with thermocouples.

We did not attempt to use the thermocouples to accurately measure gas temperature, only time-of-arrival. Because of the comparatively large size of the thermocouple bead and hence finite thermal capacitance, the thermocouple reading lags the change in the surrounding gas temperature. There are also errors due to radiation losses from the bead to the cold channel walls, and conduction losses down the thermocouple wires. Methods exist for compensating these effects. [61] Using these methods, better estimates of the gas temperatures could be obtained from the data, but we have not done so.

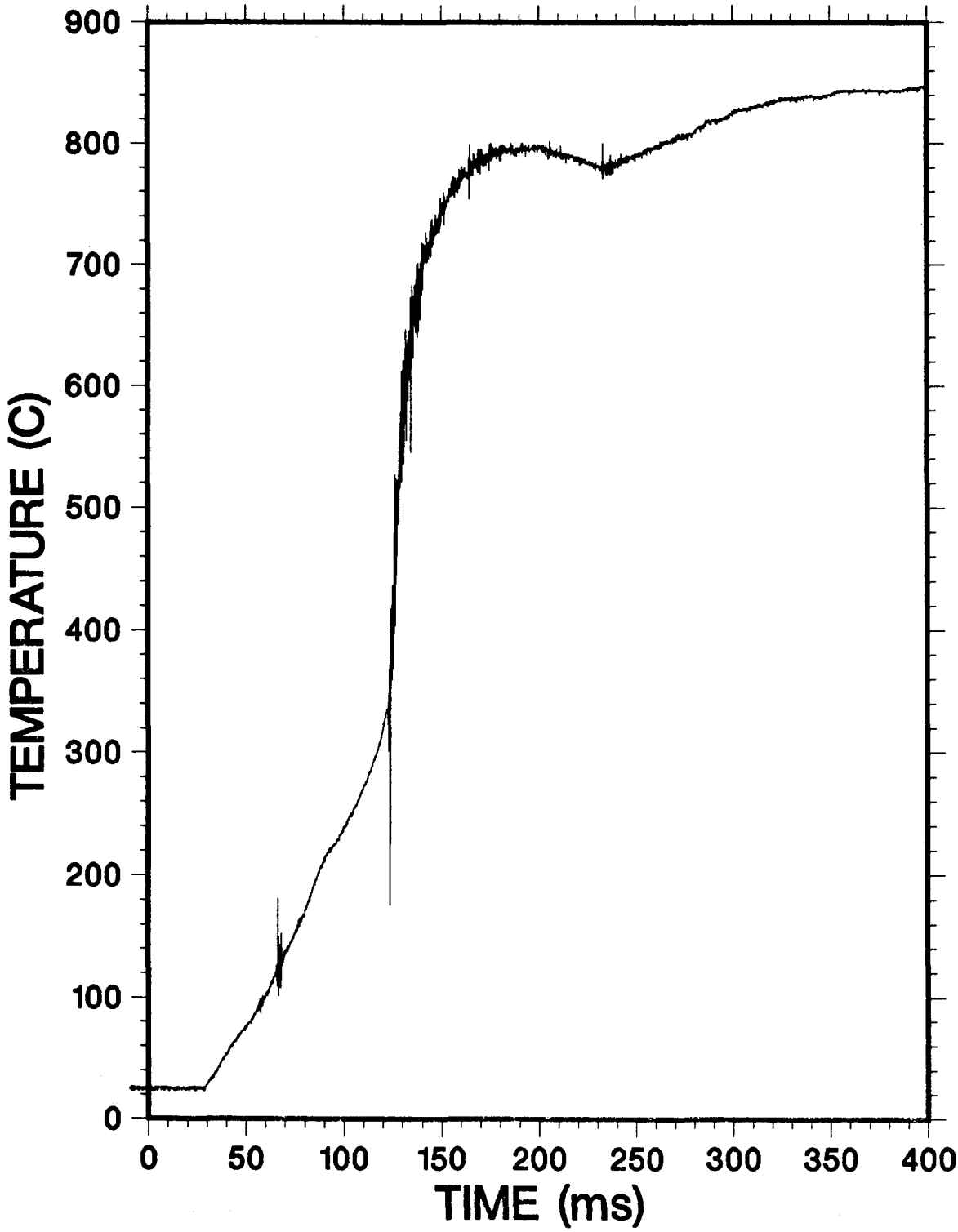

Figure 3.2. Deflagration and Detonation Time-of-Arrivals. From temperature history test F-14, Thermocouple TA7. 30.0% H_2. No top venting. No obstacles.

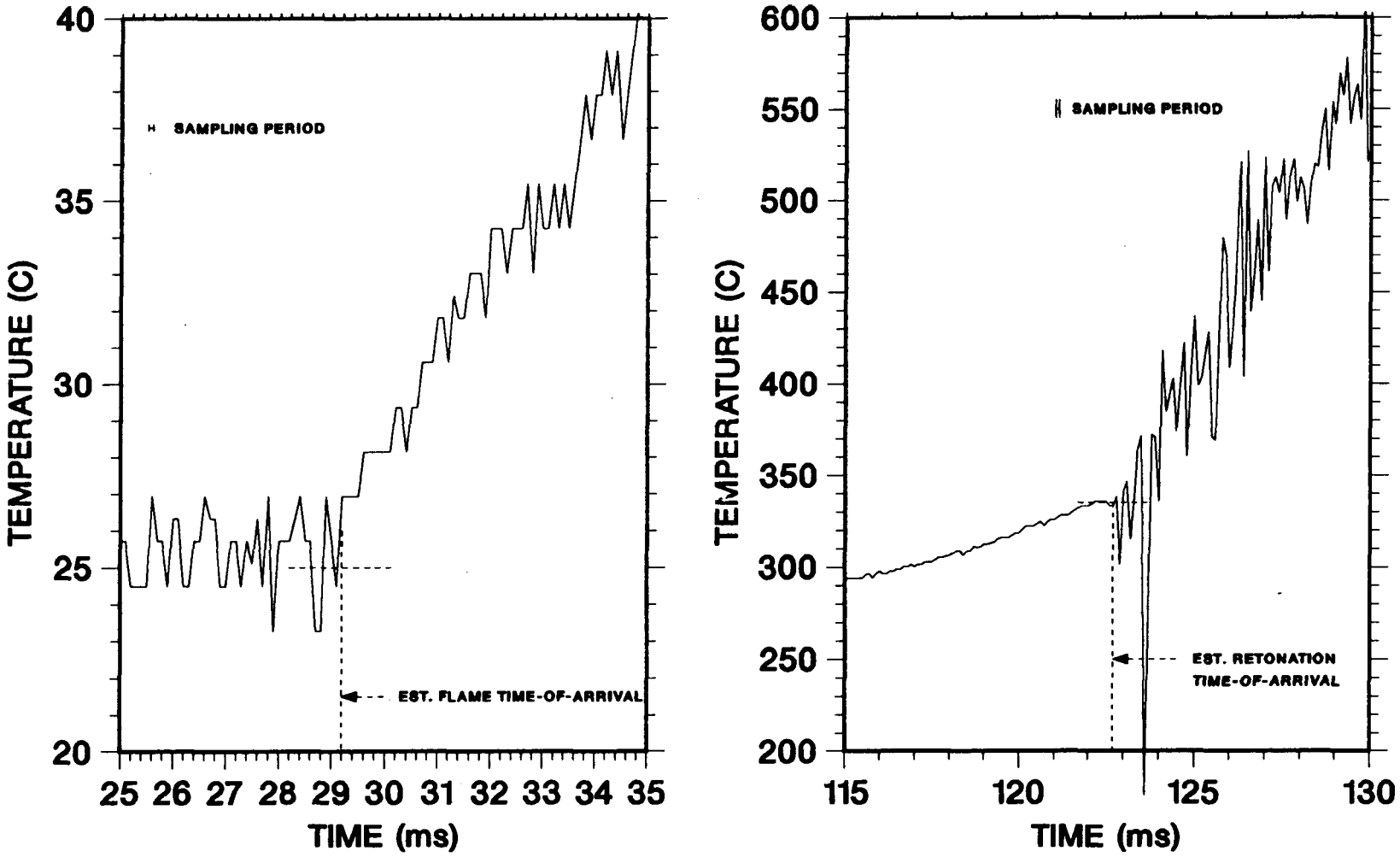

Figure 3.2. (continued)

In addition to thermocouples, we have also used two other instruments to measure flame time-of-arrival, germanium photodiodes, and lithium niobate gauges. These were "backup" detectors should the thermocouples fail to give good results. We continued to use them after the thermocouples had proven satisfactory but with no incentive to increase their number.

Germanium photodiodes (GPDs) are sensitive to the infrared radiation of hot steam. We used seven GPDs, five mounted in the optical ports, and two mounted in access pipes near the exit. This measurement differed from the thermocouple measurement in that it is along "line of sight" rather than at a point. The photodiode results become more useful in tests with more intense combustion. In tests with slow deflagrations, the signal showed a gradual rise. It was difficult to select a particular "time-of-arrival." For detonations, the signal rose abruptly. There was a clear time-of-arrival that was in excellent agreement with the results of pressure transducers and thermocouples.

Lithium-niobate gauges produce a large-amplitude output voltage when heated. We mounted two of these gauges flush on the channel walls. Initially, it was hoped that, because of their large output signal, the signal from these gauges would not require amplification but could be directly digitized. This was attractive because we had more digitizer channels than amplifiers. However, we have found that some amplification was required. Of more importance, the lithium-niobate gauge produced results in which the flame time-of-arrival was less distinct than the thermocouple data.

As the test series progressed, more high-speed cinematography was used. The cameras were run at speeds between 2000-4000 frames/second. The edge of the films contained timing marks every millisecond to determine the framing rate. The most useful view was at the channel exit perpendicular to the channel axis. In the field of view was a vertical pole with marks every foot. The position of luminous combustion fronts could be determined frame-by-frame. This was useful in determining if the front was moving at detonation speed. Also of great value was an axial view into the channel. To protect the camera from debris thrown from the channel, we placed the camera to the side of the channel and used a large front-surfaced mirror. Several mirrors were destroyed in the test series. Of less value were views through the ports in the side of FLAME. Without a means of establishing the time-after-ignition, and with the limited field of view, not much of value was seen in the port views. These views did show the presence of reverse flows during part of the test. A video camera mounted on a tower was used monitor the region for safety purposes. However, during the test the video camera was viewing the top of FLAME, and the results recorded on a VCR. With the comparatively low speed of ordinary video (30 frames/s) and low resolution, the video results were of limited

use. However, they did show that the plastic top cover was late in releasing during test F-5. From test F-26 onward, high speed motion pictures cameras were mounted above the channel and used to photograph the channel from above.

3.3 Pressure Measurement

The number, type, and location of pressure transducers used in FLAME tests is given in the Appendix. The principle type used was the Kulite model XTS-1-190. It is a quartz membrane Wheatstone bridge resistive gauge with resonant period of 10 μs. A porous metal shield, Feltmetal type 1102, was placed in front these pressure transducers to minimize the effect of "flash temperature" rise on the accuracy of the reading. An experimental study [62] has shown that pressure transducers can accurately measure hydrogen deflagration pressures using a porous metal shield. This confirmed simple theoretical results which indicate that the pressure drop through the porous metal shield is negligible for characteristic pressure rise times of the order of several milliseconds. The shield will have a detrimental effect on response to much faster pressure rises due to detonations and/or shock waves.

It is of interest to estimate the uncertainty in the pressure measurements. All the Kulite XTS-1-190 pressure transducers were initially calibrated in the Sandia Laboratory calibration laboratory, and occasionally recalibrated. The calibrations verified the factory calibrations on gauge sensitivity, zero offset and linearity. The discrepancies and nonlinearities detected were negligible. After a time some of the gauges failed due to water ingress, or due to overranging in violent tests. The failed gauges could easily be detected from their behavior. What we did not have was the capability to check the behavior of the gauges to transient pressures. The response of the gauges to rapid pressure changes (above a few kHz) was hindered by the use of felt-metal shielding previously discussed, and by the limited frequency of the digital sampling. The gains of the amplifiers used were calibrated by inputing DC voltage standards. In summary, static calibrations indicate that uncertainty in measuring slowly changing pressures was low, below a few percent. However, there was no testing of the response to more rapidly changing pressures.

Attempts were made to use Kistler and PCB quartz piezoelectric pressure transducers. These dynamic gauges can measure pressures between a low frequency limit, typically a few Hz, and an upper limit, typically about 100 kHz. These gauges gave useful information in some tests, however, they obviously were not functioning correctly in many other tests. There may have been two reasons for their failures. One reason may have been that they were operated without thermal protection to avoid degrading their fast response. There may have been flash heating effects on the response of the transducers during tests and/or

gradual thermal degradation of the transducers during the series of tests. A second reason was that after testing was completed it was recognized that the signal from these gauges to the 7612 digitizers should not have been "AC coupled" as they were in later tests. This not only filtered out the DC (0 Hz) response, but partly filtered out AC response up to about 30 Hz. Hence the failure to use DC coupling invalidated the results from these gauges in tests with slow deflagrations. We have relied on the response of dynamic pressure transducers for determining peak pressure in only two of the tests with transition to detonation: test F-14, where they were the only pressure transducers operating, and test F-12. The failure to be able to use the response of these dynamic pressure transducers in other tests with strong pressure spikes doubtless led to underestimates of the peak pressure for those tests.

3.4 Strain gauges

The locations of the 32 strain gauges on reinforcing bars in the FLAME east wall are given in Appendix A. These measurements could be used to measure the axial and bending strains of the reinforcing bars. During the pouring of concrete and imbedding of the strain gauges, several of the gauges failed. As the testing period continued, additional gauges failed. However, at the end of the testing period many of the gauges still continued to operate.

Only a cursory look at the strain gauge data was made. These brief examinations showed significant oscillations of the walls in tests with detonations and highly accelerated flames and negligible signals for tests with lower loads.

3.5 Exit velocity

For modeling purposes, it would be useful to know the flow velocities in FLAME, at least the velocity at the exit plane. We attempted to measure the exit flow velocity at the center of the exit plane of the channel. One approach was the construction of a pitot tube with a miniature pressure transducer. The pressure transducer was enclosed in the pitot tube to minimize the internal gas volume, and hence improve the transient response. Because of the very wide range in flow velocity encountered, we either had insufficient dynamic pressure to record or we overranged and damaged the fragile transducers. In the test series with obstacles, the debris from the obstacles destroyed the pitot tube. We discontinued using it.

Other simpler systems were used to measure velocity. balloons hung from strings pendulum fashion have been photographed during tests. The motion of the spheres is an indication of flow velocity. A light-weight foamed plastic "popcorn" and soap solution bubbles were introduced in the flow, but the spatial resolution of the high speed cinematography was not sufficient to enable them to be visible.

4. DATA ACQUISITION SYSTEM

4.1 Introduction

The data acquisition systems for FLAME were located in building 9920. The transducers in the FLAME channel were connected to building 9920 via roughly 100 meters of buried cables. Most of the signals were transmitted over 20 pair or 9 pair twisted shielded cable. The germanium photodiodes and the piezoelectric pressure transducer signals were transmitted via coaxial cables. All the analog signals were converted to digital form and recorded in various transient digitizer memories. Digital recording of data is much cheaper and more convenient than analog tape recording. However, for recording events with poorly known amplitudes and timing, as in flame acceleration, there are difficulties with digital recordings. This is discussed in the following paragraphs.

The primary data acquisition system was based on commercially available CAMAC (Computer Aided Measurement And Control - IEEE 583 standard) modules with a capacity of over 100 data channels. As a backup, about 40 incoming signals were simultaneously recorded on a custom built system termed DAASY. In addition, six data channels were available on Tektronix 7612 digitizers. The main advantage of having a backup data acquisition system was that different amplifier gains and sampling rates could be used. Usually one system had a fast sampling rate and low amplifier gain to accommodate a vigorous combustion, while the other system had a slower sampling rate and higher amplifier gain.

Throughout the test series there was considerable difficulty in selecting the proper amplifier gains and sampling rates. It was difficult to predict the peak pressure to be expected. Pressures varied greatly from test to test (10 to 3000 kPa). If too high an amplifier gain was selected, pressure peaks could be clipped, as in test F-19. If too low an amplifier gain was selected, much of the signal could be in the noise level, as in tests F-3 and F-5. Since flame speeds varied greatly from test to test, it was also difficult to predict the length of the test (80 ms to 27 s). If too fast a sampling rate was selected, the important events could occur after the digitizers filled their memories, as in test F-13. If too slow a sampling rate was selected, the important events could be recorded with low temporal resolution. This is the problem of finding the correct time "window" to record the test. Aside from the use of a backup data acquisition system, we were able to ameliorate the sampling rate problem by buying more digitizer memories and by using variable sampling rates with the programmable clocks. The favorite strategy used was to estimate the period of the test and

select the corresponding sampling rate to fill about 85% of the digitizer memory. The last 15% of memory was filled at a much lower sampling rate. This greatly lengthened the recording window and prevented losing the event. If the event occurred at the slower sampling rate, it would be recorded with lower time resolution. However, if the event did happen that late, often the lower resolution was adequate because the flame speeds were not high.

4.2 Primary data acquisition system

The primary data acquisition system is shown schematically in Figure 4.1. Only the flow of information from the transducers is shown. For clarity, the figure ignores the flow of information from the computer to the crate controller required to arm the devices, the possible flow of information from the programmable clocks to the computer, and the role of the computer terminals. The arrows with the thicker lines and larger heads represent the flow of information taking place "real-time" during the test; the arrows with the thinner lines and smaller heads represent the flow of information from the volatile digitizer memory to storage and/or hard copy after the test is completed. The flow of transducer information in "real-time" was from the transducer, to the amplifier, to the digitizer, to the digitizer memory, as shown in Figure 4.1. The digitizers were triggered by signals from trigger generators. The digitizer sampling rate was under the control of either an internal clock, or an external programmable clock. Just after a test, the data resided in the digitizer volatile memory. Within a few minutes after each test, we began to store the data more permanently. This second data flow was from the digitizer memory, to the digitizer, to the CAMAC crate controller, to the computer, to hard disk storage. After this had been accomplished, data was then copied to floppy disks for archival storage.

The main data acquisition system was under the control of a Digital Equipment Corporation LSI 11/23 (later upgraded to an LSI 11/73) computer. Attached to the computer were two terminals, either of which could be used, but not both simultaneously. The Tektronix 4010 graphics terminal was used to run the data acquisition programs written in Tektronix SPS BASIC and plot the results. A hard copy unit was attached to the Tektronix 4010 to obtain graphical results. The second terminal was a Datamedia DT/80. It was used for editing programs, formatting floppy disks, listing programs on a printer attached to it, etc. The computer "booted up" in the RT11 operating system. SPS BASIC was run only on the Tektronix 4010 terminal, but RT11 operations could be run on either terminal.

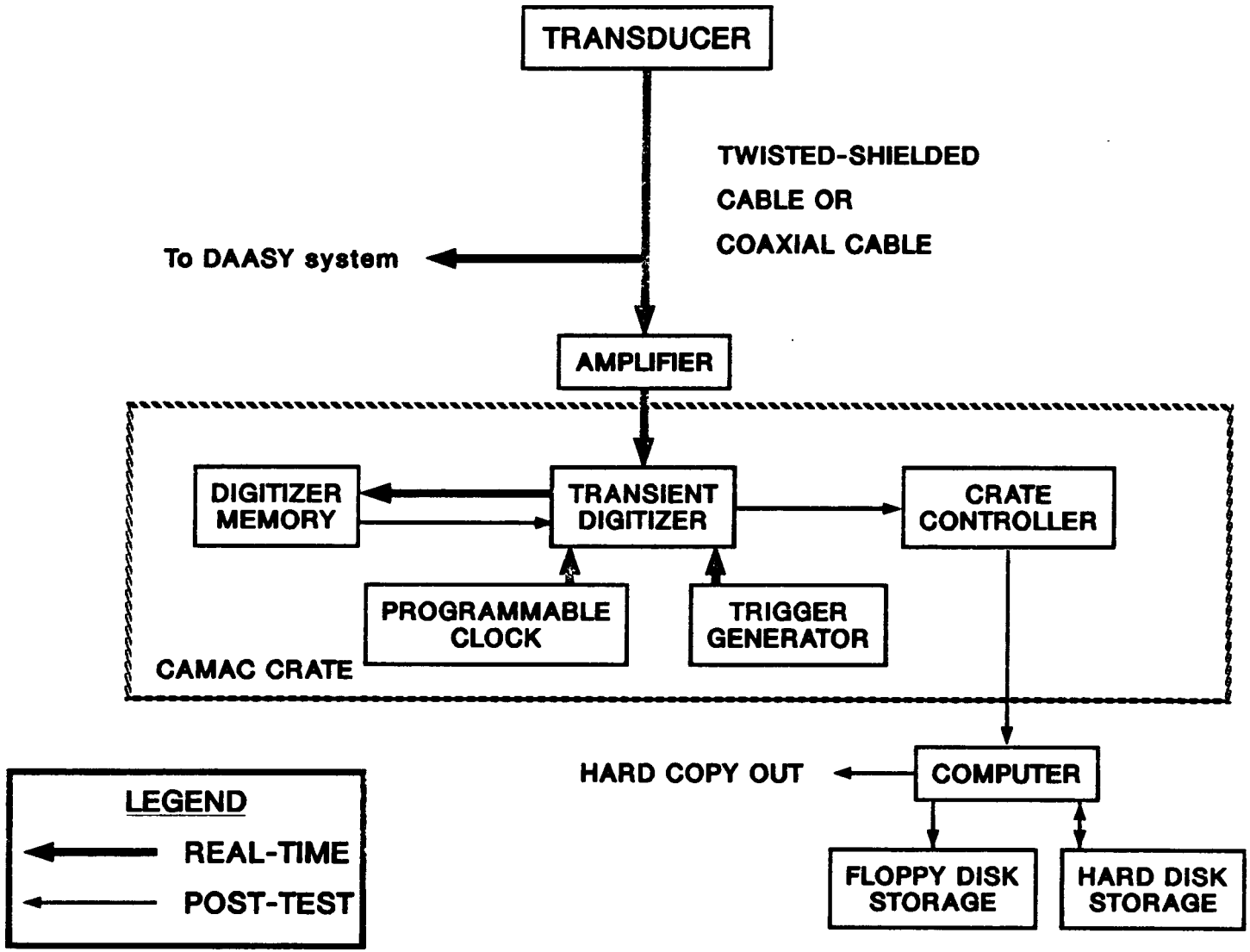

Figure 4.1. Schematic Diagram of Data Acquisition System Showing Main Flow of Information

All transducer signals requiring amplification passed through Trigtek model 205A instrumentation amplifiers. These amplifiers were in the form of fourteen rack-mounted banks of seven independent amplifiers, for a total of 98 channels. The Trigtek amplifiers gains were set by manually turning a switch on the front face of the amplifier. The possible gains ranged from 0.1 to 1000 with possible setting of (0.1,0.2,0.5,1,2,5,10,20,50 100,200,500,1000). Each amplifier had an adjustment screw so that the gain and zero could be calibrated. The Trigtek 205A amplifiers were rated from 0 Hz to 100 kHz (down 3 db).

From the amplifiers, the signal went to a transient digitizer module in a CAMAC crate. CAMAC is a standardized system consisting of CAMAC crates, crate controllers, and working modules. The crate provides electric power, mechanical support, signal and control lines to the CAMAC modules. There are 25 "slots" in each CAMAC crate. Modules may occupy one, two, or more slots, depending on the module width. Each crate must have a crate controller which is the only module which communicates with the computer. Data from working modules must flow through the crate controller to go to the computer. Likewise data from the computer to the working modules passes through the crate controller. Our primary data acquisition system contained two CAMAC crates with LeCroy 8901 GPIB interface crate controllers. The connection between the crate controllers and the LSI computer was over a General Purpose Interface Bus (GPIB - IEEE 488) highway. A GPIB connection was selected because it permitted us to also attach other non-CAMAC GPIB instruments on the highway at the price of a lower maximum data transfer rate than dedicated CAMAC data transfer highways. The working modules consisted of six BiRa 908 transient digitizers, their BiRa associated 903 memories, LeCroy 8610 trigger generators, and LeCroy 8501 programmable clocks.

4.2.1 The BiRa 908 Digitzers

The BiRa 908 transient digitizers are a three-slot-wide CAMAC module that can be programmed to simultaneously digitize data using either 32, 16, 8, or 4 active channels with a 12 bit resolution. The maximum sampling rate and the memory allocated per channel increase as the number of active channels decreases as shown in the following table. The memory per channel shown in the table is for a single 903 memory module. If two 903 modules are used per digitizer, the memory per channel would be double the values given. Up to 12 memories can be attached per digitizer.

Table 4.1
BiRa Transient Digitizer Performance

Number of Active Channels	Maximum Sampling Rate, kHz	Memory per Channel, per memory module
32	5	1K (1024)
16	10	2K
8	20	4K
4	40	8K

Most of the data was recorded with 16 active channels at speeds of 1 to 5 kHz. Up to test F-16 a single 903 memory was used with each digitizer. The value of having more memory became obvious. We purchased six additional memories to increase the number of data points per channel. Three memories were used to store pressure data on a single digitizer because of the need for high resolution pressure data over a length of the test. Two memories were used on each of four digitizers used to store thermocouple, germanium photodiode, and lithium niobate gauge data. A single memory was retained on the digitizer assigned to strain gauge data.

If under control of the internal clock, the sampling rate was constant during a test; if under the external clock, the sampling rate could be varied during a test. The digitizers and the programmable clocks were triggered by TTL level trigger pulses coming from LeCroy model TG8610B trigger generators. The trigger generators would receive trigger signals from the ignition signal or from a transducer and convert these signals into the TTL trigger pulse.

4.3 Backup DAASY system

The backup data acquisition system, the DAASY system, was limited to 40 data channels. The memory per channel was fixed at 4K, and the sampling rate was required to be constant during a test. The maximum sampling rate was somewhat higher than the CAMAC system, 80 kHz. It was run under the control of a separate Digital LSI 11/23 (later upgraded to LSI 11/73) computer. The DAASY system used a Tektronix 4010 graphics terminal for all terminal functions.

4.4 Tektronix 7612 digitizers

We made limited use of six data channels available using Tektronix 7612 transient digitizers. These devices included two

independent data channels, each with built-in amplifiers, programmable clocks, 8 bit resolution transient digitizers with sampling rates up to 200 Msamples/s, and 2K of memory per channel. The very fast sampling rates were of little value in flame acceleration studies, while the limited memory and limited resolution were problems. In contrast, the 7612s were the primary data acquisition system for detonation studies where the phenomena are faster and more predictable.

4.5 Computer language and programming

For various reasons, Tektronix's SPS BASIC was the programming language chosen for all the data acquisition systems, CAMAC, DAASY, and 7612s. The initial set of programs for arming the CAMAC devices, storing the data on hard disk, and obtaining plots of the data required inputing all parameters by keyboard each time the devices were used. The plots were of "raw data", i.e., digital level versus sample number. A second generation of programs was developed that would arm CAMAC devices using parameters from a setup file created days before the test. These programs permitted plots of "engineering data", i.e., quantities such as temperature or pressure versus time. To obtain pressure, temperature, etc., data on gauge sensitivity, amplifier gain, and signal offset were stored in a gauge file usually created before the test. See Section 5 for details of the generation of engineering units.

Two useful features of our programs deserve special mention. All our plotting routines permit creation of plots from a selected portion of a data array, as well as the entire array. This permitted detailed plots of the data in periods of interest. A second useful feature is the Graphics Input mode of the Tektronix 4010 terminal. A cross hair can be placed at a given location on a plot such as the flame time-of-arrival or a pressure peak, and the values of the coordinates at that point printed on the plot. This saved a great deal of time measuring the coordinates of the desired points.

At the start of this research, the DAASY system programs for data acquisition were not documented, were difficult to learn to use, and lacked many convenience features, such as the ability to plot a portion of a data array. During the course of the research, the DAASY programs were improved in convenience, but they were never documented or made "user friendly."

4.6 Disk storage

The data acquired by the CAMAC system was stored in a DSD 880 "Winchester" hard disk. Later this hard disk was replaced with two Digital RX02 hard disks of greater storage capacity.

Eventually, the hard disks became full. Archival storage of data was therefore done on 8-inch floppy disks. Two floppy disk copies of data were made. With the abandonment of the use of 8-inch floppy disks in newer systems, we are converting all our data storage to the newer 5-1/4 inch floppy disks. The DAASY system had no hard disk storage and relied solely on 8-inch floppy disks.

5. DATA PROCESSING

5.1 Introduction

This section discusses what was done with the data obtained in the FLAME tests to give the results shown in section 6. The first step was to convert "raw data" into "engineering variables." Raw data is in the form of an array of digitized levels. The digitized levels were converted to temperatures, pressures, voltages, etc., by the linear relation,

$$EV = (DL - DATUM)*[DS*GF/AG] + OFFSET, \qquad (5.1)$$

where EV = engineering value, pressure, temperature, etc.
DL = digital level in the data.
DATUM = digital level selected as datum.
DS = digitizer sensitivity in volts/level.
GF = gauge factor, e.g. kPa/volt, Kelvin/volt, etc.
AG = amplifier gain.
OFFSET = engineering value at the datum.

The datum was obtained by averaging a given number of the first data points, typically the first 75 points. Using the first test data points to give a datum, rather than using pretest values, minimizes the problem of zero drift of transducers. Averaging a significant number of points to obtain the datum was used to minimize error due to noise in the signal. The digitizer sensitivity of the BiRa 509 transient digitizers was fixed at 800 levels/volt throughout the testing period. The response of all the transducers used could be expressed by a linear sensitivity, the gauge factor, GF. For pressure measurements, the offset was set at zero. Hence the results are in terms of "gauge pressure." Absolute pressure can be obtained by adding the local barometric pressure to the gauge pressure. Typically barometric pressure was about 84 kPa (12.2 psia). Values of ambient pressure, temperature and humidity were recorded for the tests. Because there was no cold junction compensation for the thermocouples, and accurate values of temperature were not needed for time-of-arrival measurement, an approximate datum was used in the data reduction. Typically the datums used were 25°C in warmer weather, and 10°C in cold weather. Hence the absolute value of temperature measured could be off by ± 5°C because of errors in the datum. See section 3 for a discussion of other temperature measurement errors. The data from the germanium diodes and the lithium-niobate gauges was expressed in volts.

The sample number of the data was converted into time relative to the ignition signal as zero time. For a constant sample rate and post-trigger mode,

$$\text{Time} = (\text{Sample Number} - 1)/\text{Sampling Frequency} \qquad (5.2)$$

For constant sampling frequency in the pretrigger mode,

$$\text{Time} = \frac{(\text{Sample Number} - \text{Pretrigger points})}{\text{Sampling Frequency}} \qquad (5.3)$$

The uncertainty in the time a sample was taken relative to the ignition trigger could be up to one sample period.

In the case where two or three sampling frequencies were used, the above equations were used for the period in which the first frequency was operative, and for the second frequency,

$$\text{Time} = [\text{Time at end of first frequency period}] + \frac{[\text{Sample number} - \text{Freq. 1 samples}]}{\text{Sampling Frequency 2}} , \qquad (5.4)$$

and similarly for a third frequency.

5.2 Combustion front time-of-arrival

The main tool for determining the displacement of the combustion front as a function of time, and the corresponding velocities and accelerations, are the time-of-arrival data from thermocouples mounted on vertical rakes along the channel midplane. The combustion front time-of-arrival is therefore known at a discrete number of elevations (7 to 12) and axial positions. In cases where data was missing at one of these elevations for a given thermocouple rake, time-of-arrival data from adjacent elevations of that rake were linearly interpolated.

The time-of-arrival of the combustion fronts at axial positions other than those occupied by the thermocouple rakes, was estimated by linearly interpolating the thermocouple data for each thermocouple elevation. A plot of time-of-arrival versus axial distance for each elevation we call "combustion front trajectories." Figure 5.1a shows such combustion front trajectories for test F-14. Thermocouple data was supplemented with data from other transducers in tracking the retonation wave. The combustion front position as a function of time, isochrones, were estimated by cross plotting the axial positions of these curves at a given set of times. Combustion front profiles for the test F-14 are shown in Figure 5.1b. The horizontal speed of propagation and acceleration of the combustion front are estimated by finite differences of the thermocouple time-of-arrival data at a given elevation.

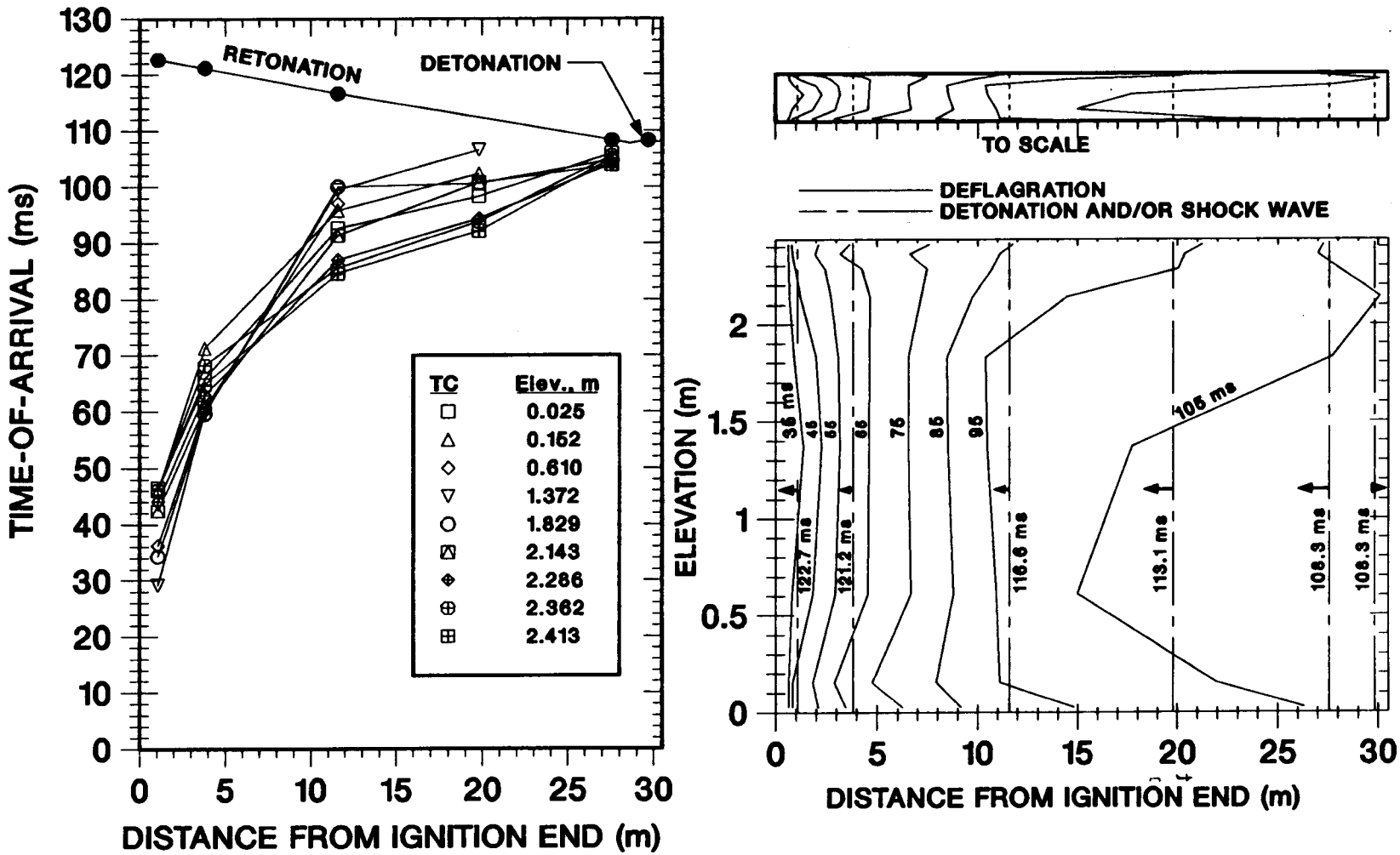

Figure 5.1. Combustion Front Trajectories and Profiles. Test F-14. 30.0% H_2. No top venting. No obstacles.

To obtain a measure of the propagation speed of the flame averaged over the channel cross section, we define the equivalent planar flame speed as the volumetric burning rate divided by the channel cross sectional area,

$$v_{eq} = \frac{1}{A_c} \frac{dV}{dt} , \tag{5.5}$$

where v_{eq} is the equivalent planar flame speed, A_c the channel cross sectional area, and V the volume of burned gas in the channel. Since we used time-of-arrival data for the flame only on the channel midplane, we estimate v_{eq} by a finite difference approximation to the following equation.

$$v_{eq} \simeq \frac{1}{h} \frac{dA}{dt} , \tag{5.6}$$

where h is the channel height and A is the burned gas area on the midplane. In general equation 5.6 will not give the same result as equation 5.5. However, in some cases it will give the same results, and in many cases will give a reasonable approximation to the results of equation 5.5. If the flame shape translates along the channel axis with constant speed, the results of both equations will be identical. If the flame front speed parallel to the channel length is a function of time and elevation, y, but not of the transverse direction, z, i.e., v= v(y,t), then the results of both equations will be identical. However, if there is a change in flame front shape in the z direction as the flame propagates down the channel, then the results of equation 5.6 will not be the same as the results of equation 5.5.

The procedure used to compute the equivalent planar flame speeds is a finite difference approximation to equation 5.6. The explanation is presented in graphical terms as shown in Figure 5.2, although the procedure is performed numerically. At time t, the combustion front is approximated by linear interpolation of estimates at the thermocouple elevations. Let the area on the midplane behind the combustion front be A(t). The small regions below the lowest thermocouple and above the highest thermocouple are excluded. The corresponding mean axial position of the combustion front,

$$X(t) = A(t)/h, \tag{5.7}$$

where h is the height of the channel, minus the distance below the lowest thermocouple and above the highest thermocouple. At a later time $(t + \Delta t)$, the area behind the combustion front is $A(t+\Delta t)$, and the mean axial position of the front is $X(t+\Delta t)$. The equivalent planar flame speed is then estimated by

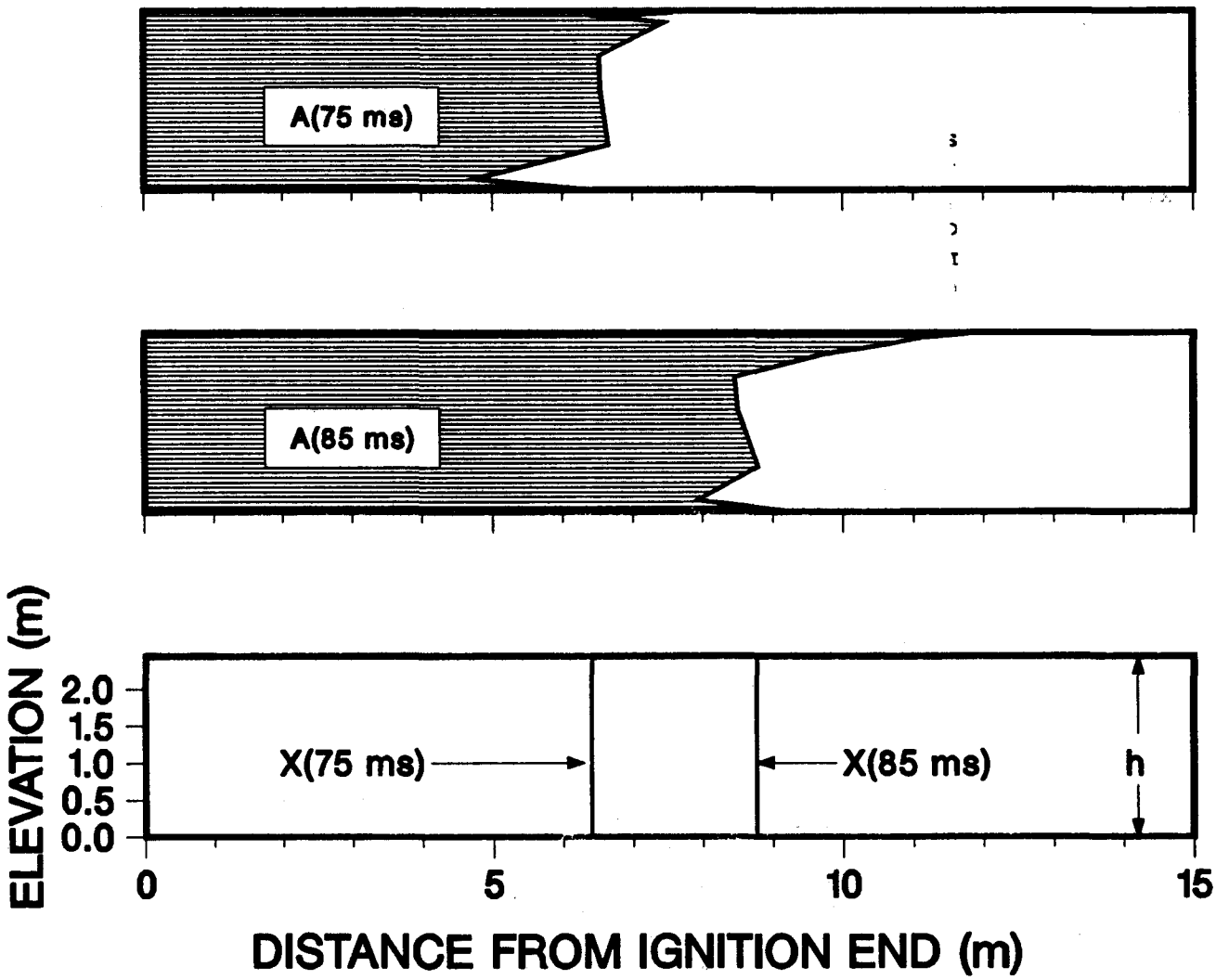

V_{eq} = [A(85 ms) - A(75 ms)]/[h*10 ms]

= [X(85 ms) - X(75 ms)]/[10 ms]

X(85 ms) = A(85 ms)/h; X(75 ms) = A(75 ms)/h

V_{eq} is the equivalent planar flame speed at

Time = 80 ms, Position = [X(85 ms) + X(75 ms)]/2

Figure 5.2. Graphical Illustration of Equivalent Planar Flame Speed

$$v_{eq} = [A(t+\Delta t) - A(t)]/(h\Delta t) = [X(t+\Delta t) - X(t)]/\Delta t \quad (5.8)$$

The value of equivalent planar flame speed thus computed is assumed to correspond to a mean axial position between X(t) and X(t+Δt), and a mean time between t and t+Δt. The graphical illustration in Figure 5.2 was taken from test F-14. For the example shown, t = 75 ms, Δt = 10 ms, A(t) is the shaded area in the top part of the figure, A(t+Δt) is the shaded area in the middle section, and X(t) and X(t+Δt) are shown in the lower section of the figure.

For tests in which there was transition to detonation, the time-of-arrival of the detonation/shock waves can be followed with the response of the pressure transducers, thermocouples, germanium diodes, and Lithium Niobate gauges. Within the spatial and temporal resolution of our data acquisition, detonations and shock waves appear to be normal to the axis of the channel, independent of elevation or width across the channel.

5.3 Pressure Measurement

The major problem with analyzing the pressure measurements is to determine which responses are valid, and which are artifacts of noise and/or transducer failure. Because there is always a period of zero gauge pressure at the start of a test, the "noisiness" of a pressure transducers signal is evident at that period. The noise may be random or consist of periodic spikes, for example, Figure 5.3 shows a noisy signal with spikes. To help judge which pressure signals were valid, the digitized pressure data was taken from site 9920 on floppy disks, and installed on the Area 5 VAX computer. For a given test, plots were made of all the pressure transducer responses using the same time interval and pressure range. This permitted overlaying the data. Although in most cases, the failure of a transducer was clear from the peculiar response, there were some cases which were not obvious. Methods of judging invalid results were developed. For example, there are several tests in which there was a slow pressure buildup followed by a large pressure spike. The peak value of the spike given by different transducers often varied considerably. Were these different values representative of large variations in peak pressure at different locations, or were they in error? If, when overlayed, the response of a transducer to the slow buildup was consistent with the results of other transducers, this was taken as an indication that the response of the transducer probably was valid. If the response of one transducer to the slow buildup was inconsistent with the results of several other transducers, this was taken as an indication that the transducer response was probably invalid, and it was discarded. All the pressure histories shown in section 6 were judged valid.

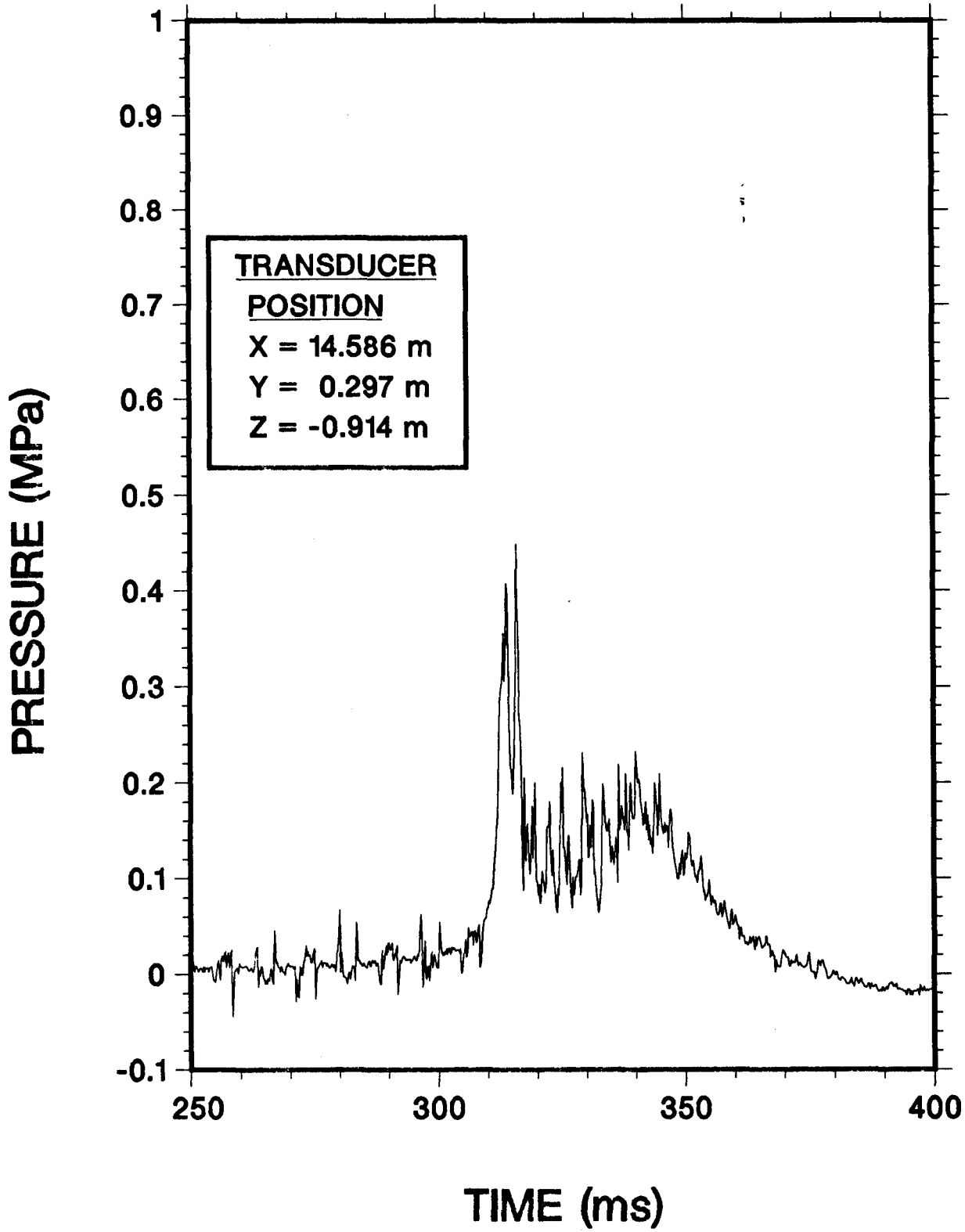

Figure 5.3. Test F-22, 15% H_2

6. EXPERIMENTAL RESULTS

6.1. Introduction

A summary of the tests is given in Table 6.1. Pressure is given to two significant figures. In the following sections, the results of tests are considered in groups with similar experimental conditions. We begin in section 6.2 with tests F-7 to F-14, tests with no obstacles in the channel and no transverse venting.

TABLE 6.1
Summary of the Test Parameters and Some Test Results

Test No. F-	Top Vent. %	H_2 Mole Fraction, %	Peak Overpress., kPa	Peak Equivalent Planar Flame Speed, m/s	Comments
		TESTS WITH NO OBSTACLES			
1	50	12.4	a	7	
2	50	19.7	2.8	54	
3	50	20.8	a	65	
4	50	28.0	20	126	
5	50	12.6	0.9	4(12)[b]	Top sheet restraint.
6	50	15.5	3.4	19	
7	0	12.0	1.2	16	
8	0	18.4	26	170	
9	0	6.9	a	1.2[c]	Limited burn.
10	0	12.3	2.6	17	
11	0	12.9	4.5	30	
12	0	24.7	95/1100[d,e]	374	DDT near exit.
13	0	12.0			All data lost.
14	0	30.0	250/2100[d,e]	932[f]	DDT near exit.
15	13	15.4	3.1	50	
16	13	17.6	10	75	
17	13	14.9			Some data lost.
18	13	18.1	36	136	
19	13	24.8	65/850[d]	160[g]	DDT at 1/3 length.
20	13	20.7	78	483	
		TESTS WITH OBSTACLES			
21	0	10-15%	650	580	No mixing fans
22	0	15.0	3100	700	DDT near exit
23	0	14.5	1200	540	
24	50	15.5	a	46	
25	50	19.7	1500	890	DDT near exit
26	50	28.5	2000	1860	Box obstacles, DDT
27	50	13.1	9	15	
28	50	14.9	9	33.4	
29	50	18.5	23	130	

DDT = Deflagration-to-Detonation Transition
a) Indicates pressure signal within the noise level.
b) Plastic top sheet restraint gave faster value early in test.
c) Indicates horizontal propagation velocity of thin layer below roof.
d) First pressure value refers to deflagration, the second to detonation.
e) Based on dynamic pressure transducers, somewhat uncertain.
f) Peak planar equivalent flame speed is highly uncertain because it was increasing rapidly near the channel exit.
g) Peak planar eq. flame speed highly uncertain due to early DDT.

6.2 Tests With No Obstacles and No Top Venting

Tests F-7 to F-14 were carried out with no top venting. The top of the channel was completely closed with steel plates. There were no obstacles in the channel other than instrumentation and mixing fans. Test F-9 was different from all the others and will be considered separately. In this section we will consider several of these tests in order of increasing hydrogen concentration, F-10, F-8, F-12, and F-14, with hydrogen mole fractions of 12.3%, 18.4%, 21.7% and 30.0%, respectively.

The combustion front trajectories for test F-10, Figure 6.1, were generated by linear interpolation of the thermocouple time-of-arrival data on the channel midplane. The corresponding combustion front profiles shown in Figure 6.1b are cross plots of the data from Figure 6.1a. They represent the flame front profiles on the midplane from 0.60 seconds after ignition to 2.60 seconds in equal time increments of 0.25 seconds. In the lower plot of Figure 6.1b the vertical scale is exaggerated compared to the axial length scale for clarity. In the smaller upper plot of Figure 6.1b, marked "TO SCALE", the two length scales are in proportion. We will use similar combustion front trajectory and combustion front profile figures in discussing many of the other tests. The slight concave downward curvature of the lines in Figure 6.1a and the small increase in distance between the combustion front profiles in Figure 6.1b indicate some flame acceleration was occurring, but it was not dramatic. The peak propagation velocity observed was 19.3 m/s, where propagation velocity is taken as the distance between two thermocouple rakes divided by the difference in time-of-arrival for thermocouples of the same elevation. The deflagration front was initially convex relative to the unburned gas. It gradually transitioned into an unsymmetrical shape concave in the lower half of the channel, inclined forward in the middle section, and nearly vertical near the top of the channel. This was a partial conversion to the "tulip" shape seen in many small-scale experiments of flame propagation in tubes. [63,64]

Pressure histories from a transducer near the ignition end and near the exit end in test F-10 are shown in Figure 6.2. These were typical of the ten pressure transducer records for this test. All pressure histories shown in this report are relative to ambient pressure, typically 84 kPa (12.2 psi). To the extent practical, all pressure history plots for a given test use the same horizontal and vertical scales so that comparisons are made easier. The Cartesian coordinates of the transducers are noted in the figures. The X coordinate is the distance from the ignition end; the Y coordinate the distance upward from the floor; the Z coordinate the distance from the channel midplane. See the Appendix for the figure which illustrates the coordinate

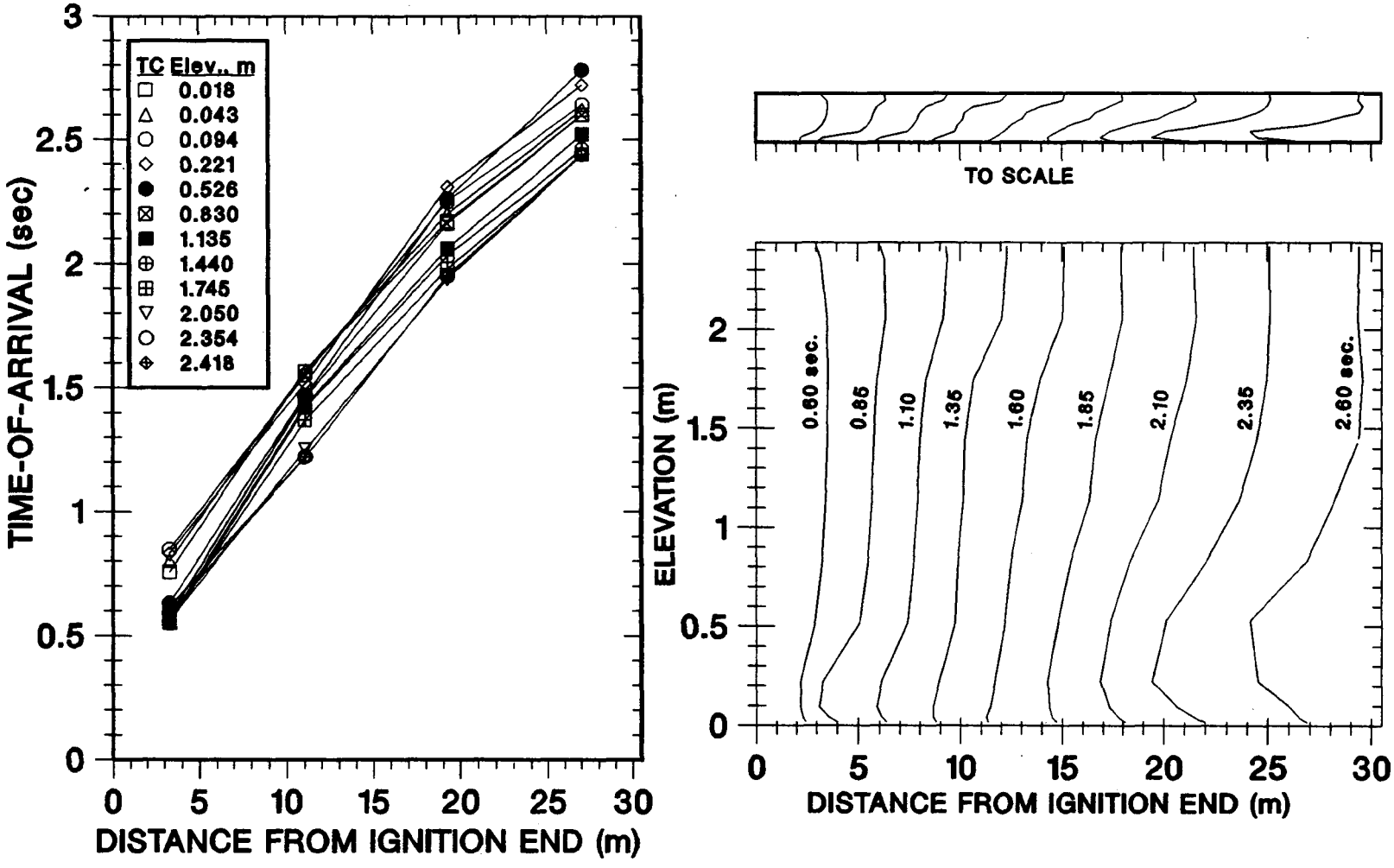

a. b.

Figure 6.1. Test F-10, 12.3% H_2

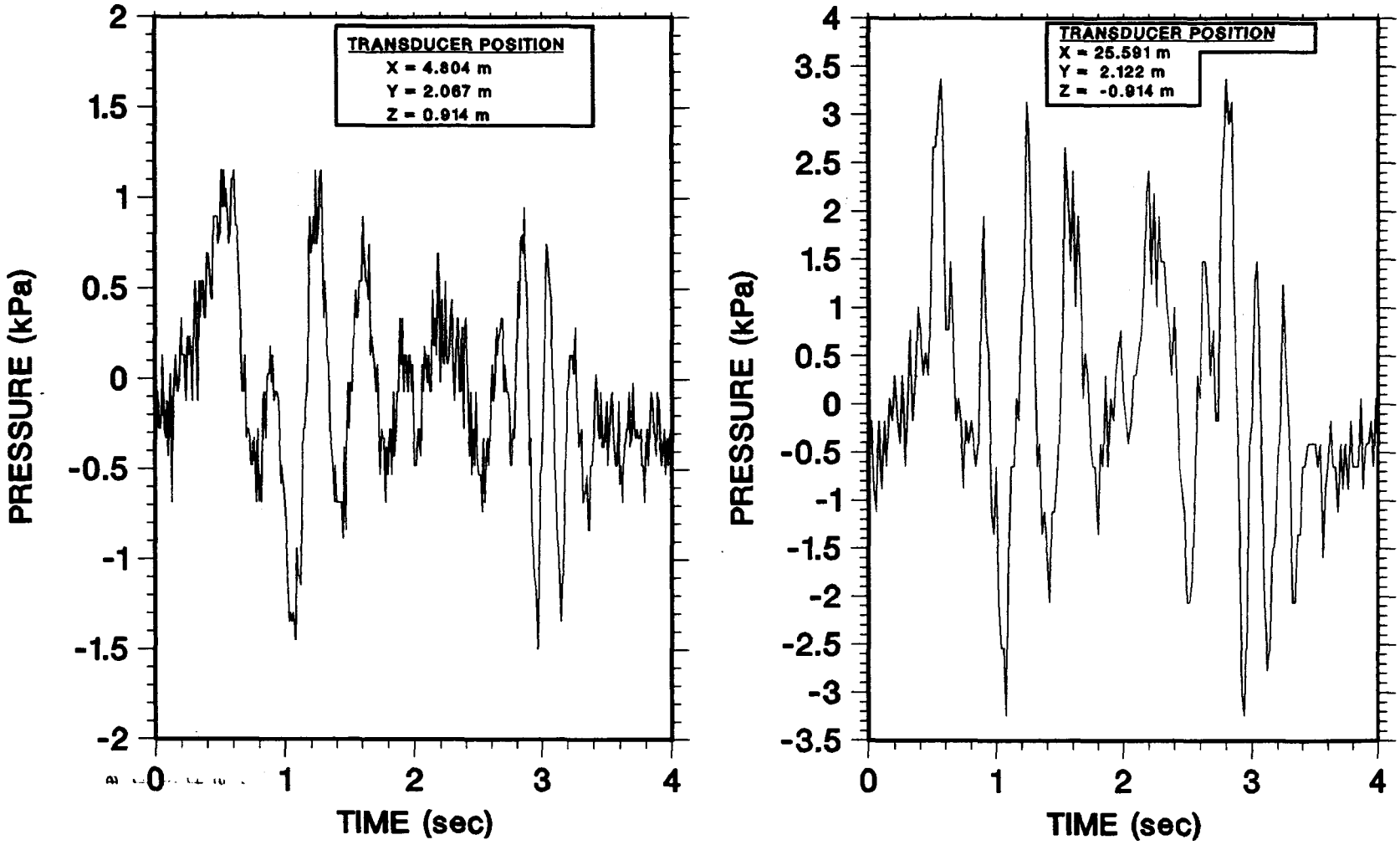

a. b.

Figure 6.2. Test F-10, 12.3% H_2

system, and for the table of pressure transducer locations. The factors which could influence the accuracy of the pressure measurements are discussed in Section 3.

The pressure histories in Figure 6.2 shows oscillations around ambient pressure of nearly equal positive and negative amplitudes. The pressures peaks were roughly 1.4 kPa (0.2 psi) near the ignition end and about 3.4 kPa (0.5 psi) near the exit end of the channel. Up to the time that the deflagration exited the channel, the period of the oscillations was about 300 ms. Just after the deflagration left the channel, at about 2.7 seconds, there was a renewed burst of oscillations with about a 200 ms period. The oscillations faded away after about 3.4 seconds. The acoustic wave travel time down the length of the channel and back was about 200 ms traveling through ambient temperature gas, and less traveling through higher temperature combustion products. Hence the axial acoustic wave travel times seem a bit less than the observed pressure oscillation periods.

In test F-8 with 18.4% hydrogen, compared to test F-10 with 12.3% hydrogen, the deflagration speeds were much higher, as shown in Figure 6.3, and the peak pressures were much higher, as shown in Figure 6.4. There was clear evidence of flame acceleration. The peak deflagration propagation speed observed was 205 m/s, and the peak equivalent planar flame speed was 170 m/s. The initially convex combustion front became inclined forward and slightly concave. The two pressure histories shown in Figure 6.4 are typical. There was one oscillation with a much larger positive than negative phase. The amplitude of the oscillations did not change much along the length of the channel.

In test F-12 with 24.7% hydrogen there was a transition to detonation near the exit. Figure 6.5 shows considerable flame acceleration. The highest propagation speed observed was 508 m/s. As in tests with lower hydrogen concentrations, the initially convex flame front gradually became somewhat concave. There was only a slight forward inclination of the front. Four pressure transducer histories for this test are shown in Figure 6.6. All the pressure histories show the same pattern, a gradual pressure rise out to about 130 ms, a second pressure rise and slight fall, and then a pressure spike. The second pressure rise occurred during the period of most rapid flame acceleration. That the spike was due to a retonation wave moving toward the ignition end is confirmed by the agreement of time-of-arrival data from pressure transducers, germanium photodiodes, thermocouples, and lithium niobate gauges. Indeed, the reflection of the retonation wave off the ignition end wall is clearly visible in Figure 6.6 and can be detected in many of the other pressure histories. The peak pressures reported were measured using Kistler piezoelectric gauges. They reported peak pressures higher than those reported by the Kulite gauges.

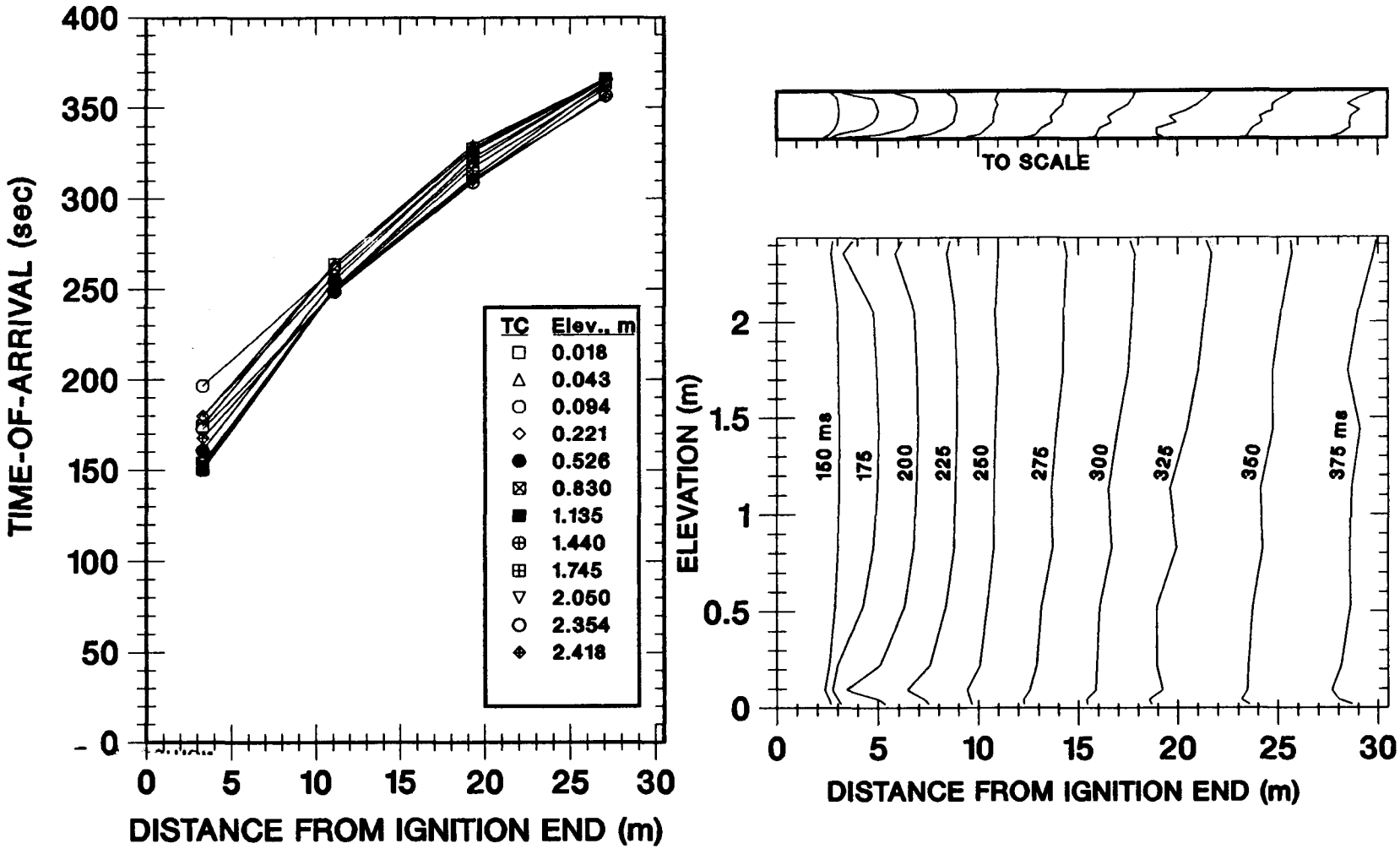

Figure 6.3. Test F-8, 18.4% H_2

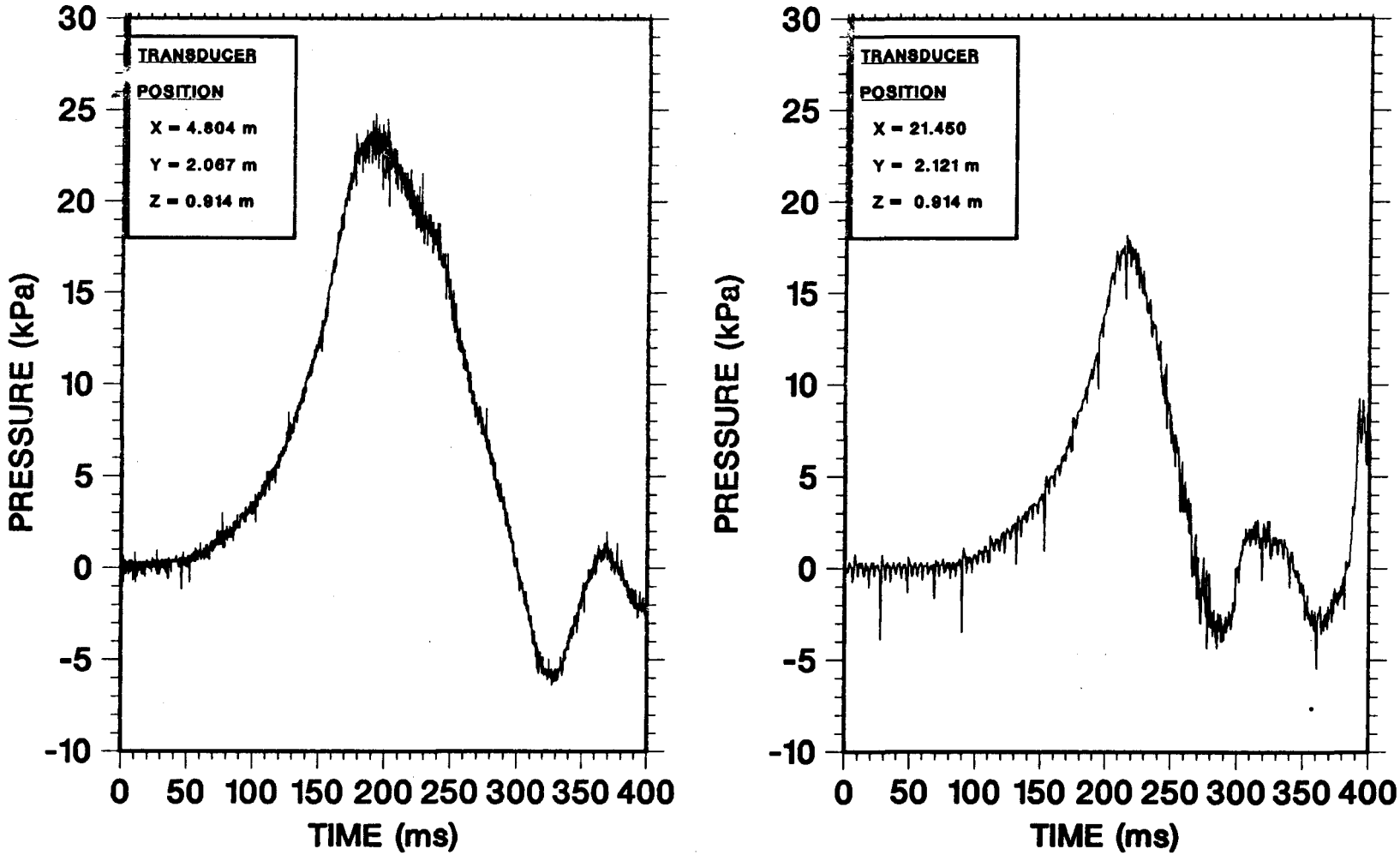

Figure 6.4. Test F-8, 18.4% H_2

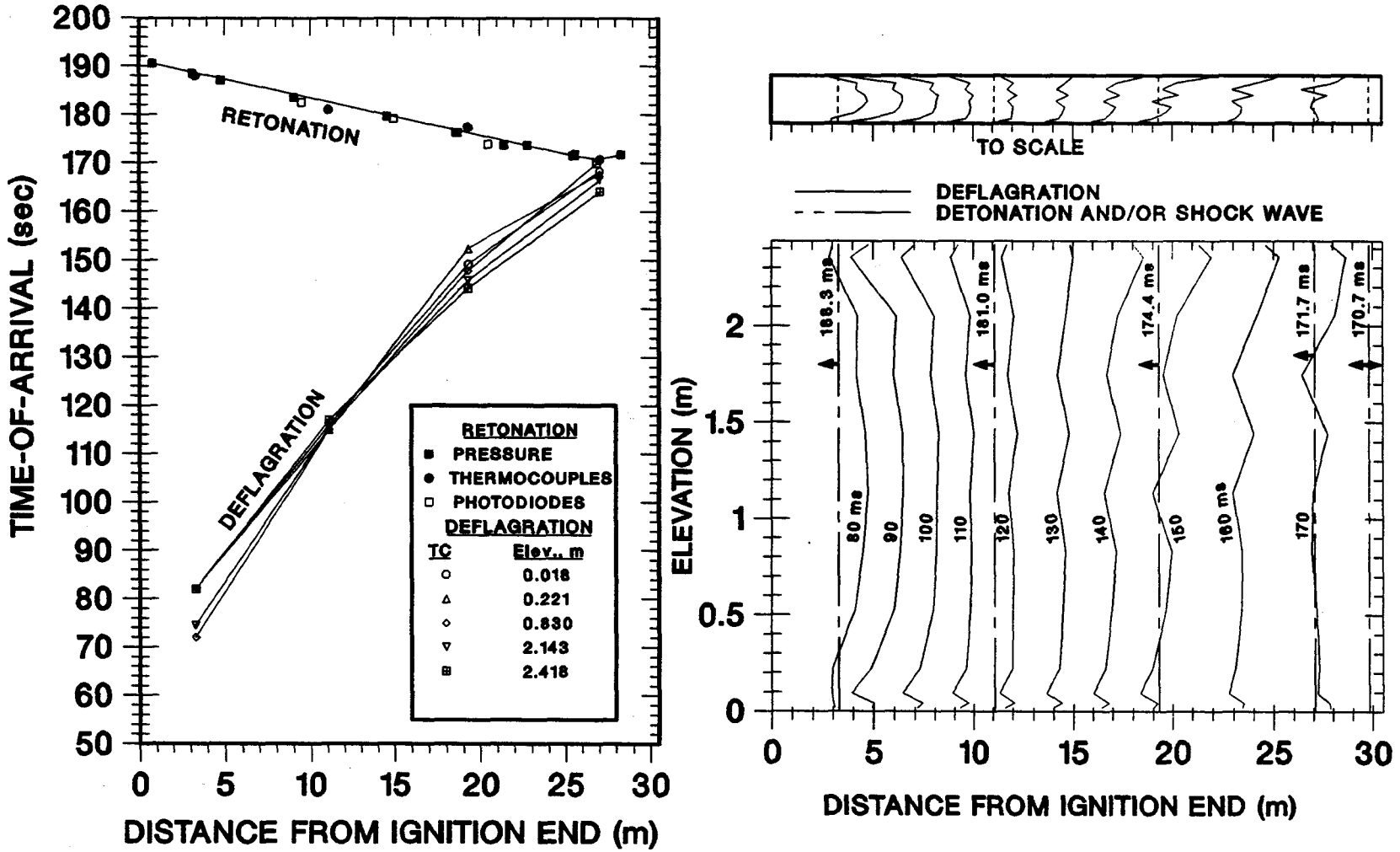

Figure 6.5. Test F-12, 24.7% H_2

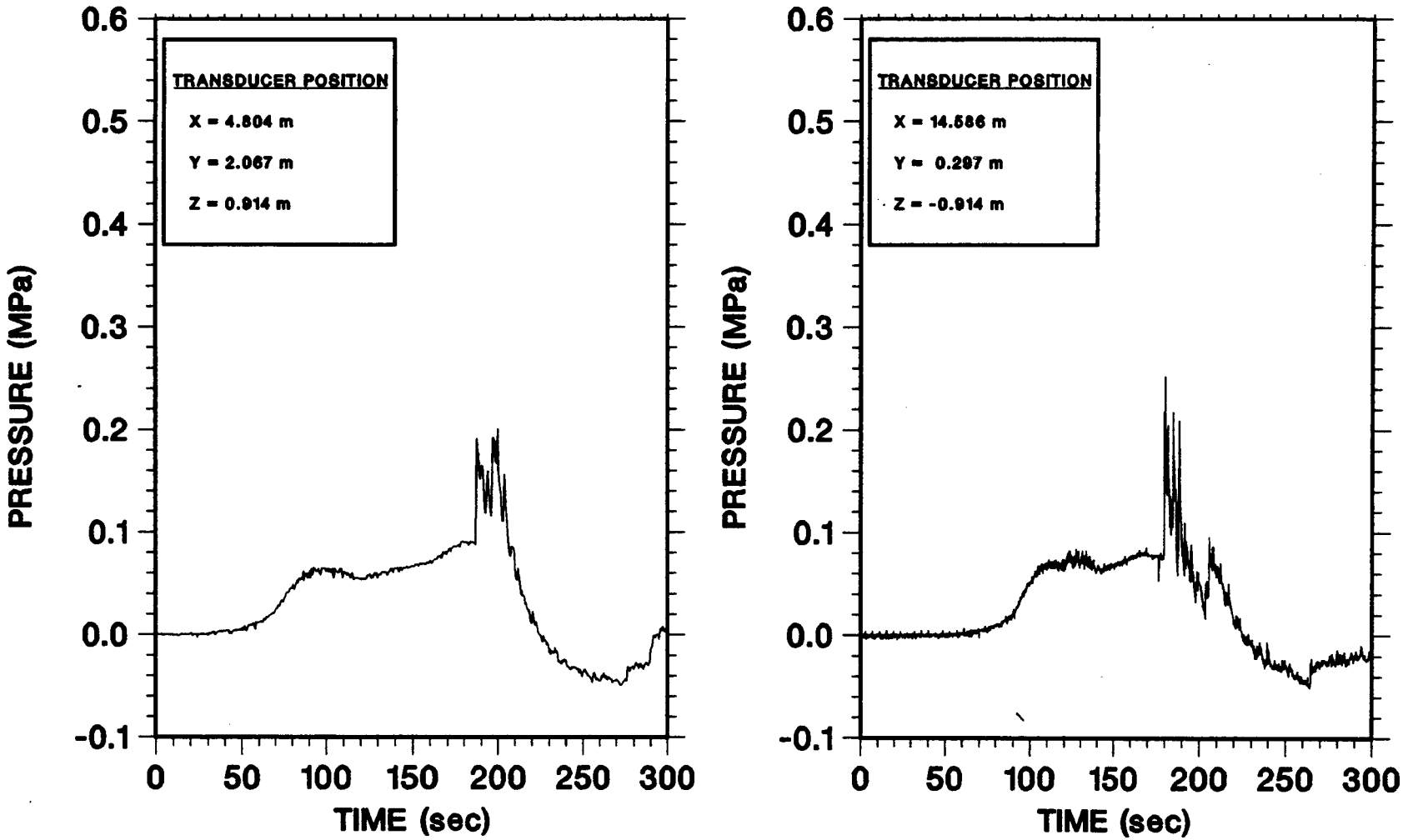

Figure 6.6. Test F-12, 24.7% H_2

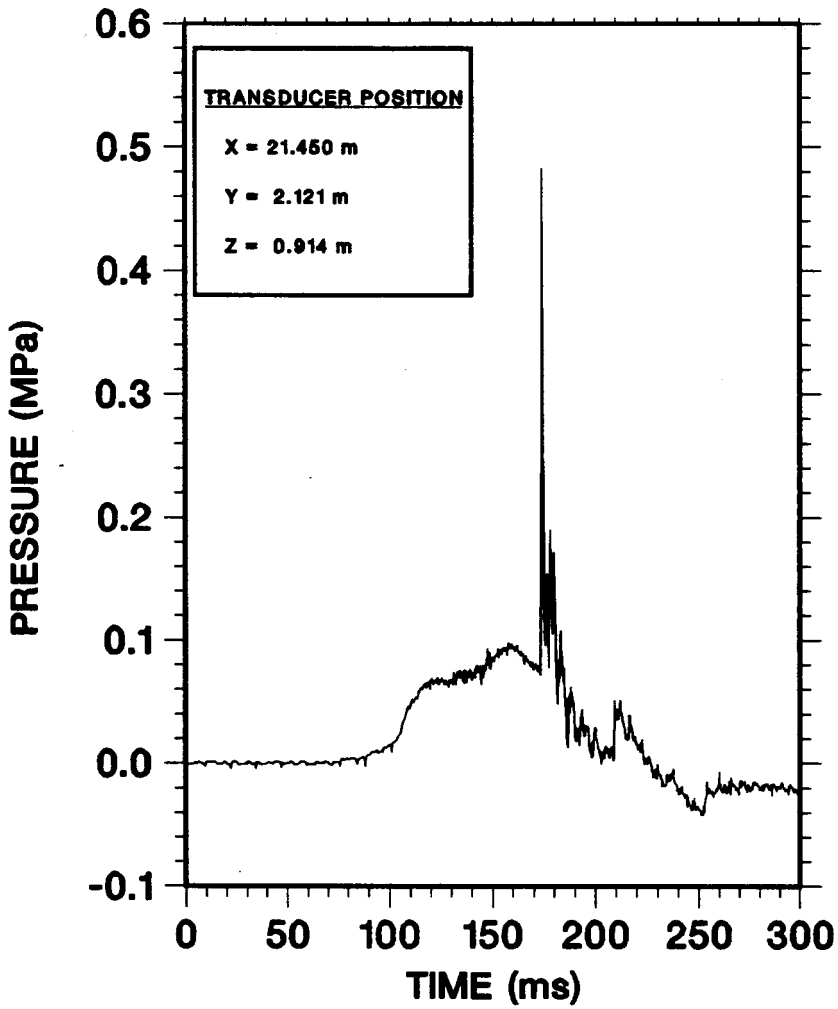

c.

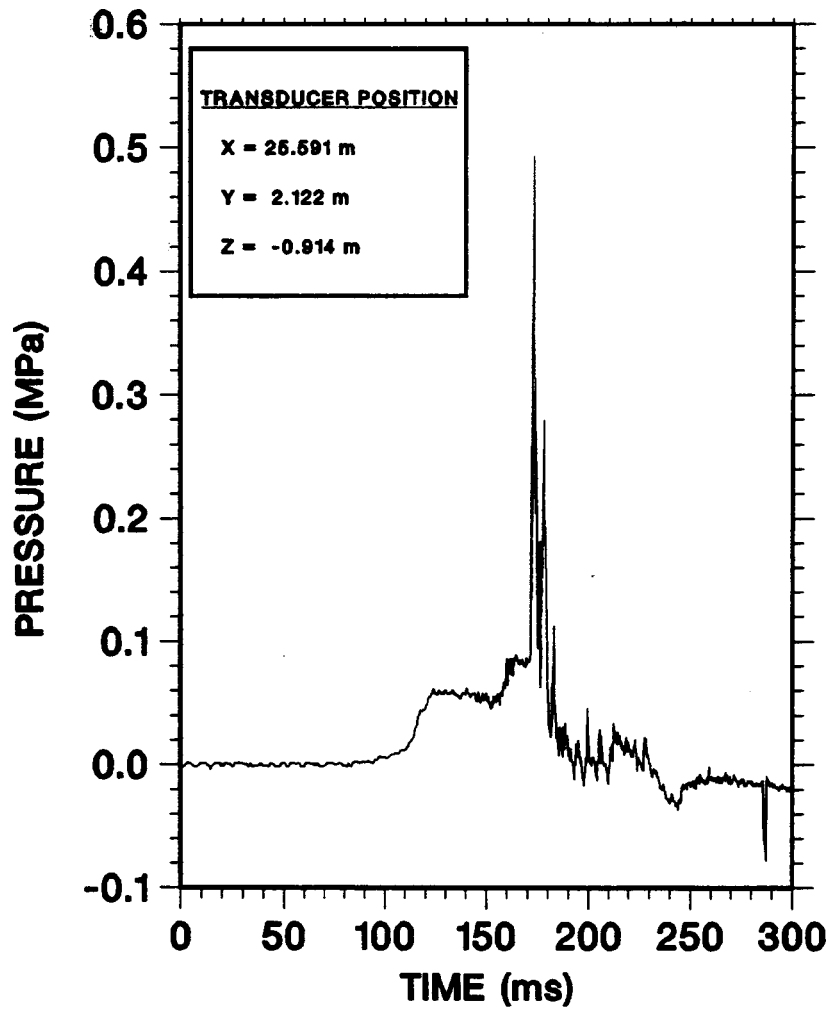

d.

Figure 6.6. (Continued)

Of great interest in this test was the location and condition at the transition to detonation. Unfortunately, the instrumentation was not set up to carefully investigate conditions near the exit, and the exact location of the transition is unknown. The transition may have been triggered by the last thermocouple rake or the mixing fan near the exit.

In test F-14 with 30.0% hydrogen none of the Kulite pressure transducers functioned. Only piezoelectric pressure transducers were operating.

The thermocouple results shown in Figure 6.7 show more pronounced flame acceleration than in test F-12. The deflagration speeds just prior to transition were large. The initially convex flame front became deeply concave. However, the location of the transition was also near the exit end of the channel as in test F-12. High-speed cinematography shows the detonation leaving the channel.

A comparison of equivalent planar flame speed versus axial position in tests F-7 to F-14 is shown in Figure 6.8. The equivalent planar flame speed was defined in Section 5. For lean mixtures with hydrogen mole fractions around 12%, the speeds are low and do not increase significantly with increasing axial distance. Flame acceleration is evident in the three tests with hydrogen mole fractions of from 18% to 30%.

In summary, for tests with no obstacles and no top venting:

1. The flame speed and peak pressure increased with increasing hydrogen concentration.

2. Flame acceleration is evident for hydrogen mole fractions of 18% and above, but not at 12%.

3. DDT first occurred at hydrogen mole fractions between 18.4 and 24.7%, near the exit.

4. The initially convex flame shape became slightly-to-strongly concave.

6.3 Tests With No Top Venting and Obstacles

It should be remembered that all the obstacle tests but one were conducted with a single obstacle configuration, simple baffles on the side walls with 33% blockage ratio. Changes in obstacle size, shape, spacing, and blockage ratio might alter the results and conclusions we draw from our obstacle tests.

The presence of obstacles dramatically increased the flame speeds, overpressures, and probability of DDT for tests

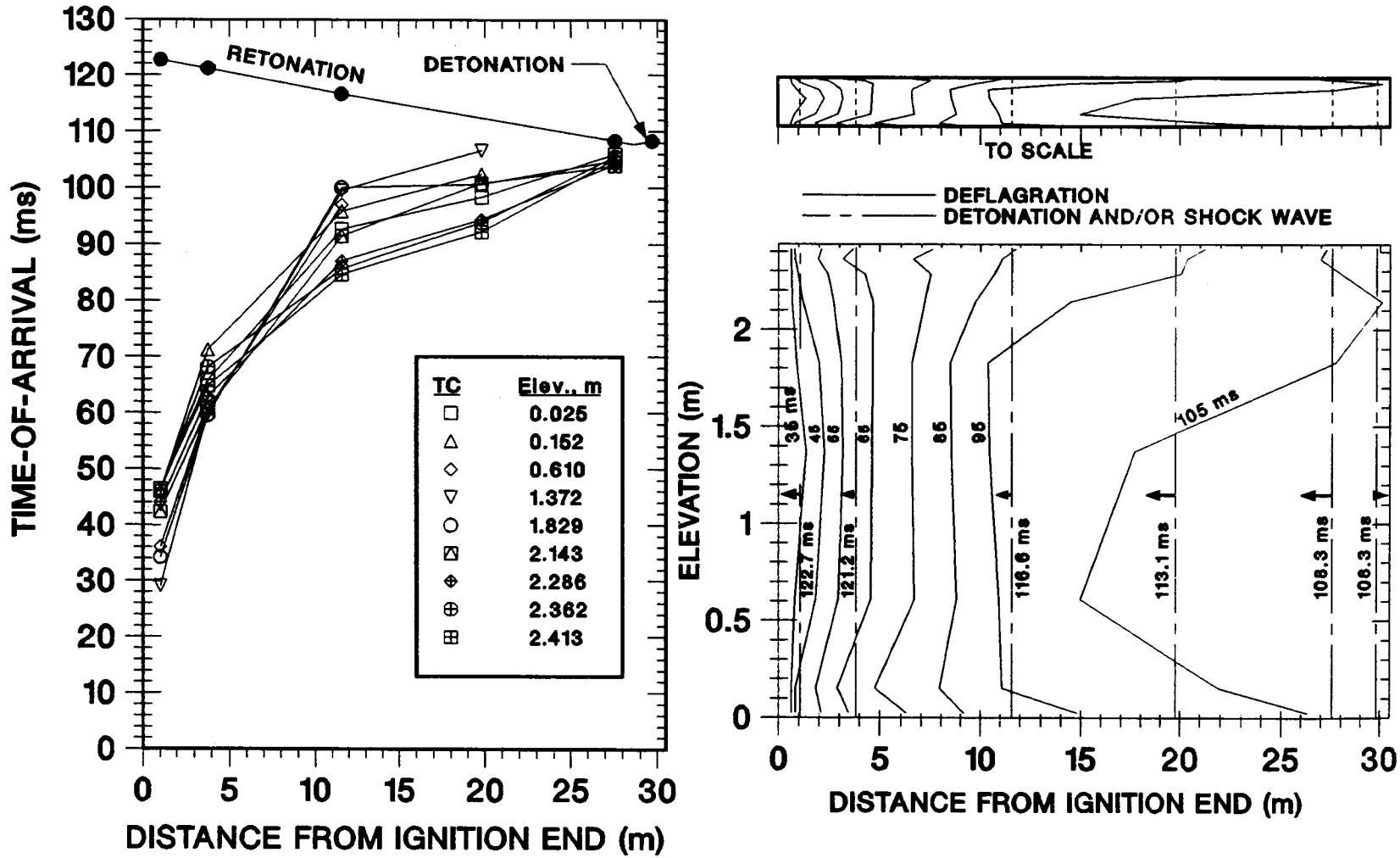

Figure 6.7. Test F-14, 30.0% H_2

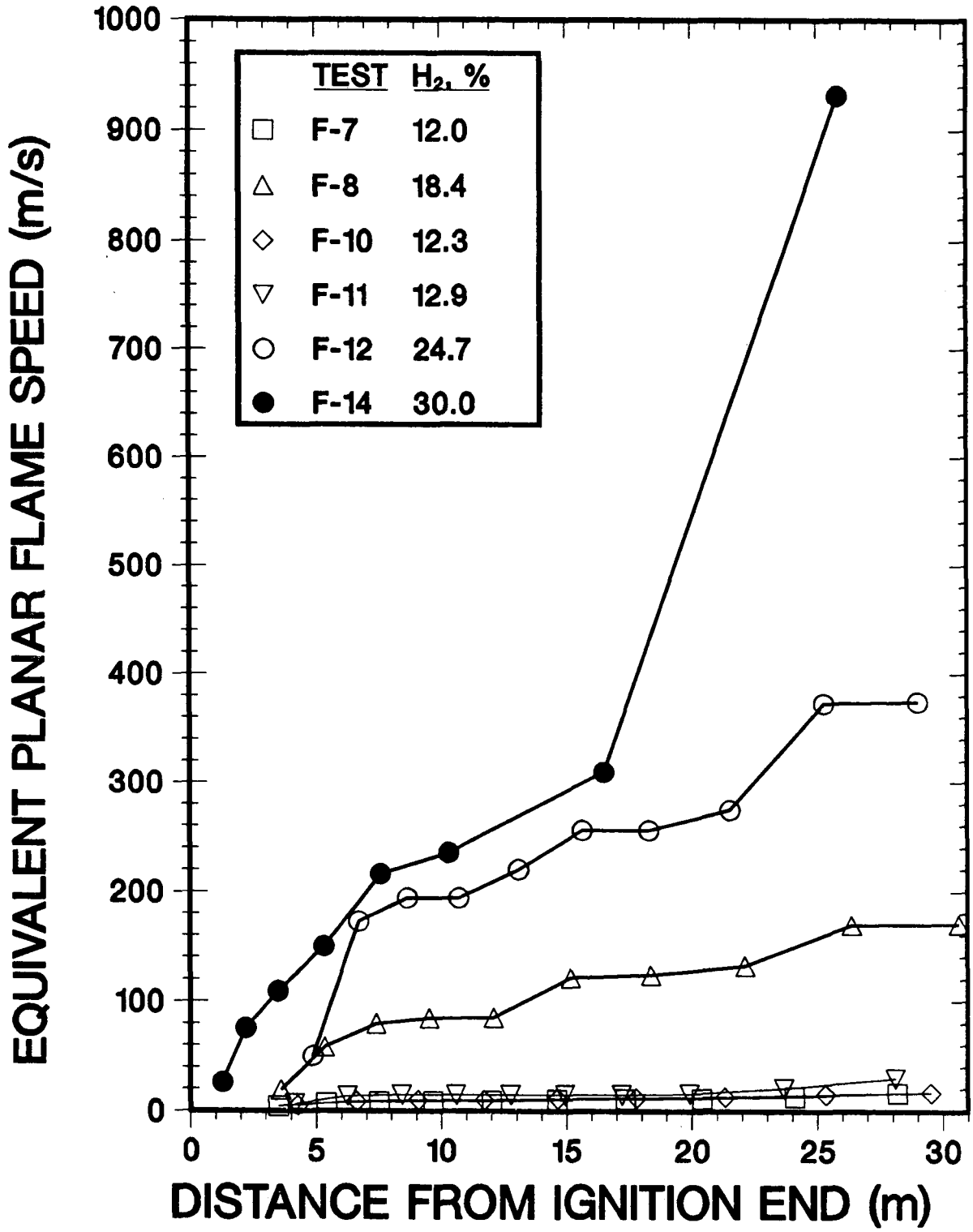

Figure 6.8. Comparison of Flame Speeds for Tests With No Top Venting and No Obstacles

with comparable hydrogen mole fractions. This section discusses the results of tests with obstacles and no top venting, tests F-21 to F-23. These obstacle tests used planar baffles attached to the side walls with a blockage ratio of 33%, as previously shown in Figure 2.3. We will present evidence that a DDT did occur in test F-22 with 15.0% hydrogen. To the knowledge of the authors, 15% hydrogen mole fraction is the leanest hydrogen-air mixture for which a DDT has been reported. Peraldi, Knystaustas and Lee [65] did observe DDT at about 16% hydrogen in a 30-cm-diameter tube with obstacles for flame acceleration and a large length/diameter ratio. The evidence for DDT in test F-22 is not as convincing as that for DDTs in tests with higher hydrogen concentrations. For test F-23 with 14.5% hydrogen, the evidence is that a DDT did not occur. A difference of 0.5% hydrogen mole fraction is within the uncertainty of the hydrogen mole fraction measurement. Nevertheless, whether we have bracketed the minimum hydrogen concentration for DDT in this geometry, or if the results indicate the stoichastic nature of DDT at the minimum hydrogen mole fraction boundary, we have found the boundary for this geometry. In test F-21, the mixing fans failed to operate. Stratification of hydrogen was observed.

The combustion front trajectories and combustion front profiles for test F-22 are shown in Figure 6.9. The large curvature of the lines in Figure 6.9, and the large increase in spacing between the combustion front profiles in Figure 6.9, illustrate the large flame acceleration produced by the presence of obstacles. The combustion front trajectories indicate two regions, the first ten meters and the last twenty meters. In approximately the first 10 meters, initially convex deflagration front takes 300 ms to accelerate to a planar front traveling at about 760 m/s. The planar front continues to move at this speed for the last 20 meters of the channel. This speed corresponds to choked conditions in the burned gas. The deflagration is moving at a speed near the lower Chapman-Jouguet point relative to the unburned gas ahead of it. In one-dimensional flow, this is the fastest speed a deflagration can propagate.

Four representative pressure histories for Test F-22 are shown in Figure 6.10. Near the ignition end, Figure 6.10, the pressure rise is gradual. Although there are numerous small pressure spikes, the peak pressure is small, 0.22 MPa (32 psi). Further from the ignition end, a dominant pressure spike develops that becomes large in magnitude and more abrupt in onset. Near the exit, Figure 6.10, the spike has a peak of 3.12 MPa (452 psi). In Figure. 6.11, the peak pressures indicated by the pressure transducers in tests F-22 and F-23 are plotted as a function of distance from the ignition end. The reader is cautioned that the accuracy of individual peak pressure values can be significantly in error due to noise and lack of temporal resolution. However, the trend shown should be correct. The

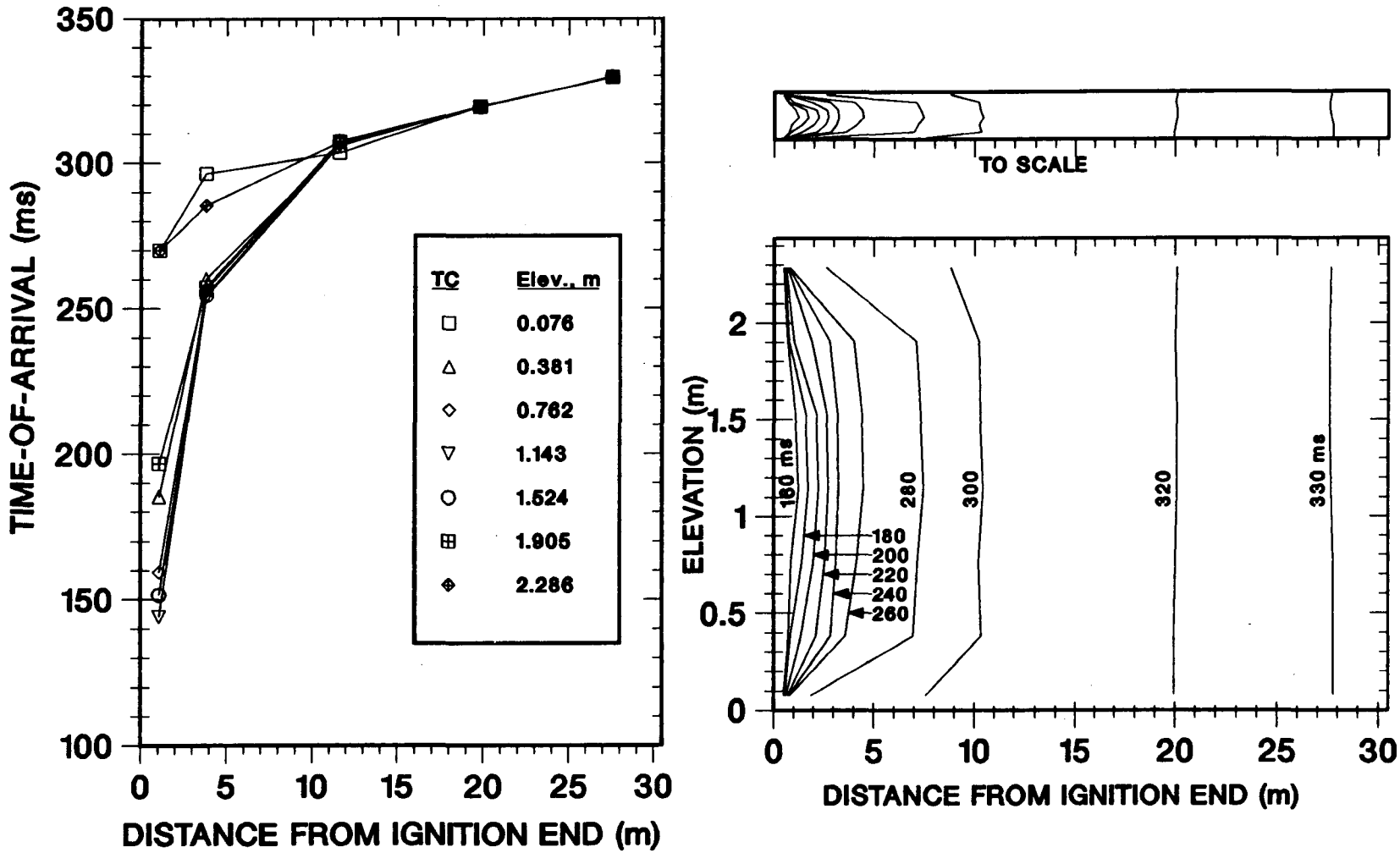

Figure 6.9. Test F-22, 15.0% H_2

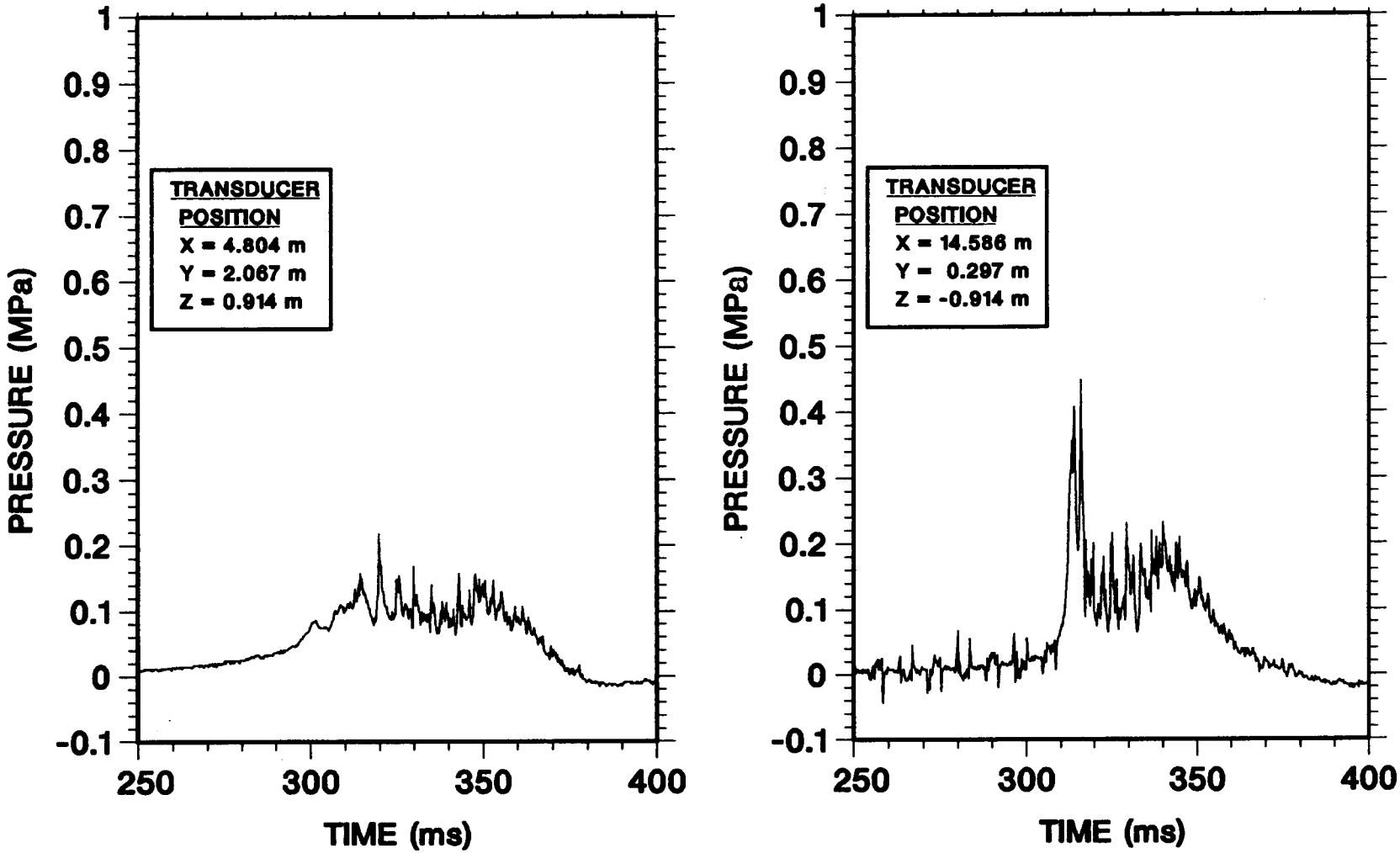

Figure 6.10. Test F-22, 15.0% H_2

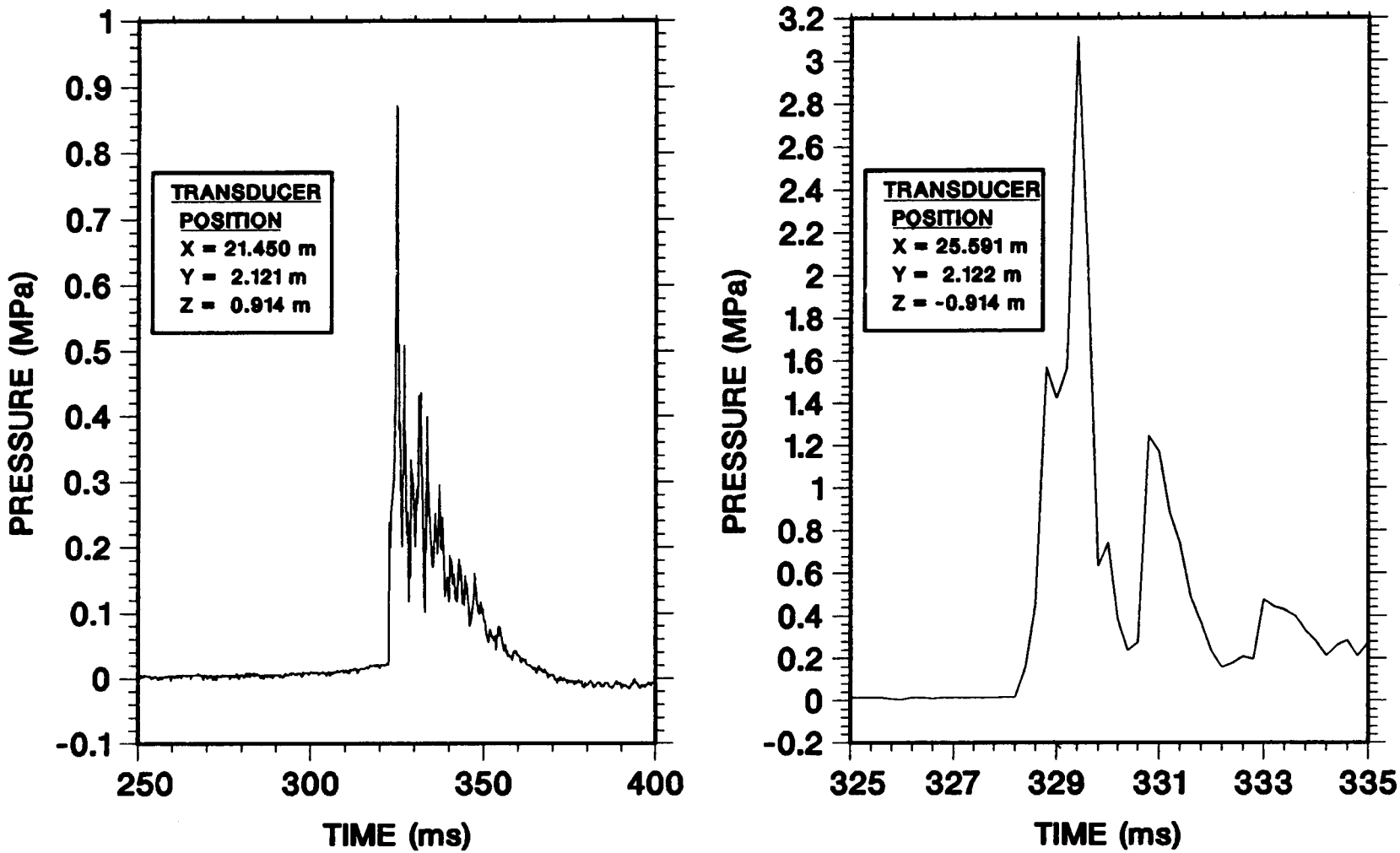

Figure 6.10. (Continued)

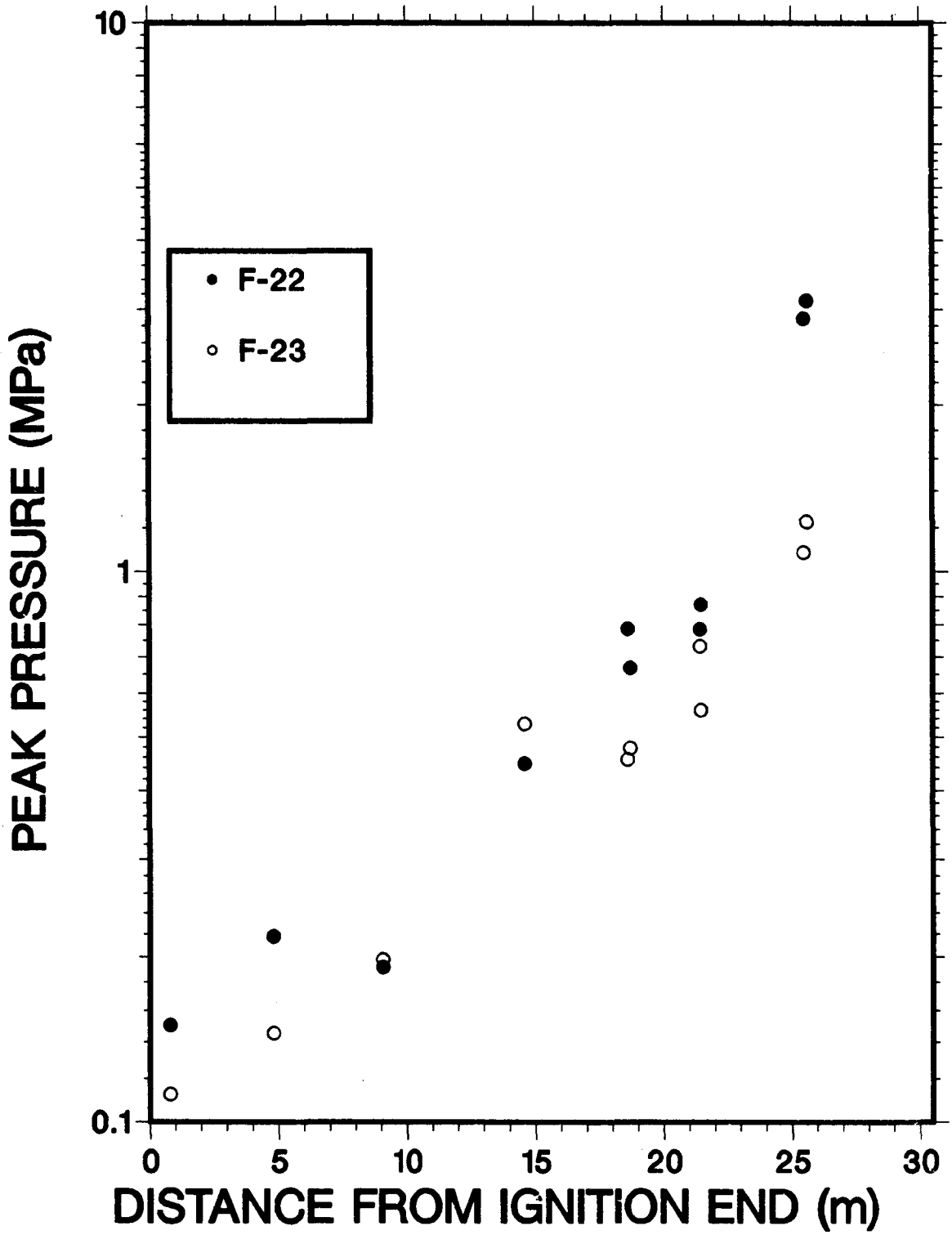

Figure 6.11. Tests F-22 and F-23. Measured peak pressures.

increase in peak pressure with increasing distance from the ignition end is clearly shown to be dramatic. For Figure 6.10, the peak pressure/initial pressure ratio of the spike is about 38 (ambient pressure = 0.084 MPa). This corresponds to a shock wave of Mach number of 5.7, a value in the range of detonation wave numbers. This is one piece of evidence that a DDT occurred. However, there is no evidence of a retonation wave. At the time the combustion wave exited the channel, many of the obstacles had been broken off the walls of the channel. The obstruction of the obstacles remaining on the walls, and of the debris flying through the channel, may be the reason a returning retonation wave was not seen.

The detonation cell width, λ, for a 15.0% hydrogen-air mixture is about 360 mm. Hence the ratio of gap size between the obstacles, d = 1219 mm (4 ft), to detonation cell width, was $d/\lambda \simeq 3.4$. DDT has been observed for ratios of d/λ that low, with the observed combustion front being a "quasi-detonation". Quasi-detonations are highly disturbed detonations traveling significantly below the detonation C-J speed. The ratio of the unobstructed channel width, W, to λ was $W/\lambda \simeq 5.0$. Benedick, Knystautas, and Lee [66] have shown that a detonation could propagate from a rectangular opening to an open space when $W/\lambda \simeq 9$ for this FLAME channel aspect ratio. The presence of the ground under the bag will tend to support the shock wave on that plane and prevent the extinguishment of a detonation after it exits the channel. Hence, the mixture used in test F-22 could undergo DDT in the channel and is marginally able to continue to propagate outside the channel. This discussion should be kept in mind when the photographic data is discussed in the next paragraph.

The evidence for a DDT in test F-22 rests on two pieces of data, the high pressure seen near the exit previously discussed, and the speed of a luminous wave seen exiting the channel. There was no evidence of a combustion wave moving at detonation speed inside the channel from the thermocouples, pressure transducers, or germanium photodiodes. The DDT must have occurred near or at the channel exit. High-speed cinematography (3854 frames/s) taken perpendicular to the channel axis shows the motion of a moderately to weakly luminous wave exiting the channel. The luminous front was observed on seven frames. The speed of the wave was determined by comparing the position of the wave on consecutive frames of film. In particular, the position of the wave on each frame was determined by observing the position of the sharp break in slope of the plastic bag at the top and bottom positions due to lateral expansion behind a compressive wave. The wave position was measured on a digital position imaging screen. Shown in all frames was a vertical pole with reference stripes each 0.305 m (1 foot) apart. The distances between these stripes on the imaging screen was used as a distance standard.

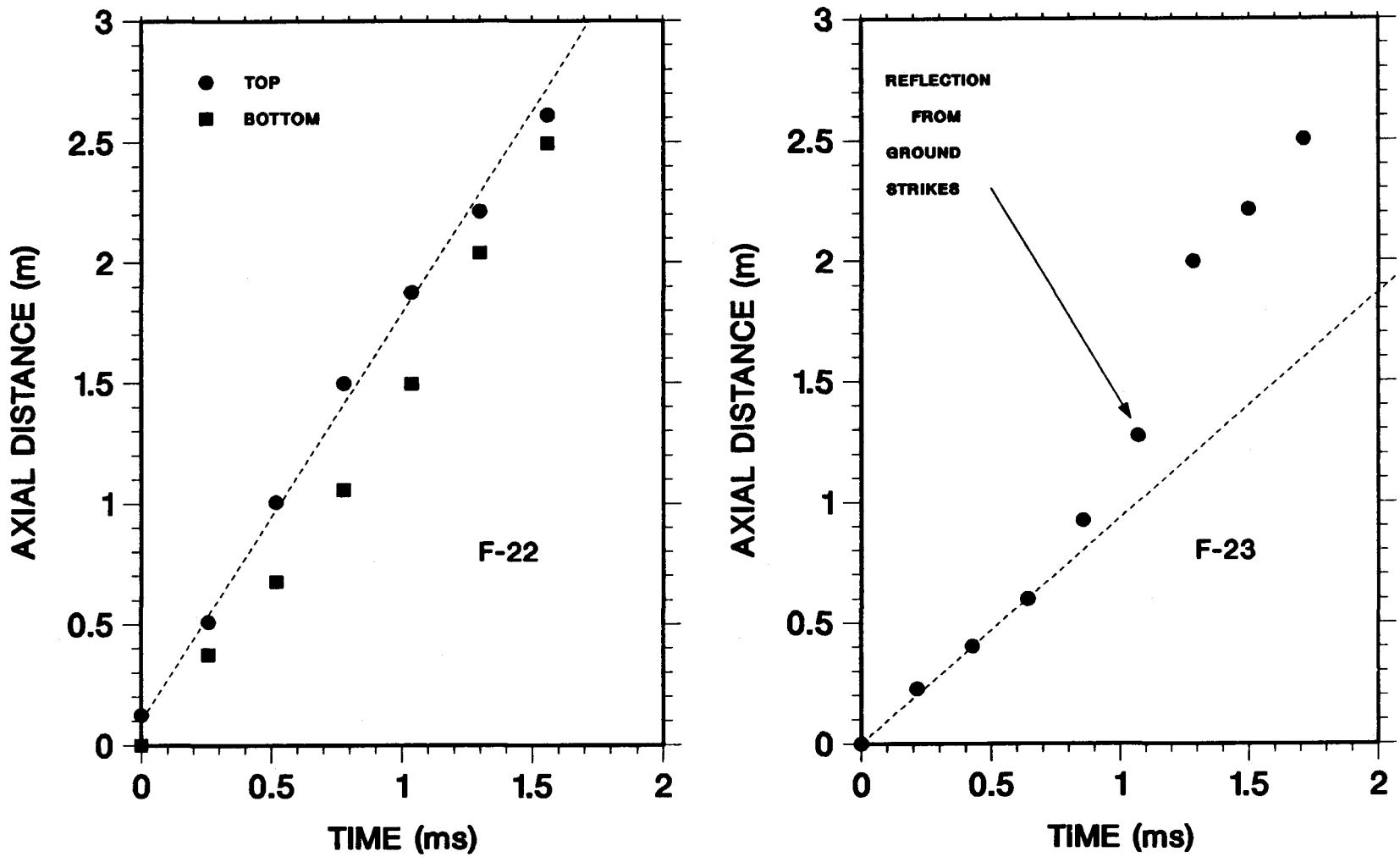

Figure 6.12. Tests F-22 and F-23. Trajectory of Wave Exiting Flame Channel.

Since the pole was closer to the camera than the FLAME exit, a correction for parallax was made, increasing the measured distances by 18%. The results are shown on Figure 6.12. The luminous front is seen to move at a nearly constant speed of 1686 m/s relative to the ground. This is above the C-J detonation velocity of 1516 m/s. The difference can be due to the motion of the unburned gas out of the channel. High-speed cinematography looking into the channel showed explosive growth of bright luminous fronts from the obstacles and the last rake, but did not clearly show these fronts covering the entire cross section as would be expected by a detonation. In summary, it appears that there was a deflagration-to-detonation transition in test F-22. If a self-sustaining detonation was not achieved, the pressures in the channel and wave speed outside the channel were not less than those expected of a detonation.

The experimental results for test F-23 are shown in Figures 6.13 and 6.14. The combustion front trajectories are similar to those for test F-22, except the times-of-arrival are somewhat later, corresponding to lower flame speeds. The propagation speed down the last 10 meters of channel was 620 m/s. The peak pressures observed for test F-23 are shown with those of test F-22 on Figure 6.11. They show a similar trend, increasing with distance from the ignition end, but the values near the channel exit are lower. The largest peak pressure/initial pressure ratio seen was 14, corresponding to a shock wave Mach number of 3.5, below that required for a detonation. High-speed cinematography (4675 frames/s) at the channel exit showed the motion of a very-weakly luminous wave exiting the channel. Using the same technique as in evaluating the data from test F-22, the position of the wave at the top the the confining bag is shown in Figure 6.12. The points do not lie on a straight line. The large change in slope near the sixth point coincides with the arrival of a reflected wave from the ground. Consequently, we believe the slope given by the first points is representative of the speed of the wave coming from the channel into an open space. This velocity is about 935 m/s, below the C-J detonation speed of 1496 m/s. High-speed cinematography looking into the channel show no evidence of detonation or even strong local explosions. In summary, the evidence shows that a DDT did not occur in test F-23. It appears that the two tests F-22 and F-23 have closely bounded the conditions for DDT.

Test F-21 was interesting because of an error made in preparation of the test. The air supply to the air-driven mixing fans was cut off. Analysis of gas samples taken at the upper locations indicated a hydrogen mole fraction of 15%, while gas samples at the lower locations at the lower locations indicated a hydrogen mole fraction of 10%. During the filling of the FLAME channel, hydrogen enters the channel through three widely separated ports low in the far wall. It appears the jets lost

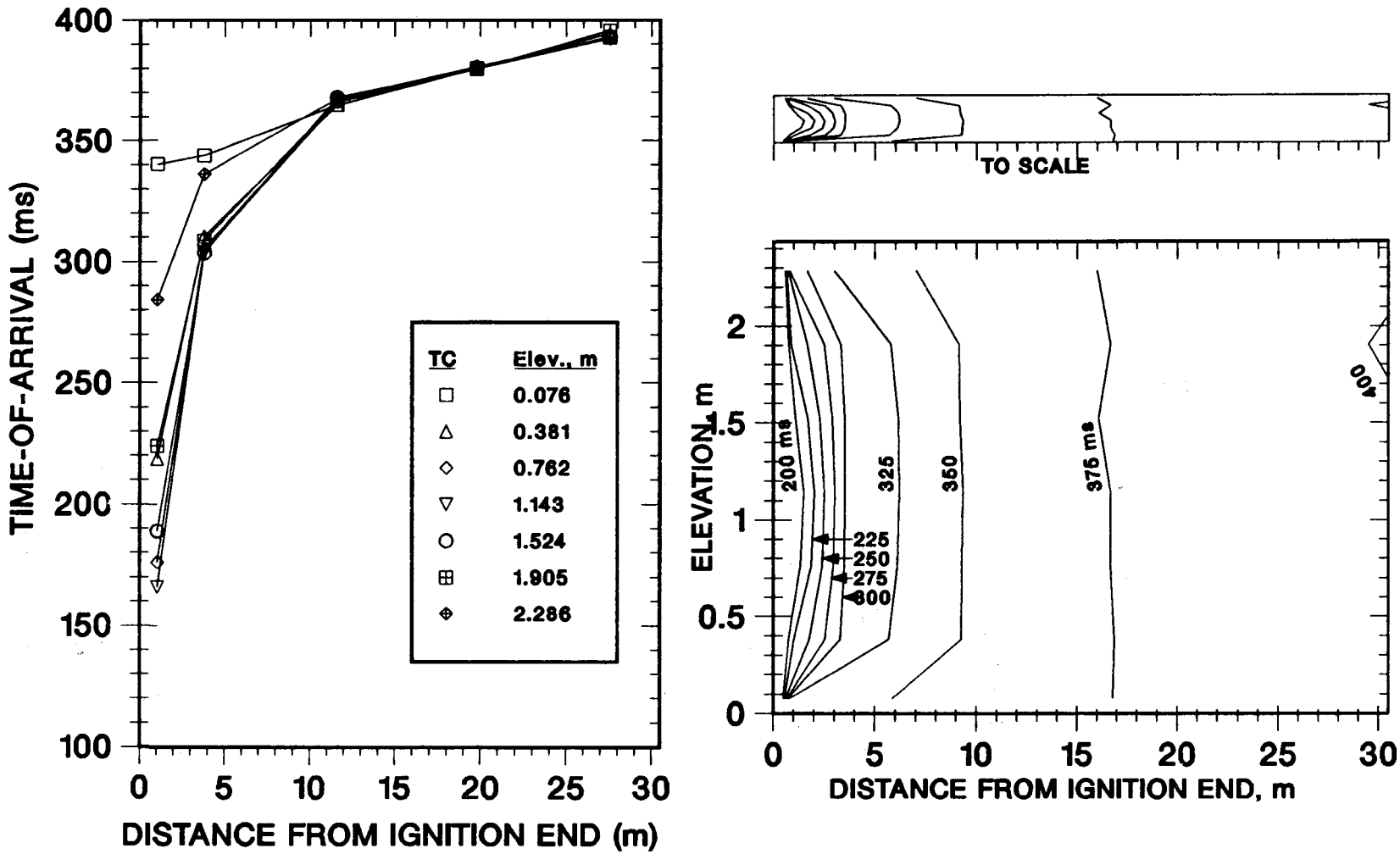

Figure 6.13. Test F-23, 14.5% H_2

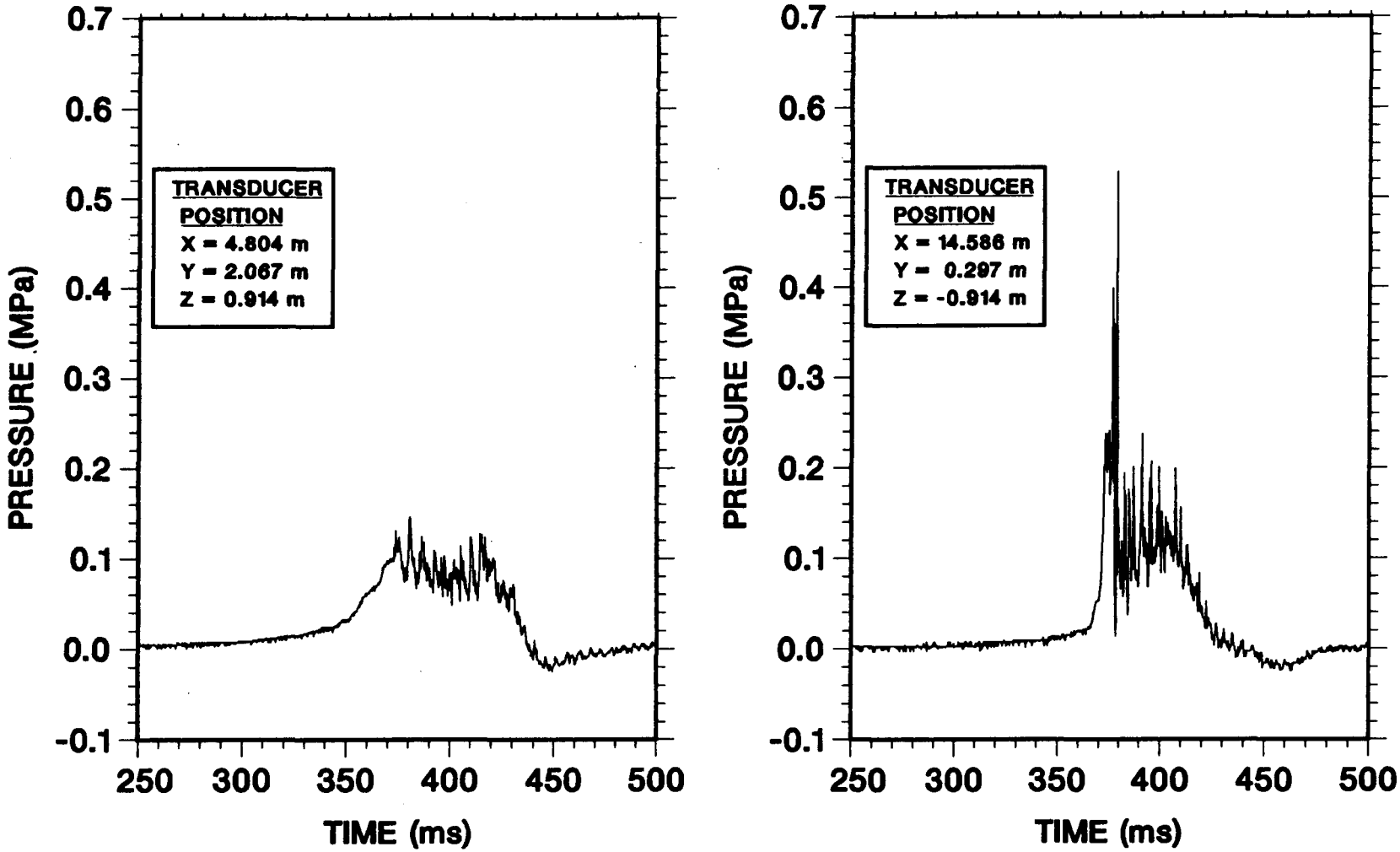

Figure 6.14. Test F-23, 14.5% H_2. No top venting. 33% blockage ratio. Pressure histories.

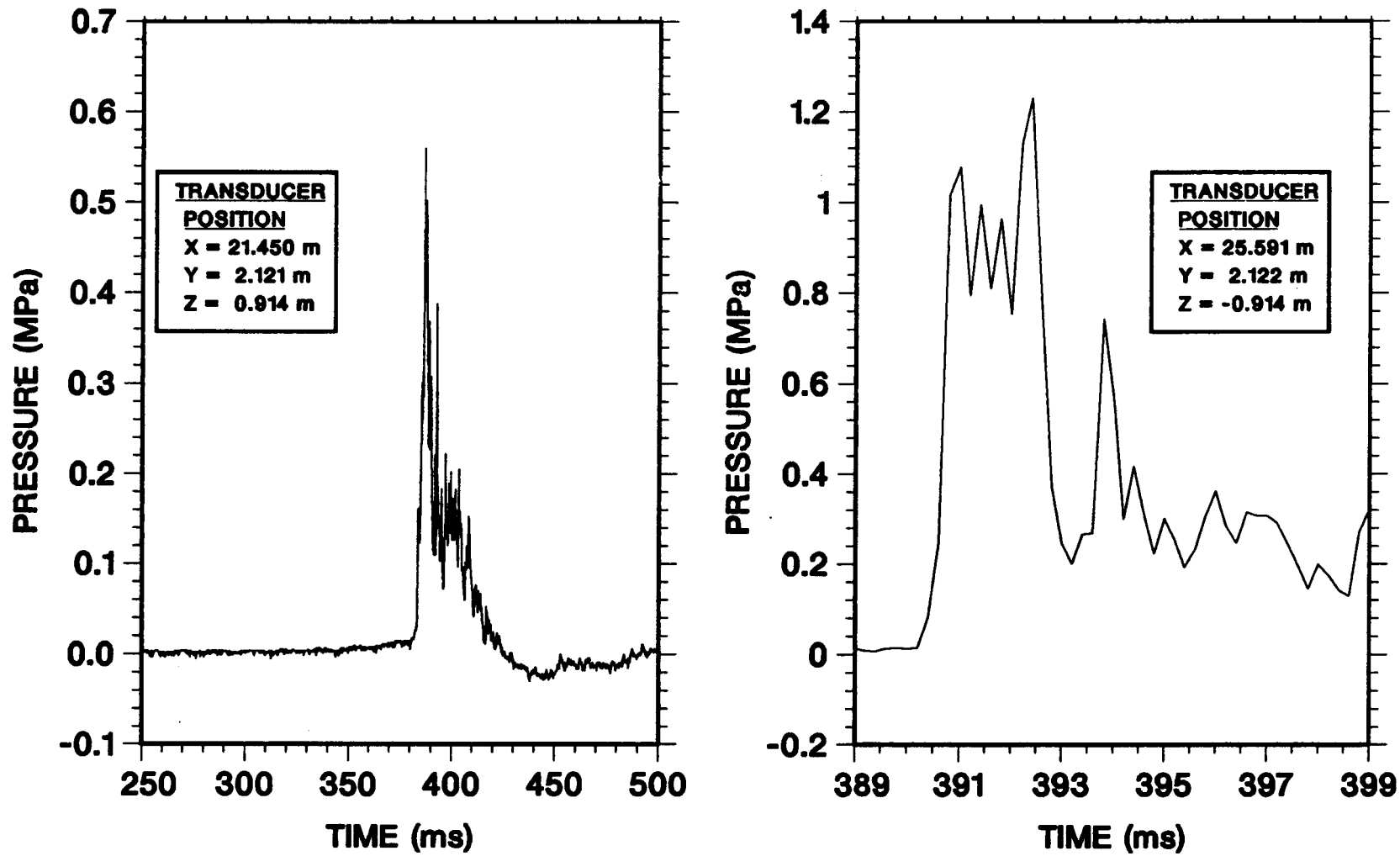

Figure 6.14. (Continued)

their momentum rapidly because of the low mass density of hydrogen and drifted upward to the ceiling. Calculations done with the HMS code by J. Travis confirmed this explanation. [67]. The deflagration front trajectories and fronts shown in Figure 6.15 show that the flame travelled slower near the bottom than the top in the first ten meters. After that axial distance, the front tended to be vertical and planar.

The equivalent planar flame speed versus axial distance for tests F-21 to F-23 is shown in Figure 6.16. The lines representing the results for the three tests are nearly the same for the first twenty meters. The equivalent planar flame speeds tend toward asymptotic values in the last section of the channel, with the richer mixtures giving a higher speed.

In summary, for tests with obstacles in the channel and no top venting:

1. The flame speeds and pressures are much higher than in comparable tests without obstacles.

2. The flame accelerates toward speeds corresponding to choked conditions in the burned gas, $\simeq$ 500 - 700 m/s.

3. Transition to detonation was seen at 15% hydrogen.

6.4 Tests With 50% Top Venting and No Obstacles

Tests F-1 to F-6 had 50% of the top covered with steel plates. Prior to each test, the entire top was covered with a thin plastic sheet. The expectation was that the sheet would quickly be destroyed causing minimum restraint to gas flow. The results of tests F-1 - F-4, and F-6 follow a consistent pattern. Test F-5 had some anomalous results. In test F-5, the top sheet was observed not to fail until the flame had progressed part way down the channel. We will consider tests F-2, F-4, and F-6 in detail. The pressure rises for these tests were low. In two tests, F-1 and F-3, the pressure signals were in the noise level. We will examine the pressure response only for the test with the highest hydrogen mole fraction tested, test F-4 with 28.0% hydrogen. In none of these tests was there a detonation. We will consider these tests in order of decreasing hydrogen mole fraction.

For test F-4 with 28.0% hydrogen, the deflagration front trajectories and profiles are shown in Figure 6.17. In Figure 6.17a, for each elevation, the lines of time-of-arrival versus distance from the ignition end are nearly straight and parallel. The time-of-arrival at any given axial distance monotonically decreased with increasing elevation from the floor. As shown in Figure 6.17b, this means the deflagration propagated down the

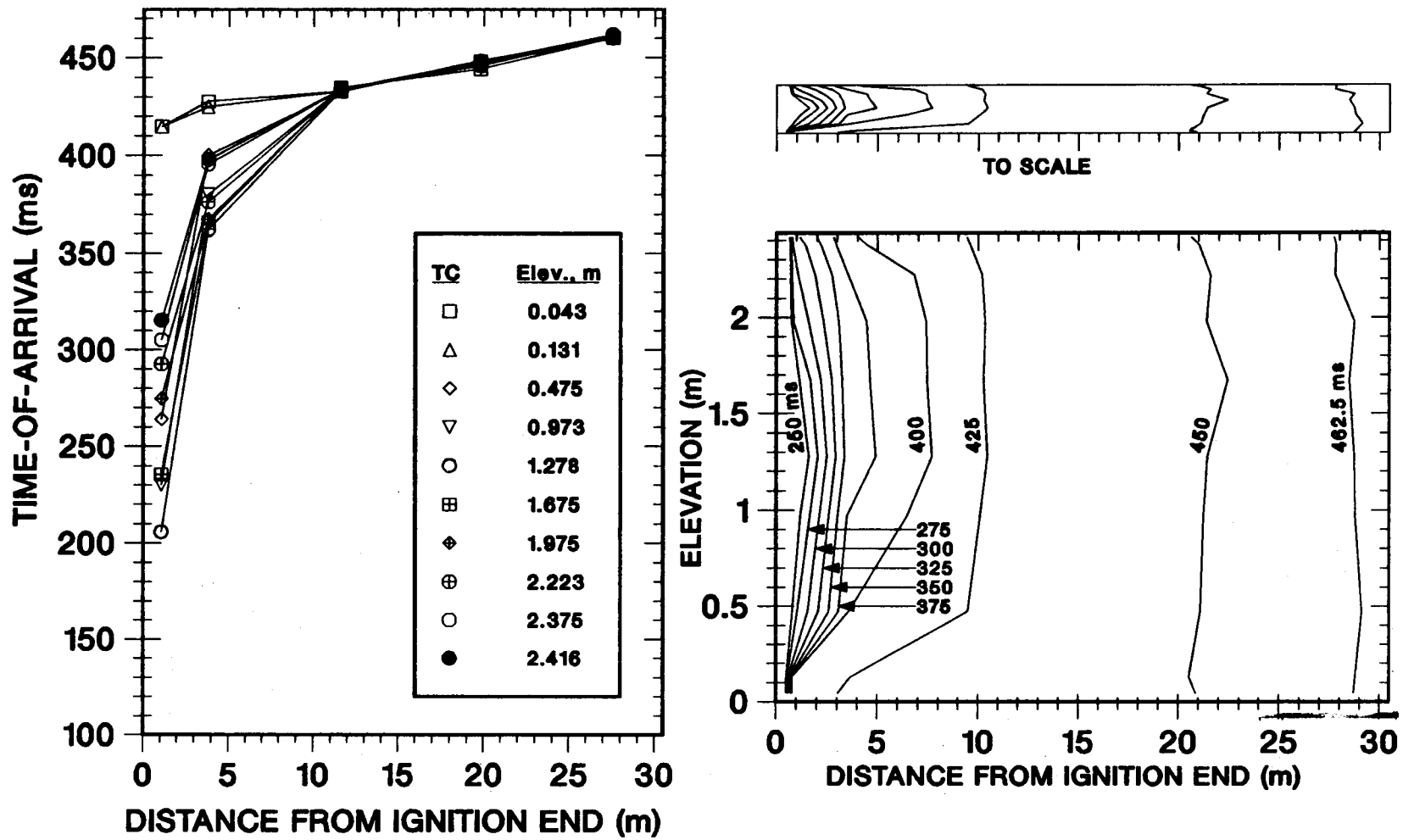

Figure 6.15. Test F-21, 10-15% H_2. No top venting. 33% blockage ratio. Combustion front trajectories and profiles.

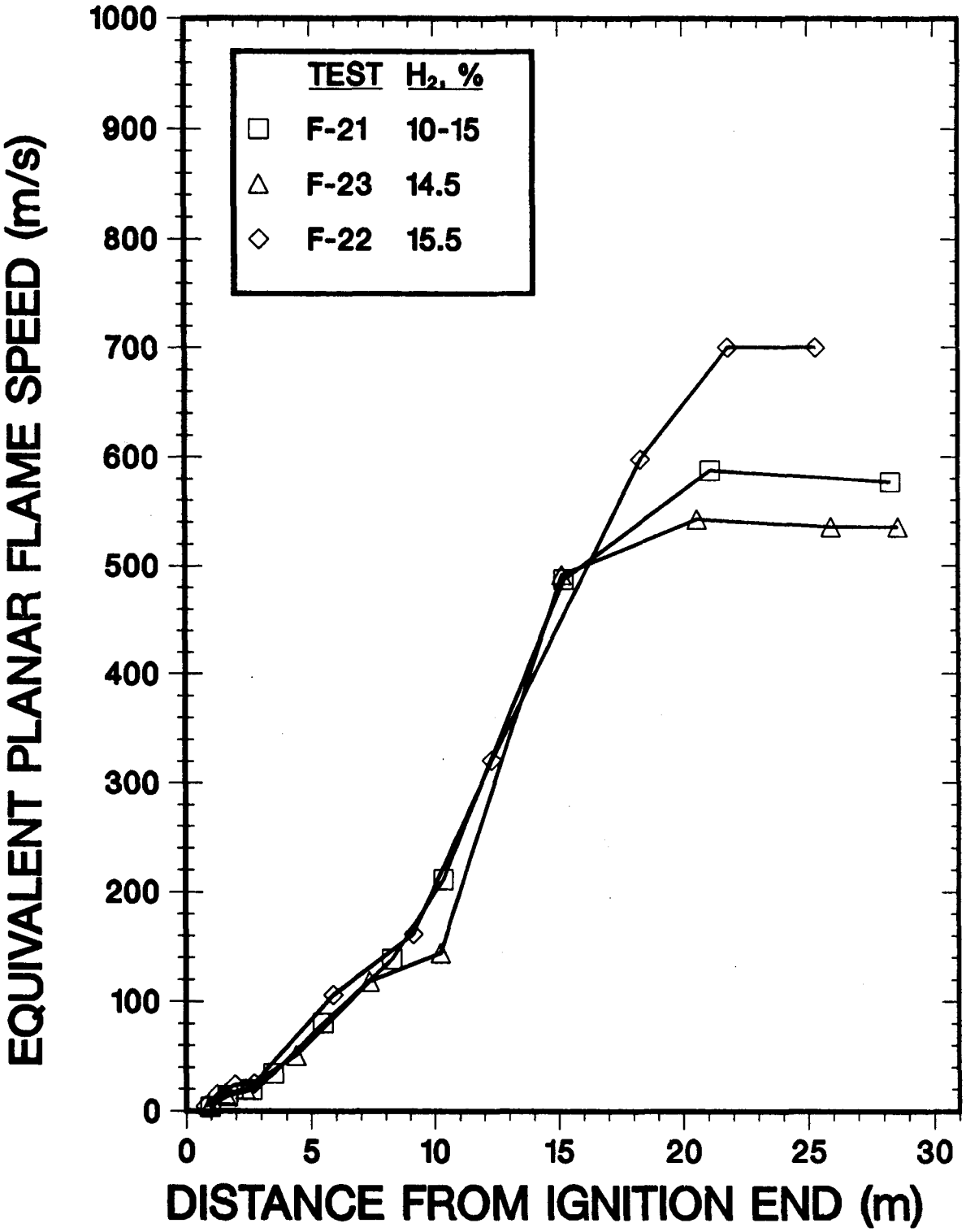

Figure 6.16. Comparison of Flame Speeds for Tests With No Top Venting and Obstacles

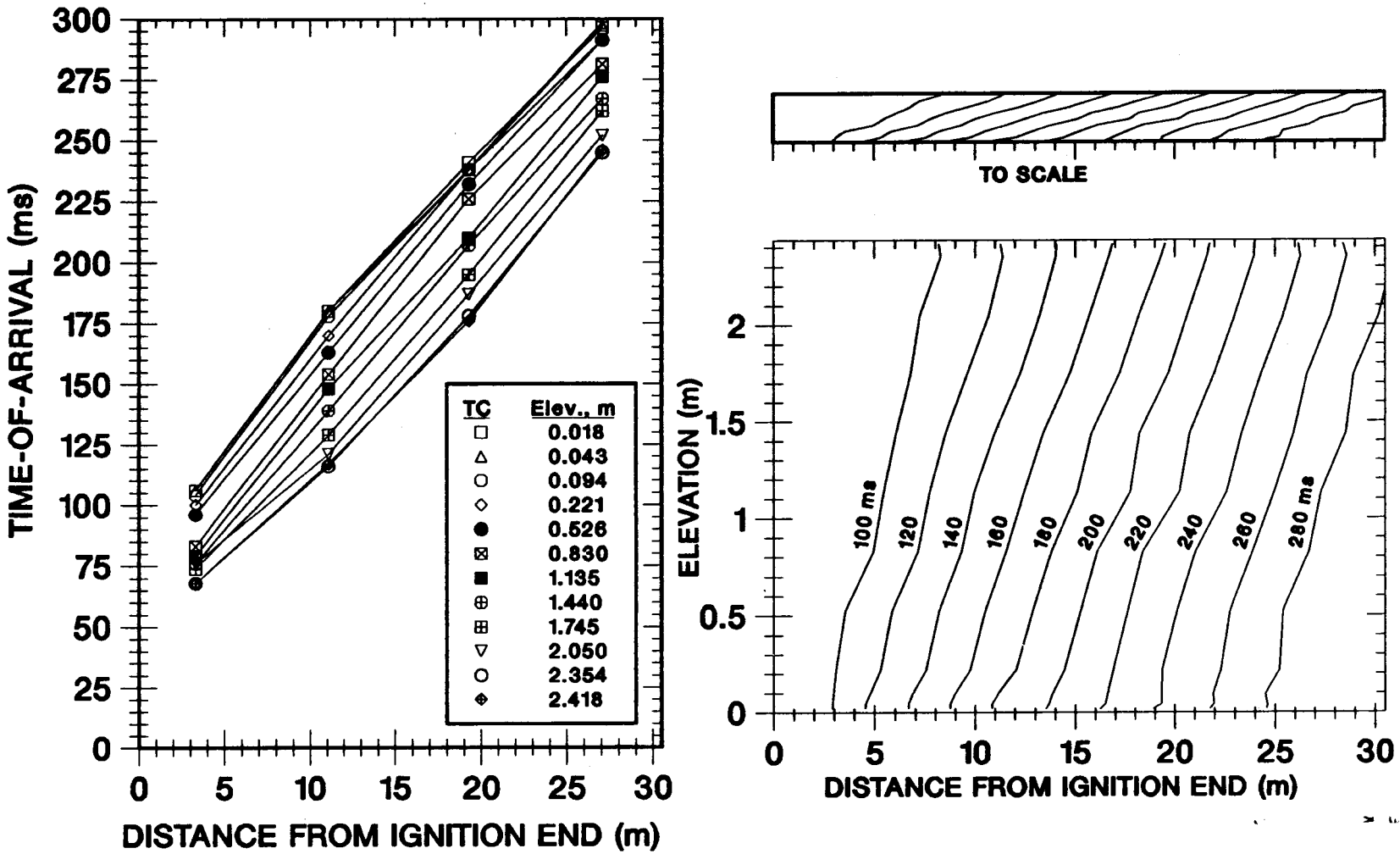

a. b.

Figure 6.17. Test F-4, 28.0% H_2

channel at nearly constant speed, 126 m/s. The flame profile was inclined forward from the vertical by about 70 degrees. There was no flame acceleration.

Pressure histories from four transducers used in test F-4 are shown in Figure 6.18. The initial smooth pressure rise up to 40 ms in Figure 6.18a may correspond to the time before the top plastic sheet fails. This period of smooth pressure rise diminished further from the ignition end. The smooth pressure rise was followed by a period of rapid pressure oscillations, with periods typically about 2 ms. Periods this short can only be associated with venting out the top and pressure waves transverse to the channel axis. The peak pressures shown in Figures 6.18a and 6.18b occur at about 70 ms, when the flame front has only moved a few meters from the ignition end. The peak pressure occurred somewhat later in Figures 6.18c and 6.18d, but still before the arrival time of the flame. It appears that the peak pressures were associated with the transient processes soon after ignition, and that after the steadily propagating flame was achieved, the resultant overpressures were less than 10 kPa.

Figure 6.19 shows the combustion front trajectories and profiles for test F-2 with 19.7% hydrogen; Figure 6.20 shows the combustion front trajectories and profiles for test F-6 with 15.5% hydrogen. The flame speeds decrease as the hydrogen mole fraction decreases. Aside from the lower speed, the pattern of steeply inclined flame fronts with uniform propagation speed down the channel is the same for all three tests considered, and for F-1 and F-3.

The results of test F-5 shown in Figure 6.21 are clearly different from the other five tests. The comparatively high initial flame velocities for test F-5 are inconsistent with those of the other tests. This is evident in Figure 6.22. However, further from the ignition end, the behavior changes. The equivalent planar flame speed drops to levels comparable to test F-1 with about the same hydrogen mole fraction. Video pictures of this test show that the plastic top sheet did not fail early in test F-5 as in the other five tests. We believe this is the cause of the anomalous behavior.

In summary, for the tests with 50% top venting and no obstacles:

1. There was no flame acceleration and no DDT, even for nearly stoichiometric mixtures.

2. The flame front was planar and steeply inclined from the vertical with the top leading.

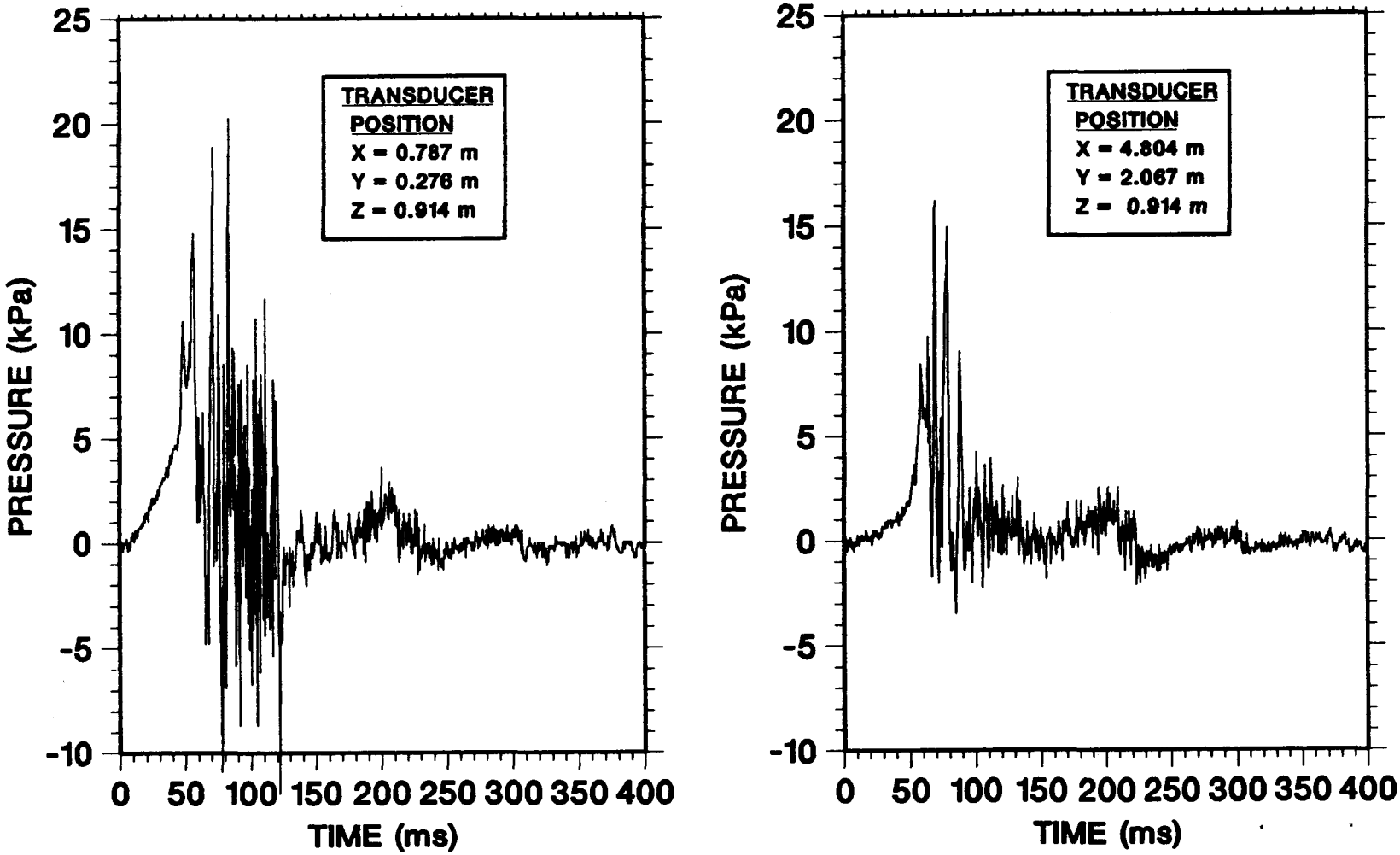

Figure 6.18. Test F-4, 28.0% H_2. 50% top venting. No obstacles. Pressure histories.

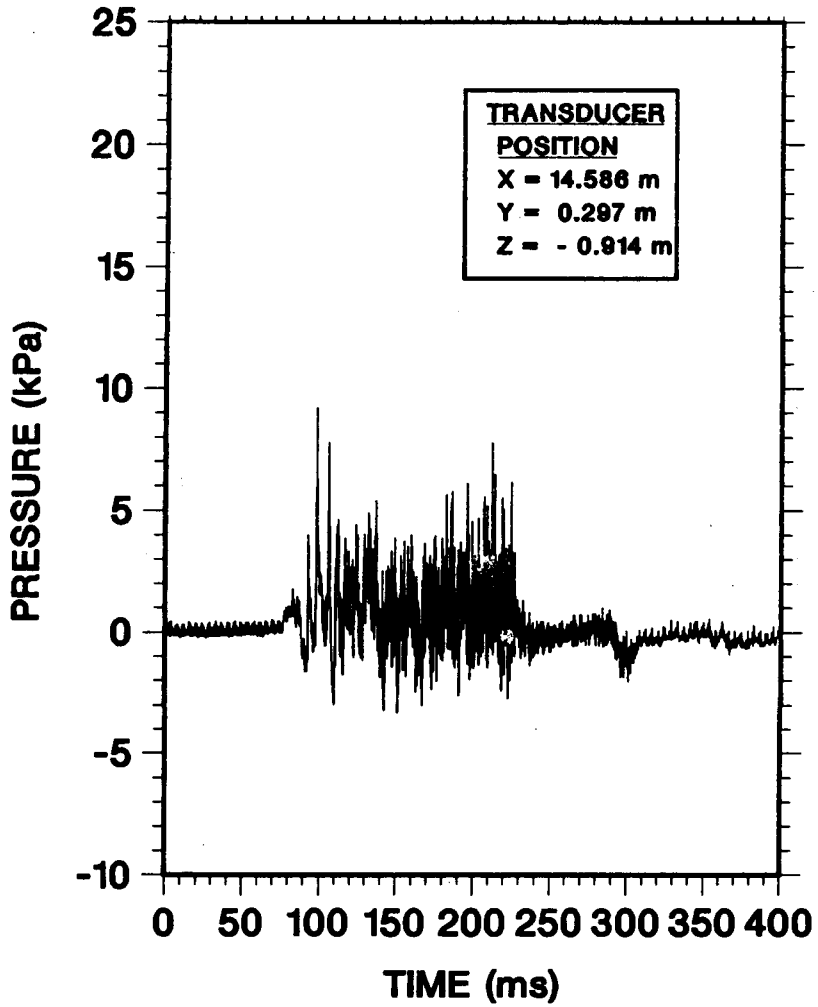

c.

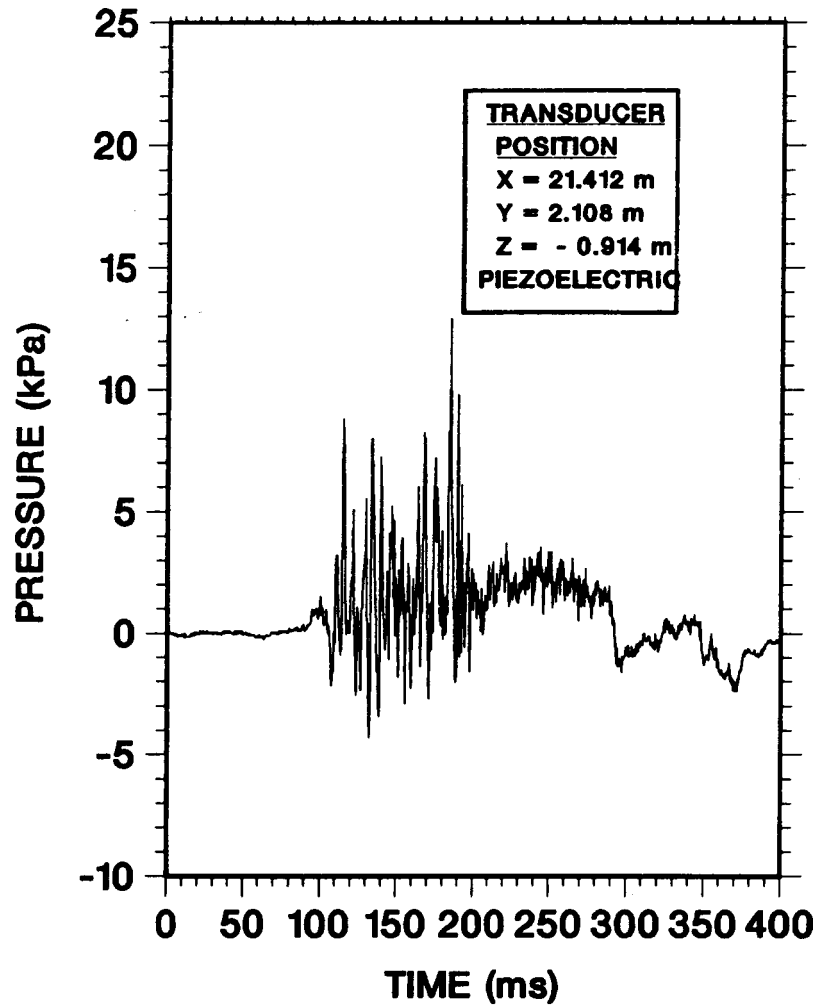

d.

Figure 6.18. (Continued)

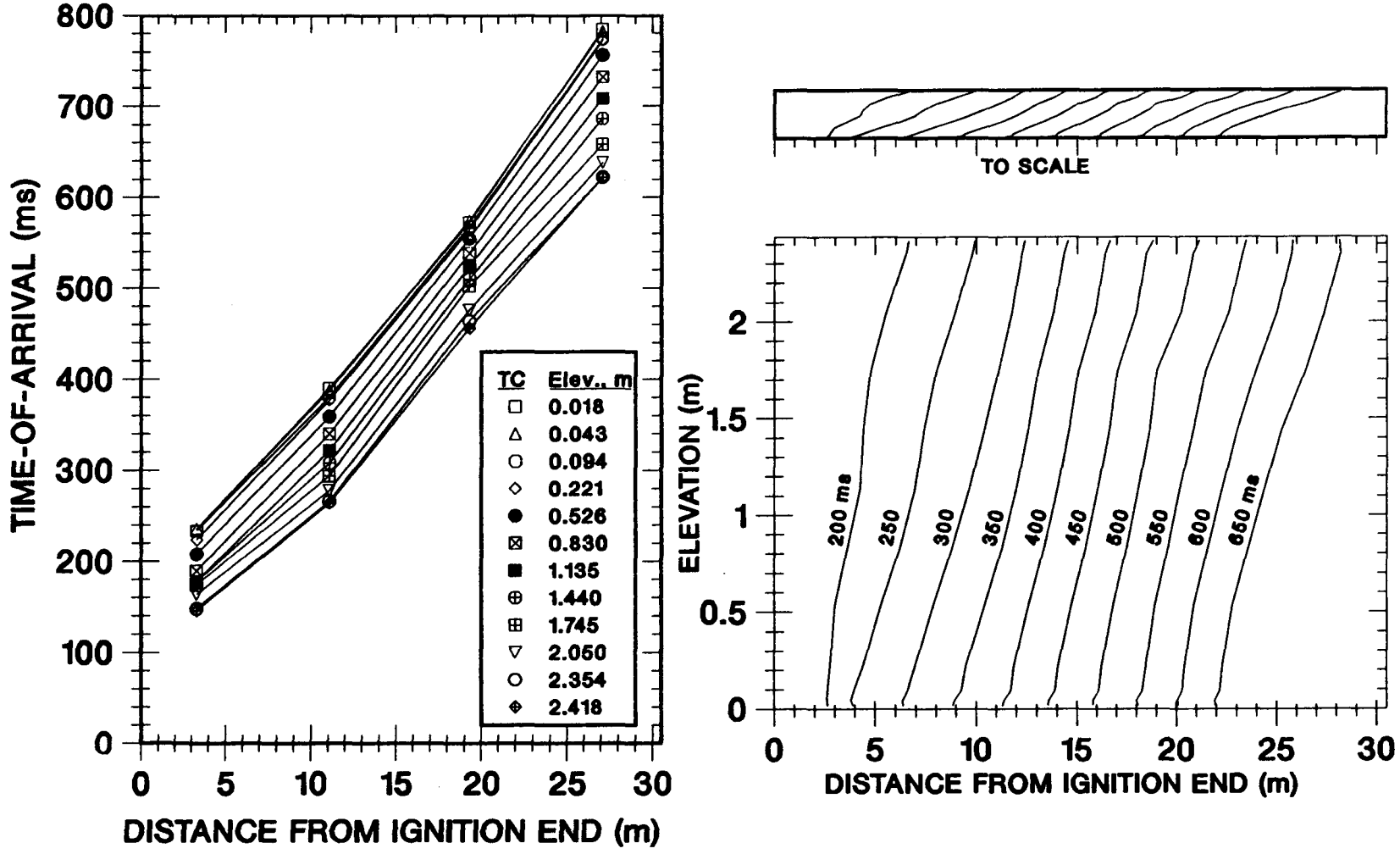

Figure 6.19. Test F-2, 19.7% H_2. 50% top venting. No obstacles. Combustion front trajectories and profiles.

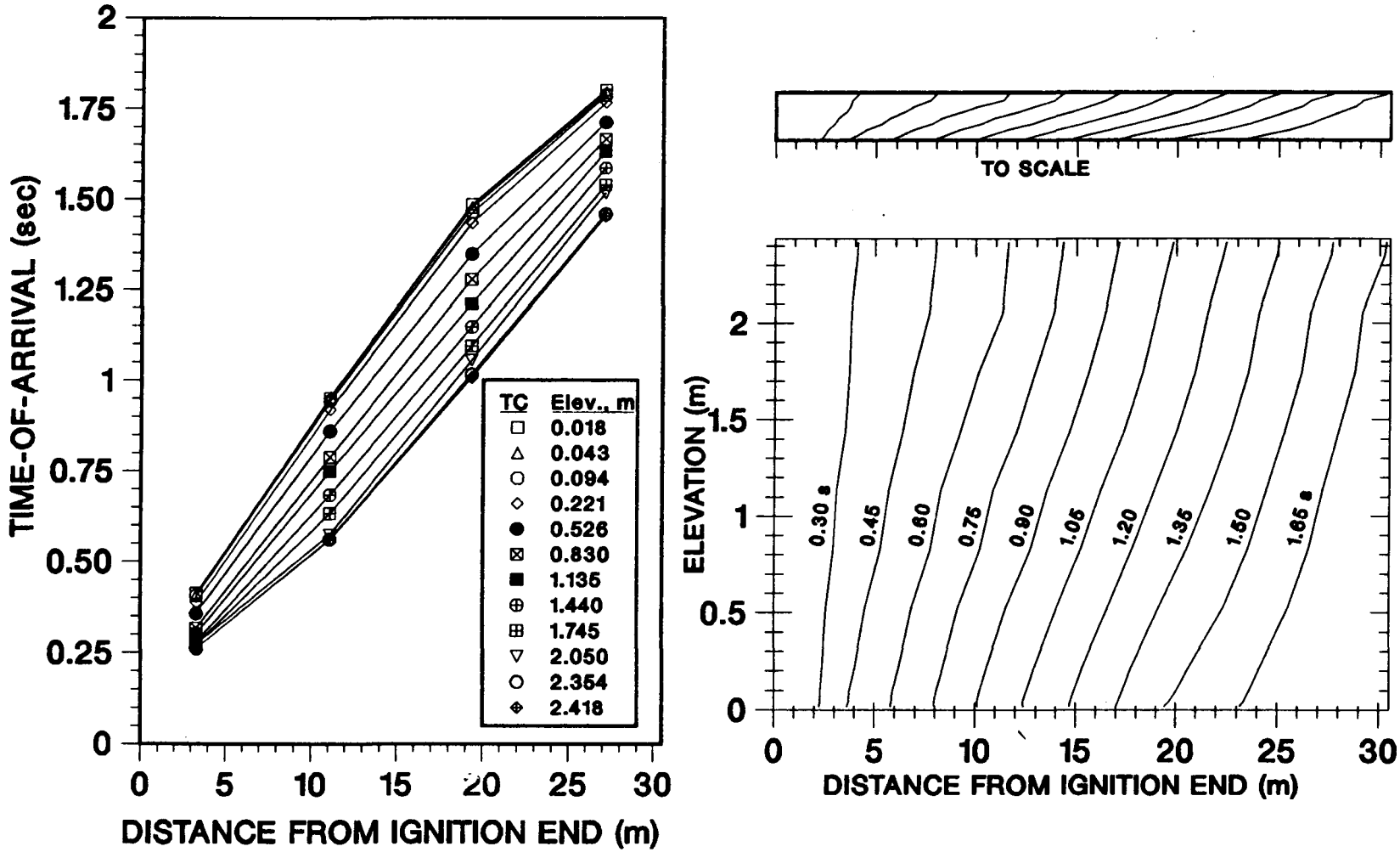

Figure 6.20. Test F-6, 15.5% H_2. 50% top venting. No obstacles. Combustion front trajectories and profiles.

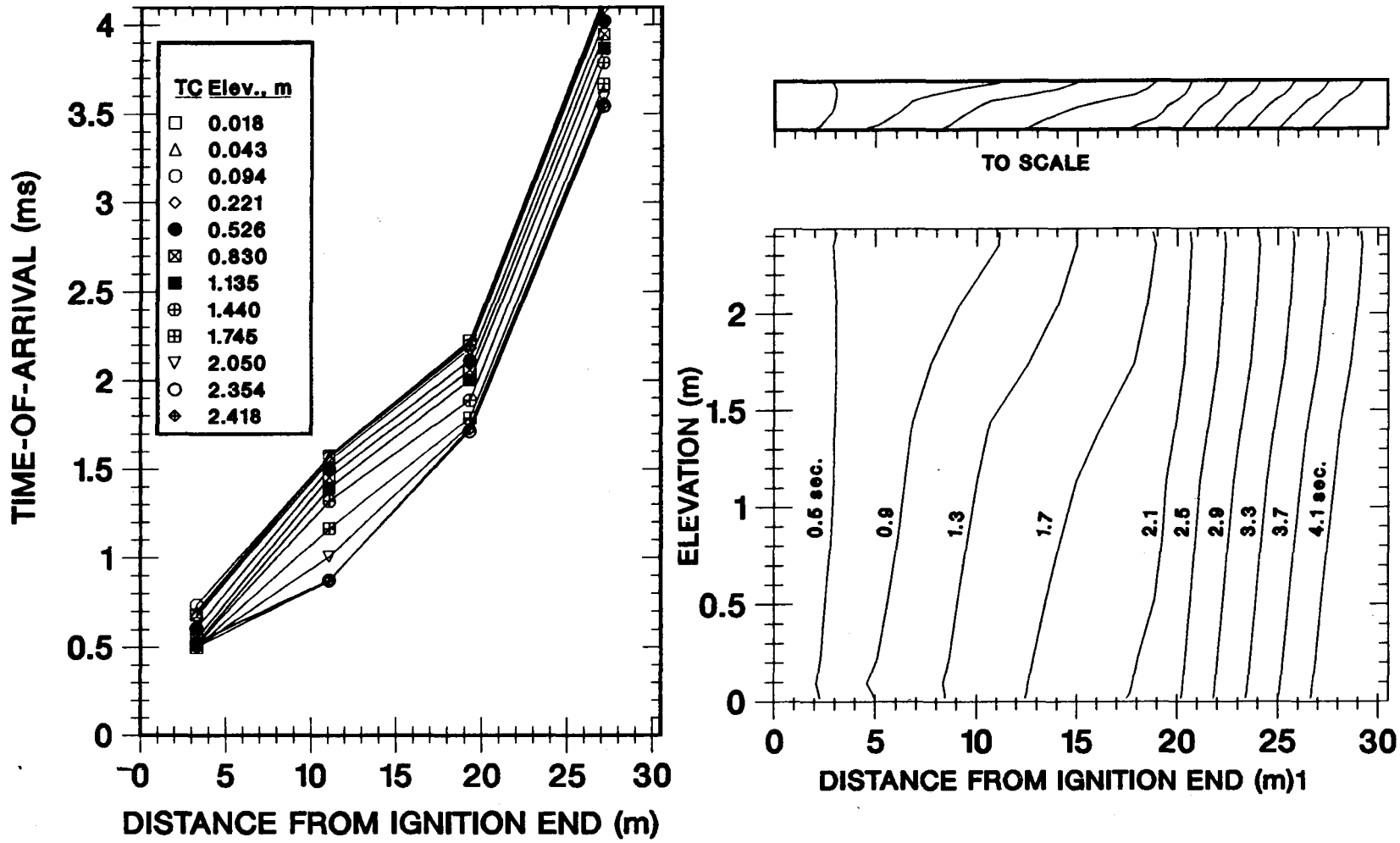

Figure 6.21. Test F-5, 12.6% H_2. 50% top venting. No obstacles. Combustion front trajectories and profiles.

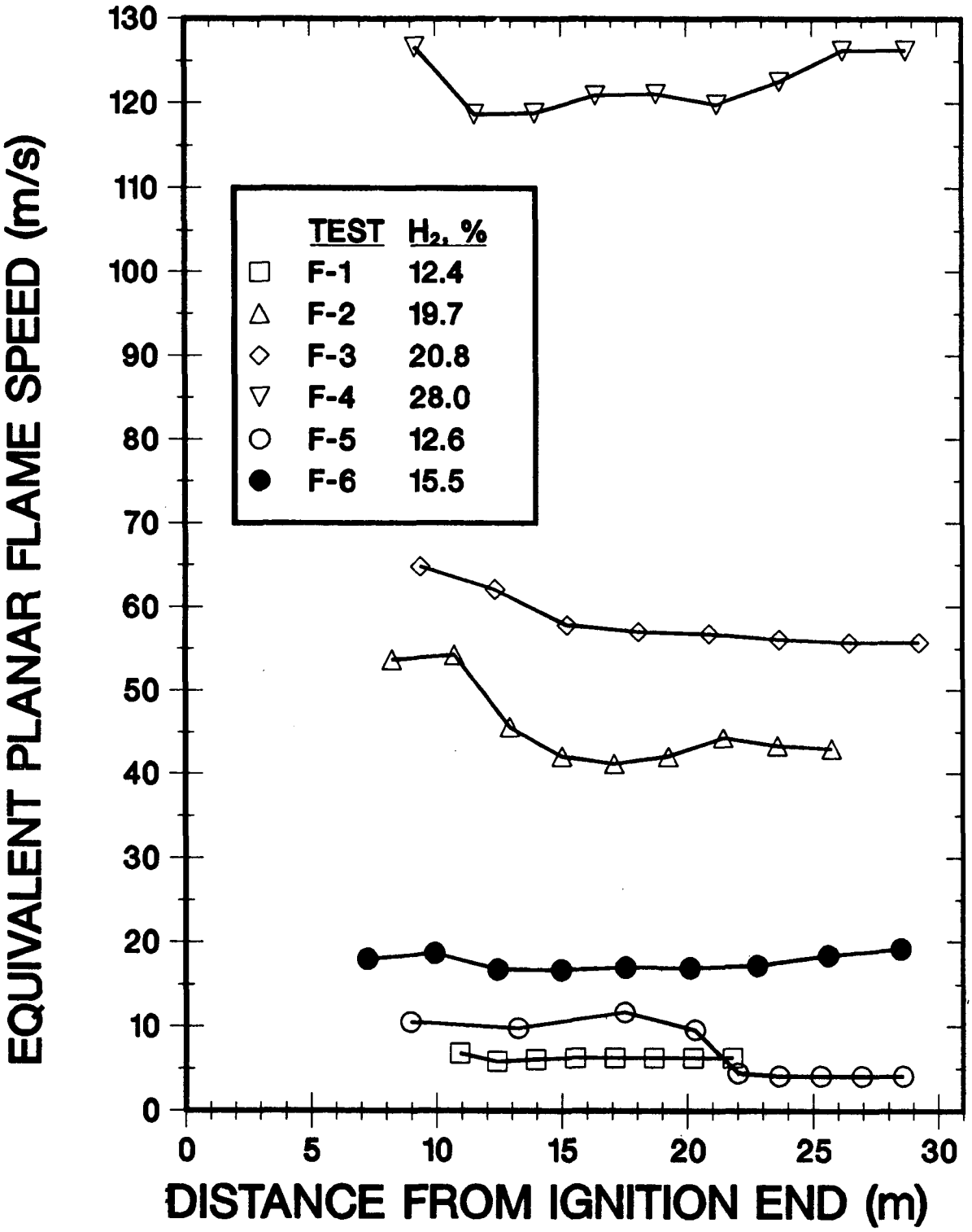

Figure 6.22. Comparison of Flame Speeds for Tests with 50% Top Venting and No Obstacles

3. The flame propagation speed increased with increasing hydrogen mole fraction.

4. The overpressures were low and the peaks were associated with initial transient effects and not the steady flame propagation.

6.5 Tests With 50% Top Venting and Obstacles

Tests F-24 to F-29 were carried out with 50% top venting and obstacles. Test F-26 used obstacles that simulated the geometry of the upper plenum region of an ice condenser pressurized water reactor containment. At one time members of the reactor safety community expressed the opinion that DDT was impossible in a geometry as open as that of test F-26. This test confirmed that flame acceleration by obstacles, even with only 11% blockage ratio can cause a DDT in a vented geometry. We will first consider test F-26. All the other tests considered here used the the obstacle geometry with planar baffles of 33% blockage ratio previously discussed. We will discuss those tests in order of increasing hydrogen mole fraction.

The combustion front trajectories and profiles for test F-26 are shown in Figure 6.23. From Figure 6.23a, it is clear that the transition to detonation occurred about 7 meters from the ignition end, between the second and third thermocouple rakes. A rightward wave, the detonation, was observed moving at 2000 m/s. A leftward wave, the retonation, was observed moving at about 2000 m/s. Test F-26 was the only test with obstacles in which a retonation wave was observed. The combustion front profile at 65 ms in Figure 6.23b is a crude estimate since there were no thermocouple rakes near the DDT. Four representative pressure histories of test F-26 are shown in Figure 6.24. Near the ignition end, Figure 6.24a, the pressure history shows a gradual pressure rise, fluctuations, the retonation wave, and more fluctuations. Through most of the channel the pressure transducer response looked like Figure 6.24c. There was a single detonation wave with an abrupt rise to about 1.0 MPa (145 psi). The higher narrow peak shown in Figure 6.24d of 1.5 MPa (220 psi) was not observed by any other pressure transducer, even one at the same axial distance from the ignition, but which was located on the other side of the channel. Nevertheless, there is no indication that the transducer was not responding correctly.

The results from test F-24 with 15.5% hydrogen and obstacles with 33% blockage ratio are shown in Figure 6.25. The deflagration accelerated, but the highest propagation speed observed was 82 m/s. The initially convex flame front became concave relative to the unburned gas. The overpressures were low, in the noise level.

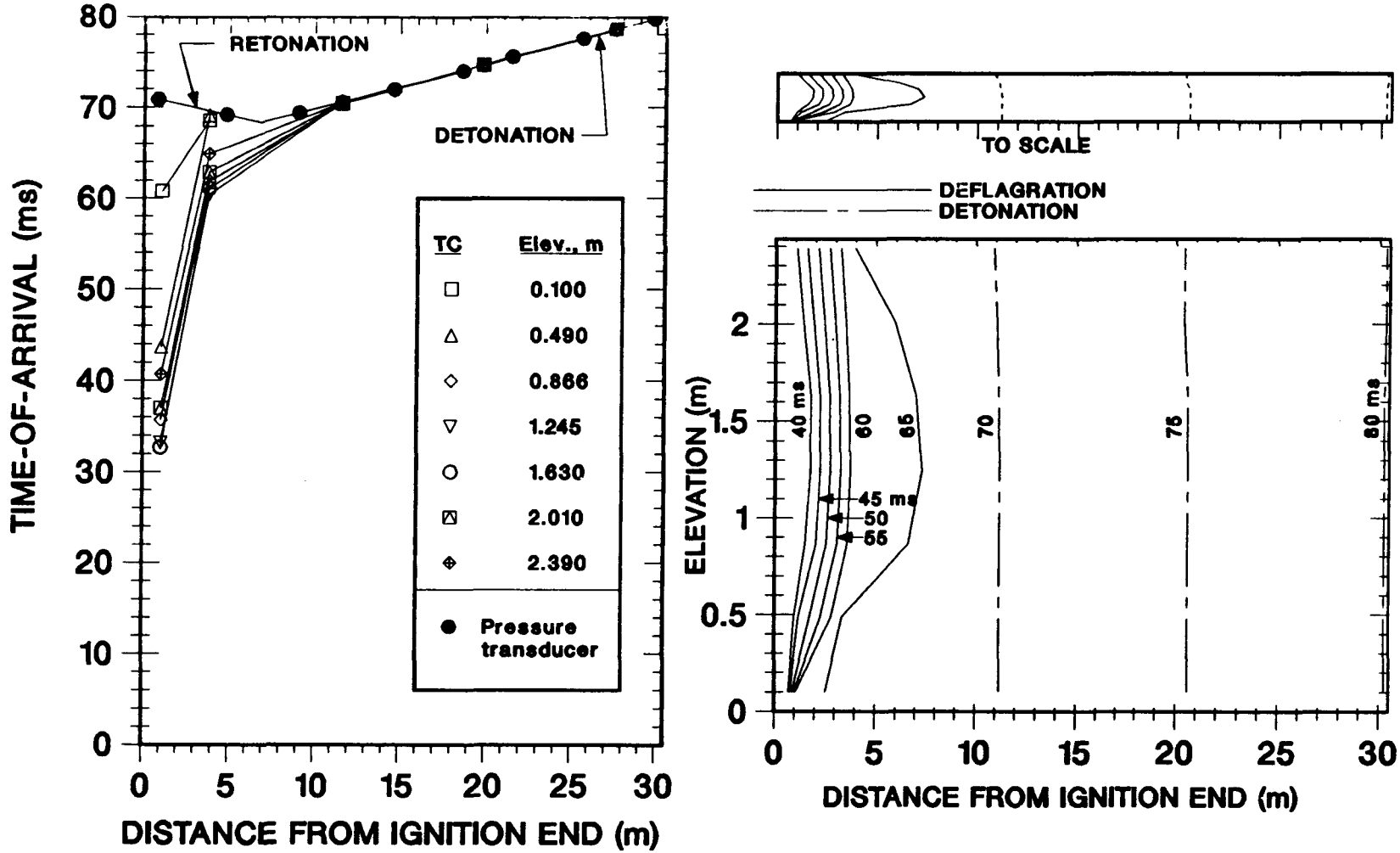

a. b.

Figure 6.23. Test F-26, 28.5% H_2. 50% top venting. 11% blockage ratio. Combustion front trajectories and profiles.

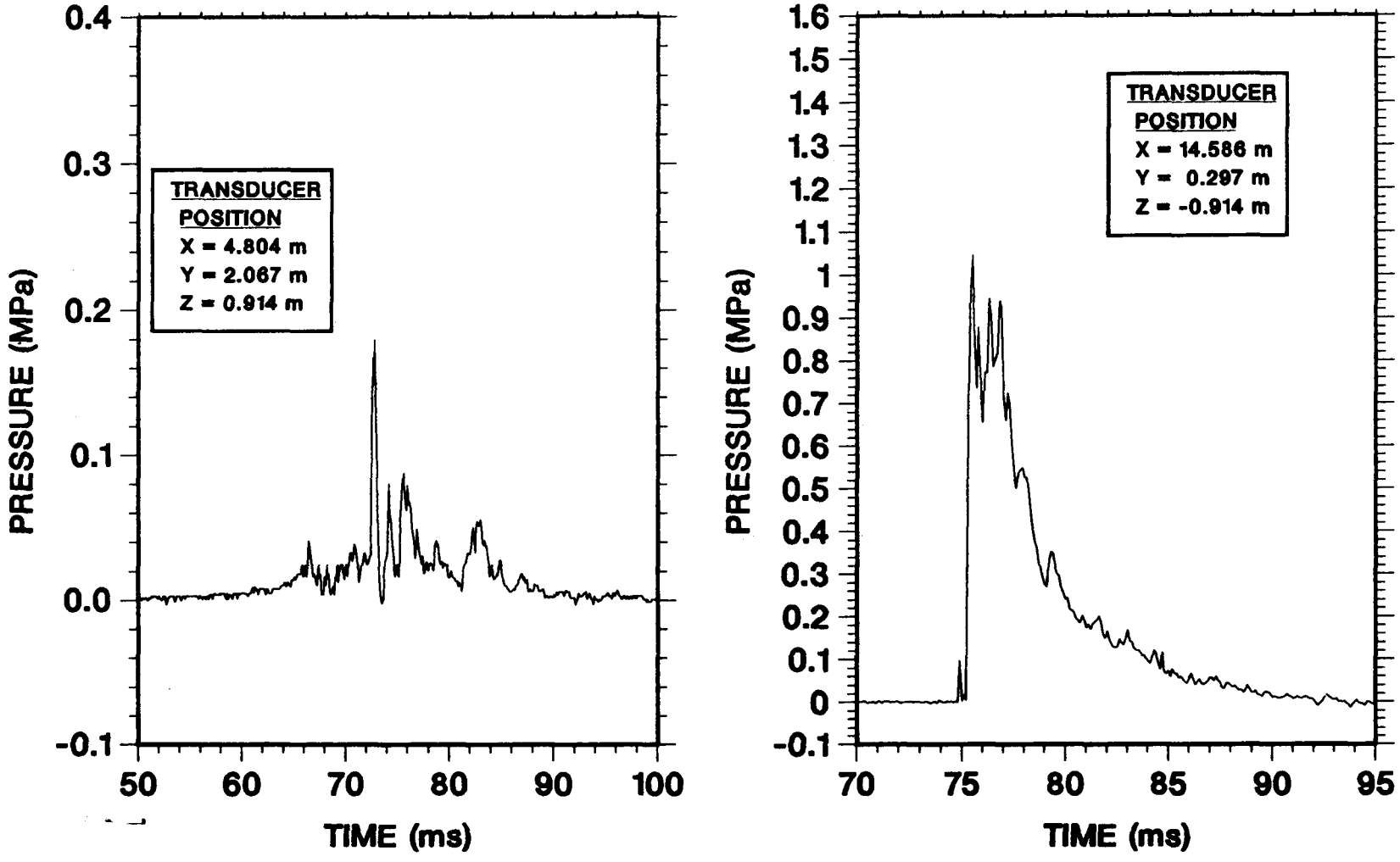

Figure 6.24. Test F-26, 28.5% H_2. 50% top venting. 11% blockage ratio. Pressure histories.

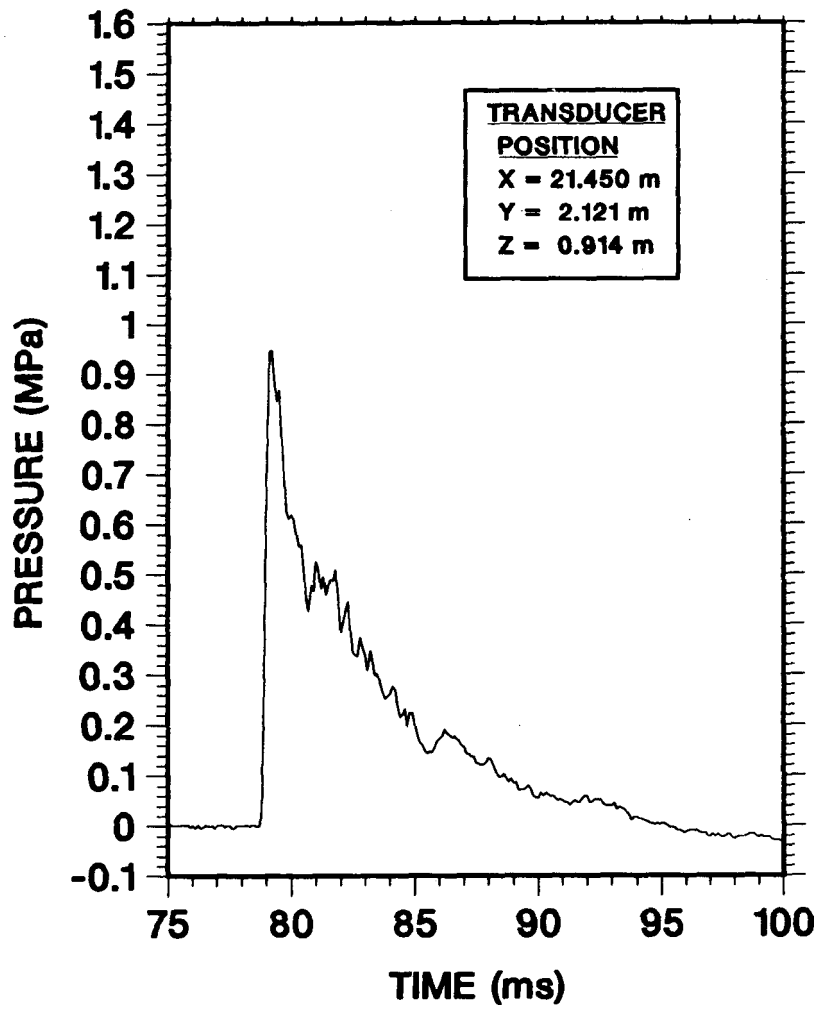

c.

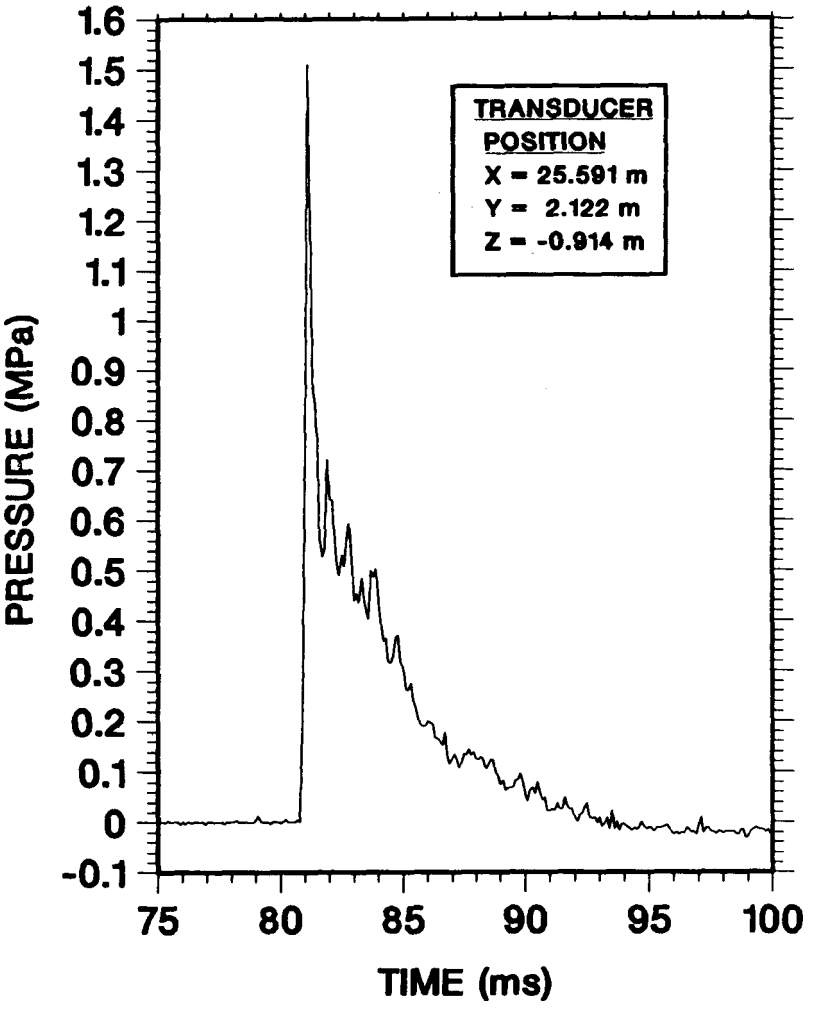

d.

Figure 6.24. (Continued)

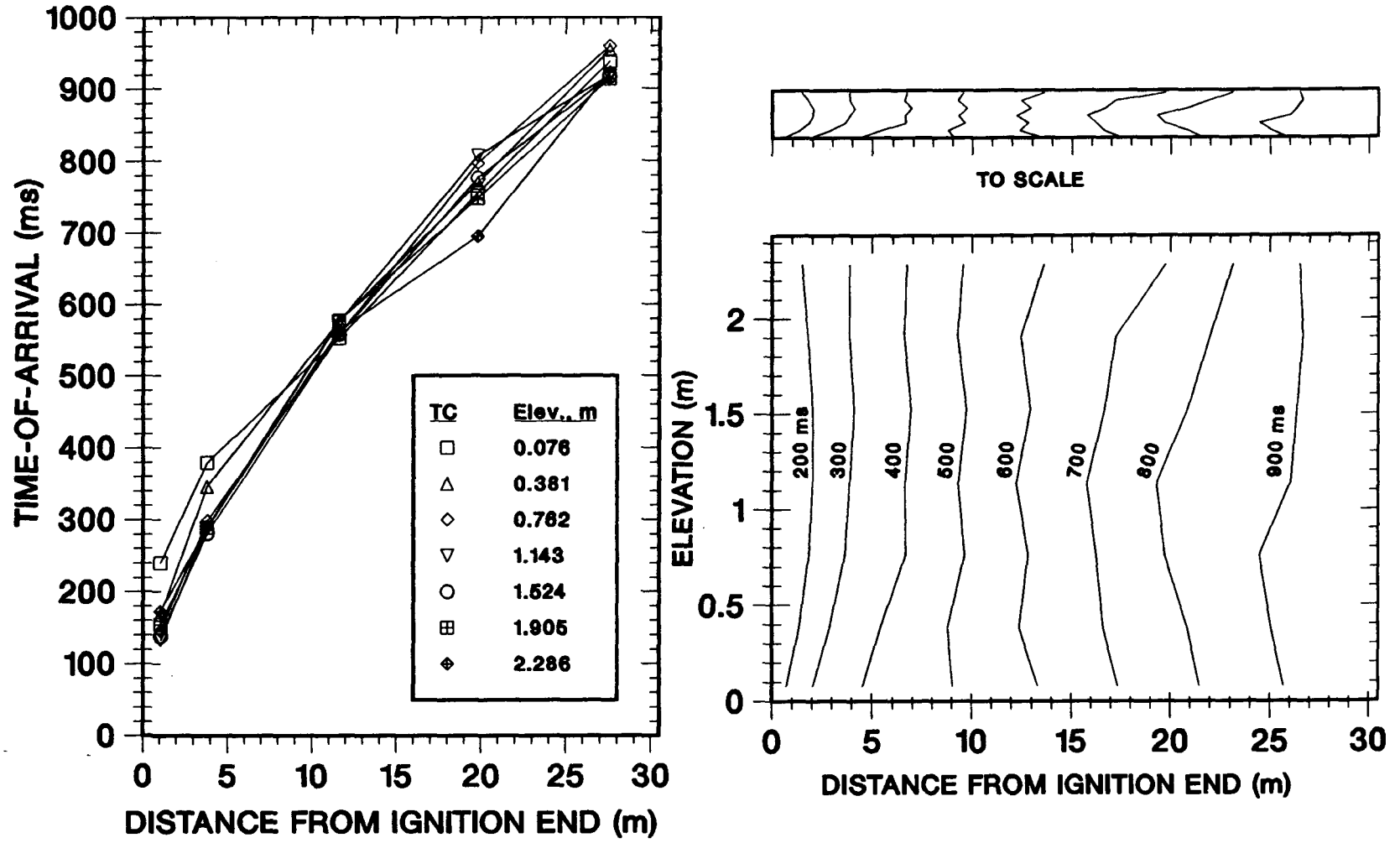

Figure 6.25. Test F-24, 15.5% H_2. 50% top venting. 33% blockage ratio. Combustion front trajectories and profiles.

The results from test F-29 with 18.5% hydrogen are shown in Figures 6.26 and 6.27. The acceleration of the deflagration is more pronounced than in test F-24. The highest observed deflagration propagation speed was 100 m/s. The initially convex flame shape becomes slightly concave. The peak pressures shown in Figure 6.27 were associated with an oscillating burst that appears to move down the channel with the flame. The magnitude of the peak pressures was low, under 25 kPa.

The results of test F-25 with 19.7% hydrogen are shown in Figures 6.28 and 6.29. Compared to test F-29, the flame speeds are much faster, flame acceleration was more pronounced, and the overpressures were much higher. Figures 6.29 shows as we move down the channel, the pressure peaks increase and the onset of the peak pressure becomes more abrupt. The pressure trace in Figure 6.29d, at 25.5 meters from the ignition end, is similar to that of a detonation. High-speed cinematography looking into the channel shows the formation of a bright luminous front which soon occupies the entire channel cross section. High-speed cinematography (2896 frames/s) perpendicular to the channel exit shows a luminous wave in five consecutive frames. A linear regression of the axial position versus time of the luminous wave shows it moved at a speed of 1616 m/s. The linear fit to the data had little scatter. This compares to the C-J speed of 1690 m/s relative to the unburned gas for 19.7% hydrogen-air mixture. The detonation cell width for such a mixture at 82 kPa, 300 K, is about 60 mm. Hence $d/\lambda \simeq 20$, and $W/\lambda \simeq 60$. The physical dimensions are larger than critical for DDT and propagation of the detonation from the channel into open space. The evidence appears to indicate that a transition to a self-sustaining detonation was achieved in test F-25. To the knowledge of the authors, this is the leanest hydrogen-air mixture in which a DDT was seen in a geometry with transverse venting.

Figure 6.30 summarizes the variation in equivalent planar flames speeds versus axial distance for these tests, excluding test F-26. The equivalent planar flame speeds increase monotonically down the channel and do not appear to reach a plateau. At each axial position, the equivalent planar flame speeds observed increase rapidly with increasing hydrogen mole fraction.

In summary, for tests with 50% top venting, the presence of obstacles

1. Greatly increased the flame speeds and overpressures compared to similar tests without obstacles.

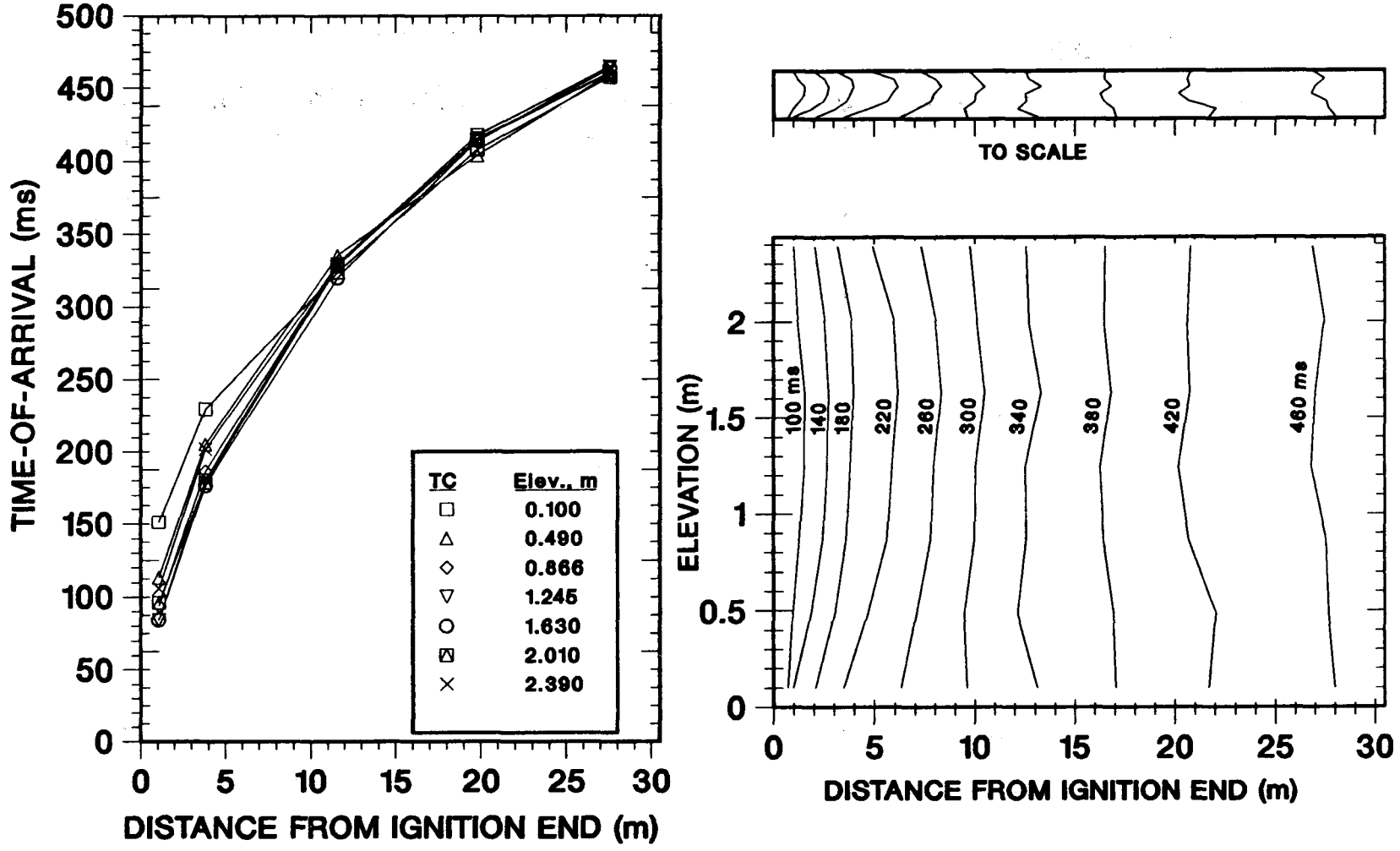

Figure 6.26. Test F-29, 18.5% H_2. 50% top venting. 33% blockage ratio. Combustion front trajectories and profiles.

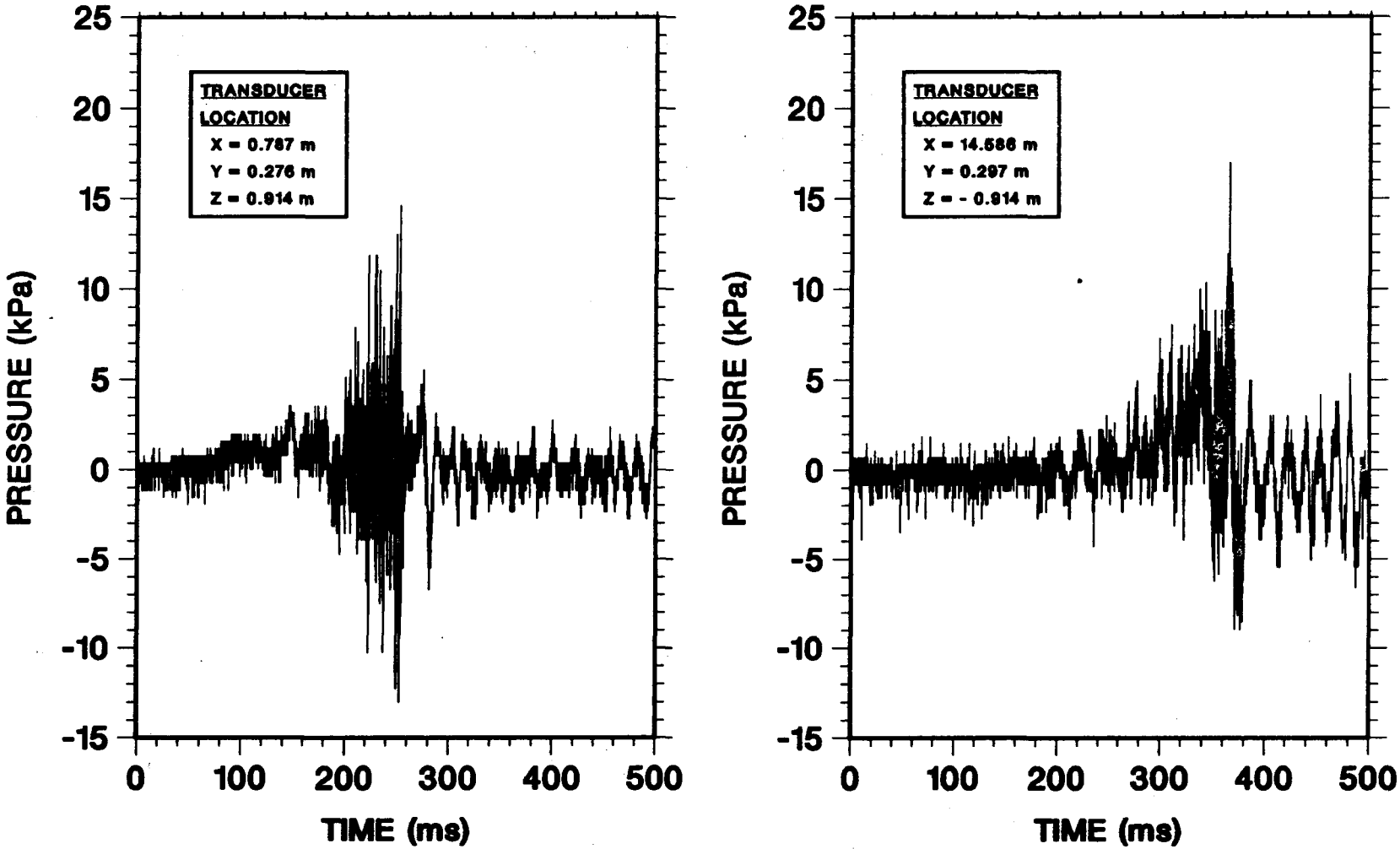

Figure 6.27. Test F-29, 18.5% H_2. 50% top venting. 33% blockage ratio. Pressure histories.

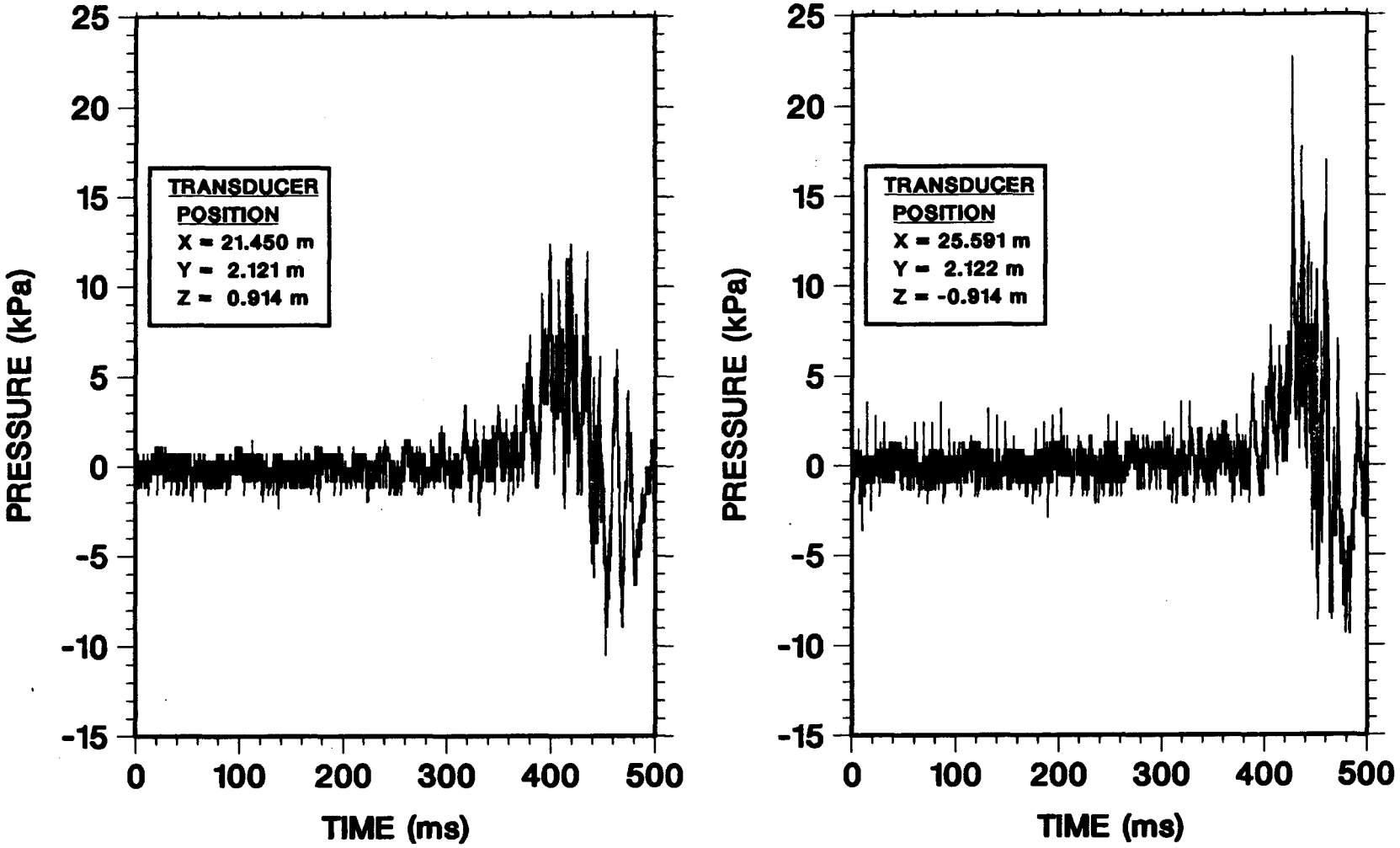

Figure 6.27. (Continued)

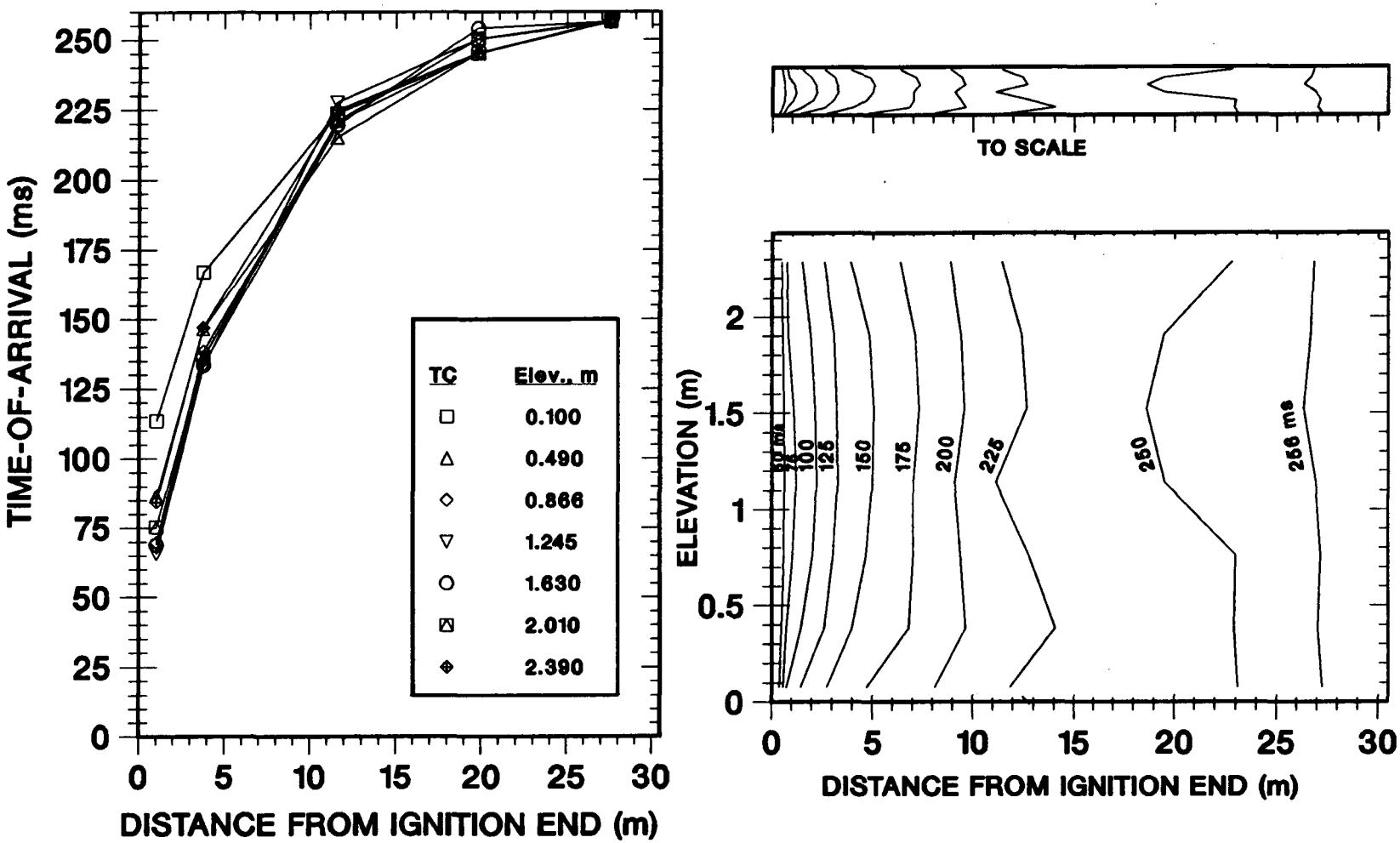

Figure 6.28. Test F-25, 19.7% H_2. 50% top venting. 33% blockage ratio. Combustion front trajectories and profiles.

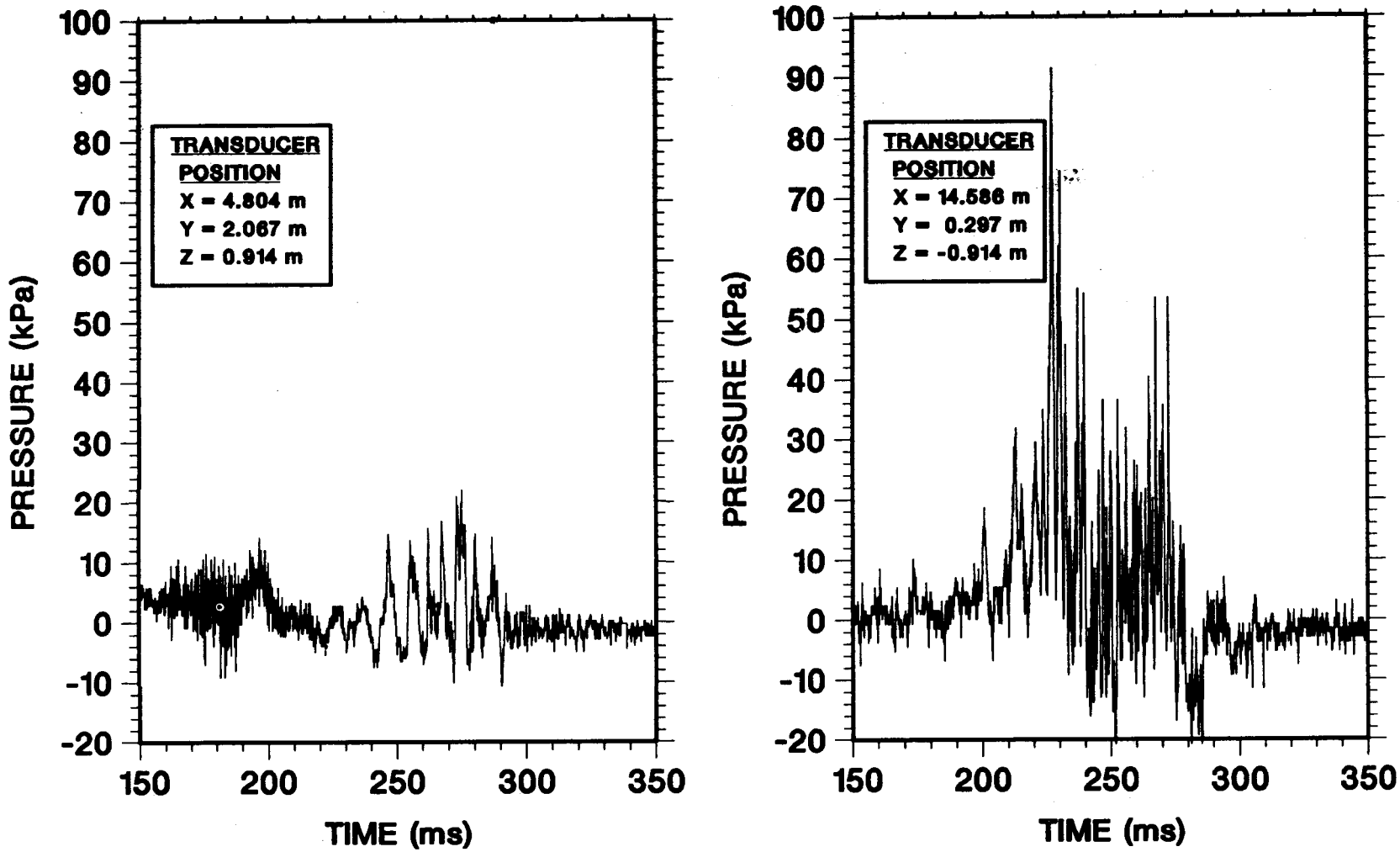

Figure 6.29. Test F-25, 19.7% H_2. 50% top venting. 33% blockage ratio. Pressure histories.

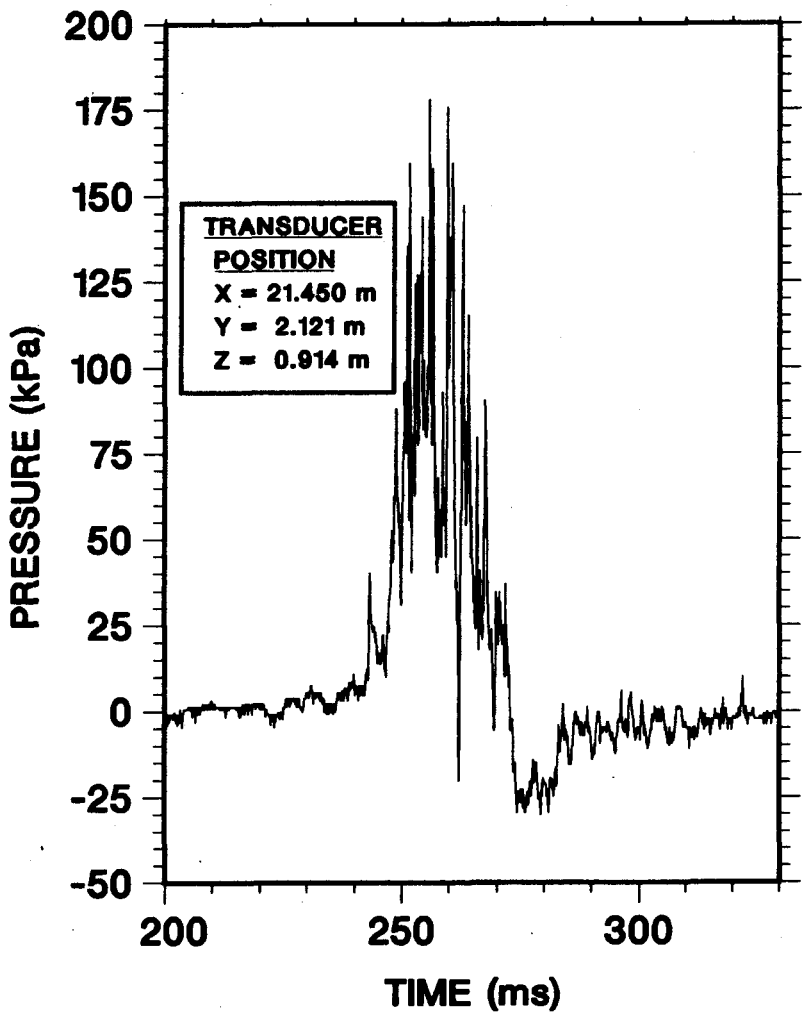

c.

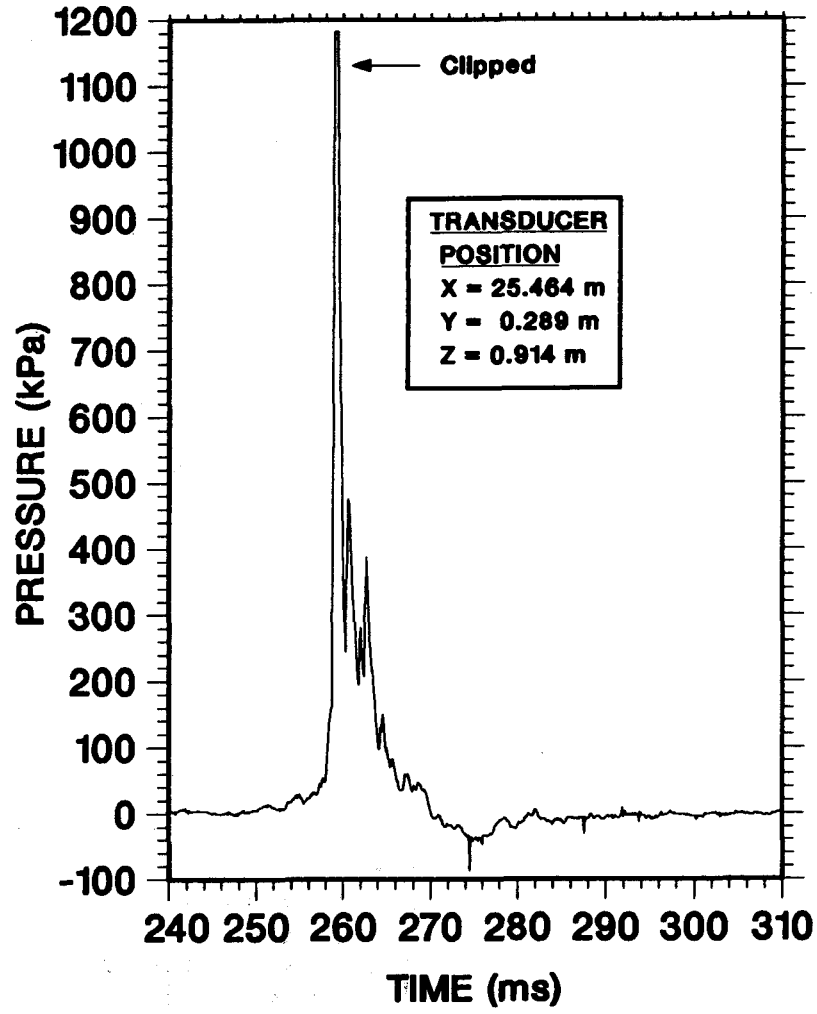

d.

Figure 6.29. (Continued)

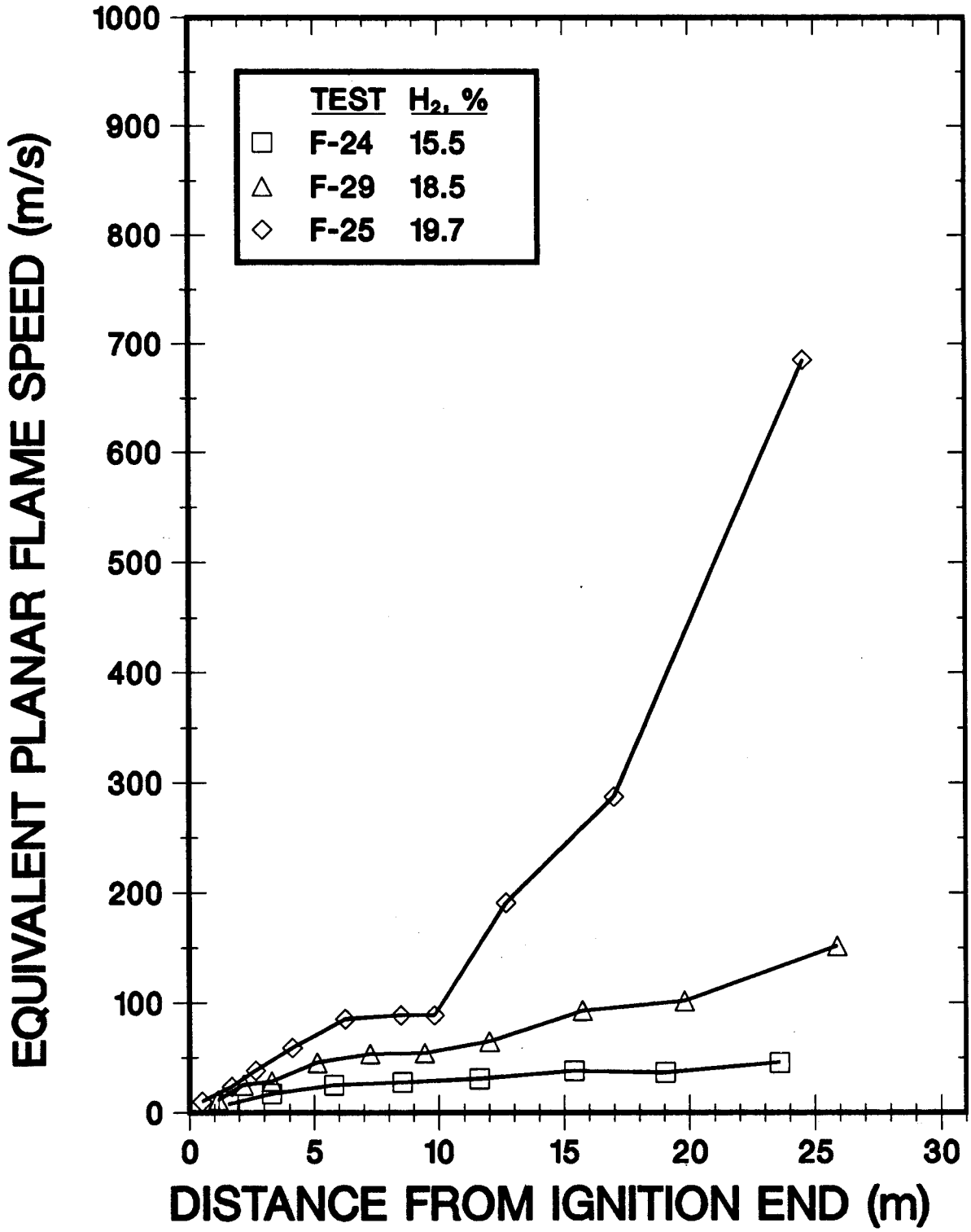

Figure 6.30. Comparison of Flame Speeds for Tests With 50% Top Venting and Obstacles

2. Showed flame acceleration continuing down the length of the channel, whereas there was no flame acceleration without obstacles.

3. Underwent DDT at 20% hydrogen, while there was no DDT without obstacles even at 28% hydrogen.

6.6 Tests With 13% Top Venting and No Obstacles

In tests F-15 to F-20, all but 13% of the top of the channel was covered with steel plates. The entire top was covered with a thin plastic sheet to act as a gas seal. There were no obstacles in the channel other than the mixing fans and the thermocouple rakes. It was expected that the results would be intermediate between those for tests with 50% and with no top venting. This was not what was observed. For the leaner mixtures, hydrogen mole fractions below 18%, the hypothesis was true. For the more reactive mixtures, the results were more violent than in tests without top venting.

Test F-15 with 15.4% hydrogen is an example of the expected behavior. The results of test F-15 are shown in Figures 6.31 and 6.32. Compared to a test with 50% top venting, F-6 with 15.5% hydrogen, shown in Figure 6.20, the flame speeds are higher as are the overpressures. However, compared to a test without top venting and leaner mixture, F-10 with 12.3% hydrogen, the overpressures are similar, as shown in Figure 6.2. As in next three tests to be discussed, the combustion front profile changes from initially a convex shape to a deeply concave one, with the top end travelling faster than the bottom. Also as in the next three tests, the pressure response near the ignition end, Figure 6.32a, shows a pressure peak at an early time, which must correspond to transients just after ignition, and a late burst. The further from the ignition end, the smaller the initial pressure peak until it is unobservable midway down the channel. The late time pressure burst moves down the channel from the exit end to the ignition end. In test F-15 its magnitude at the exit end was similar to that at the ignition end, but higher peaks were seen at some of the transducers midway down the channel.

The shape of the combustion front of test F-16 with 17.6% hydrogen, shown in Figure 6.33, is similar to that of test F-15 except that the speeds are higher and the faster propagation speed of the flame near the top plates compared to the floor is more pronounced. The pressure histories shown in Figures 6.34 for test F-16 are similar to that of test F-15, except that the magnitude of the overpressures is higher. The results for test F-18 with 18.1% hydrogen shown in Figures 6.35 and 6.36, and for test F-20 with 20.7% hydrogen shown in Figures 6.37 and 6.38, are again similar. The speeds and overpressures increase rapidly with increasing hydrogen content, but the flame shapes, flame acceleration, and pressure histories are similar. However, the magnitude of the flame speeds and the peak overpressures become higher than for comparable tests with no top venting.

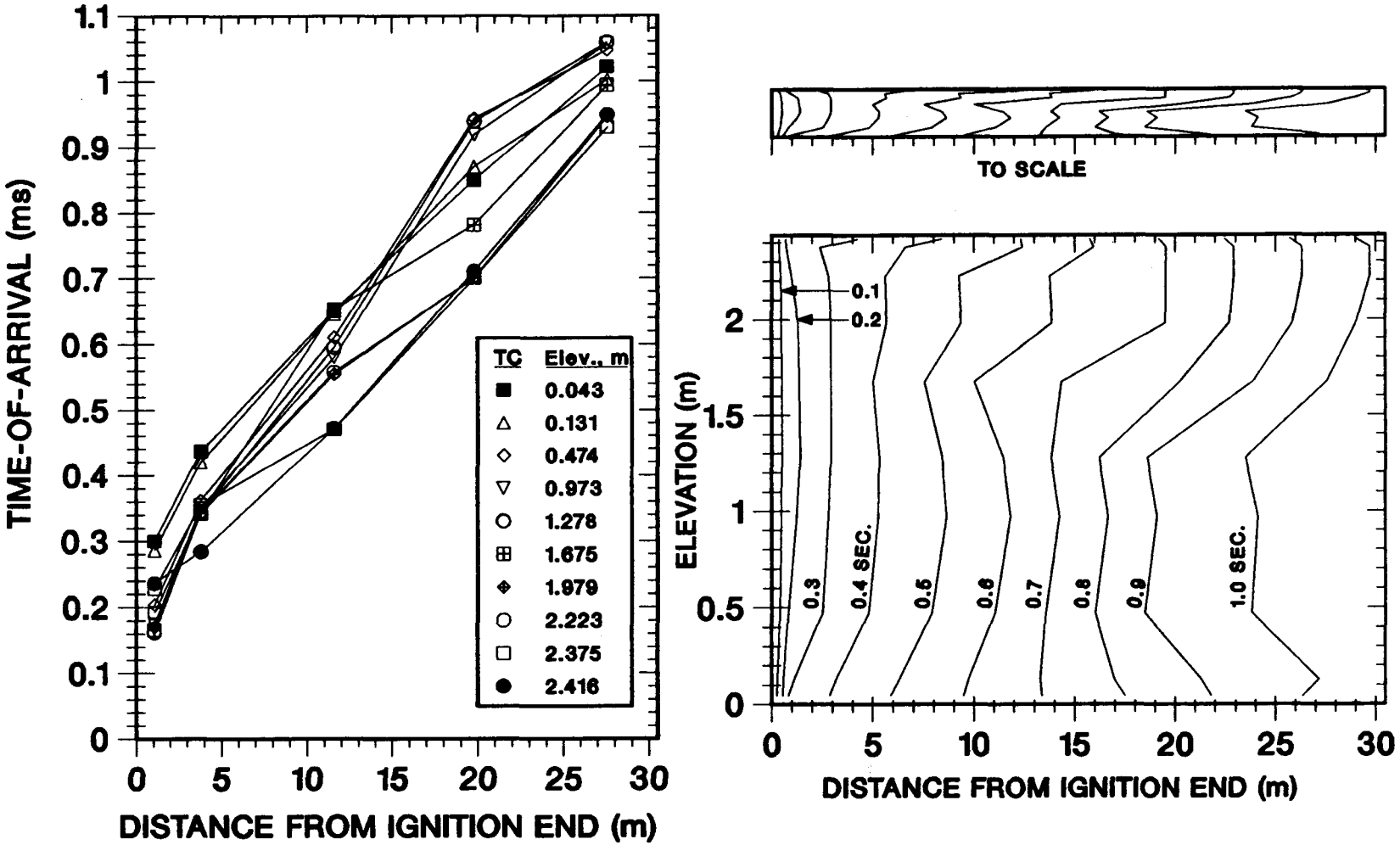

Figure 6.31. Test F-15, 15.4% H_2. 13% top venting. No obstacles. Combustion front trajectories and profiles.

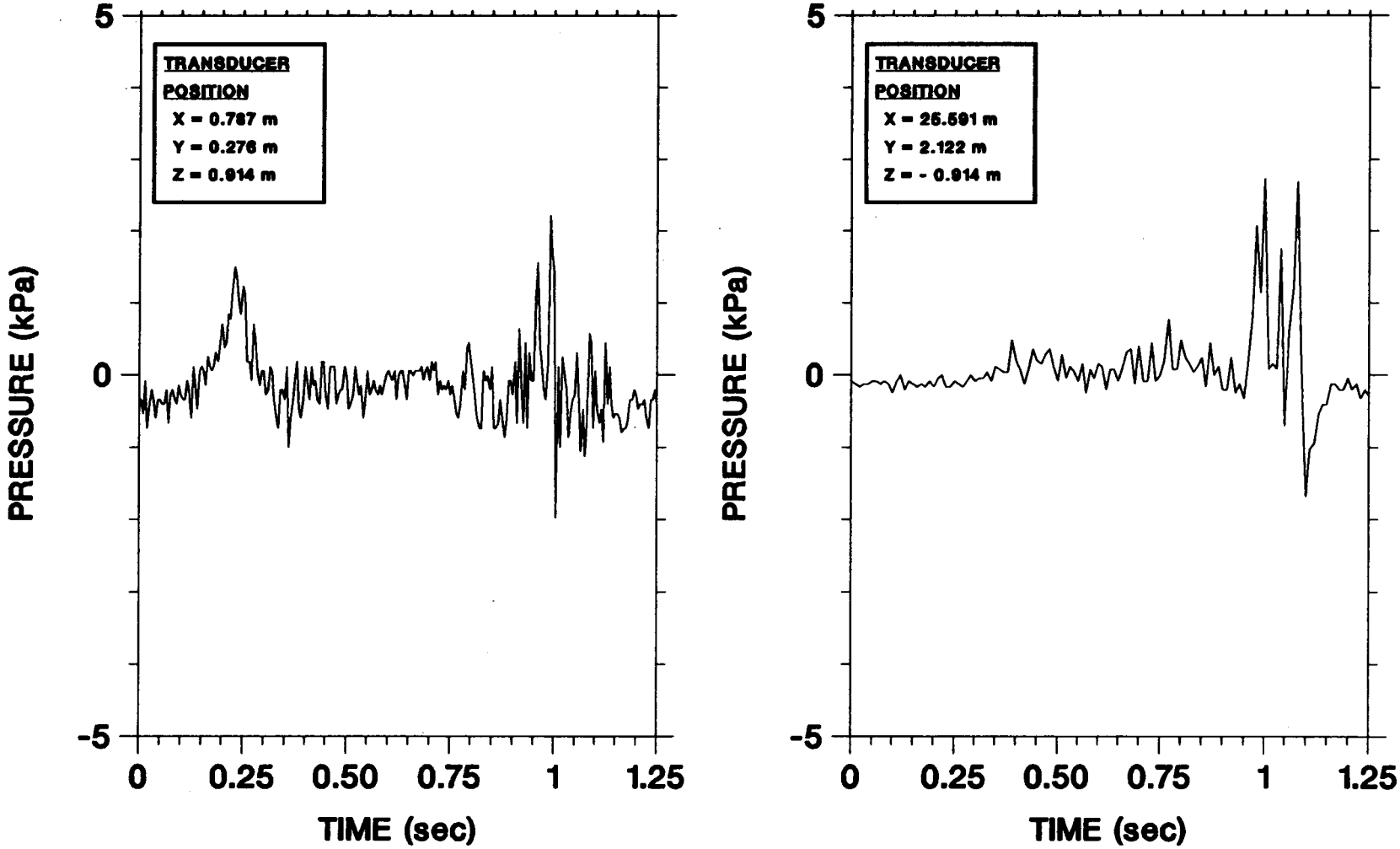

Figure 6.32. Test F-15, 15.4% H_2. 13% top venting. No obstacles. Pressure histories.

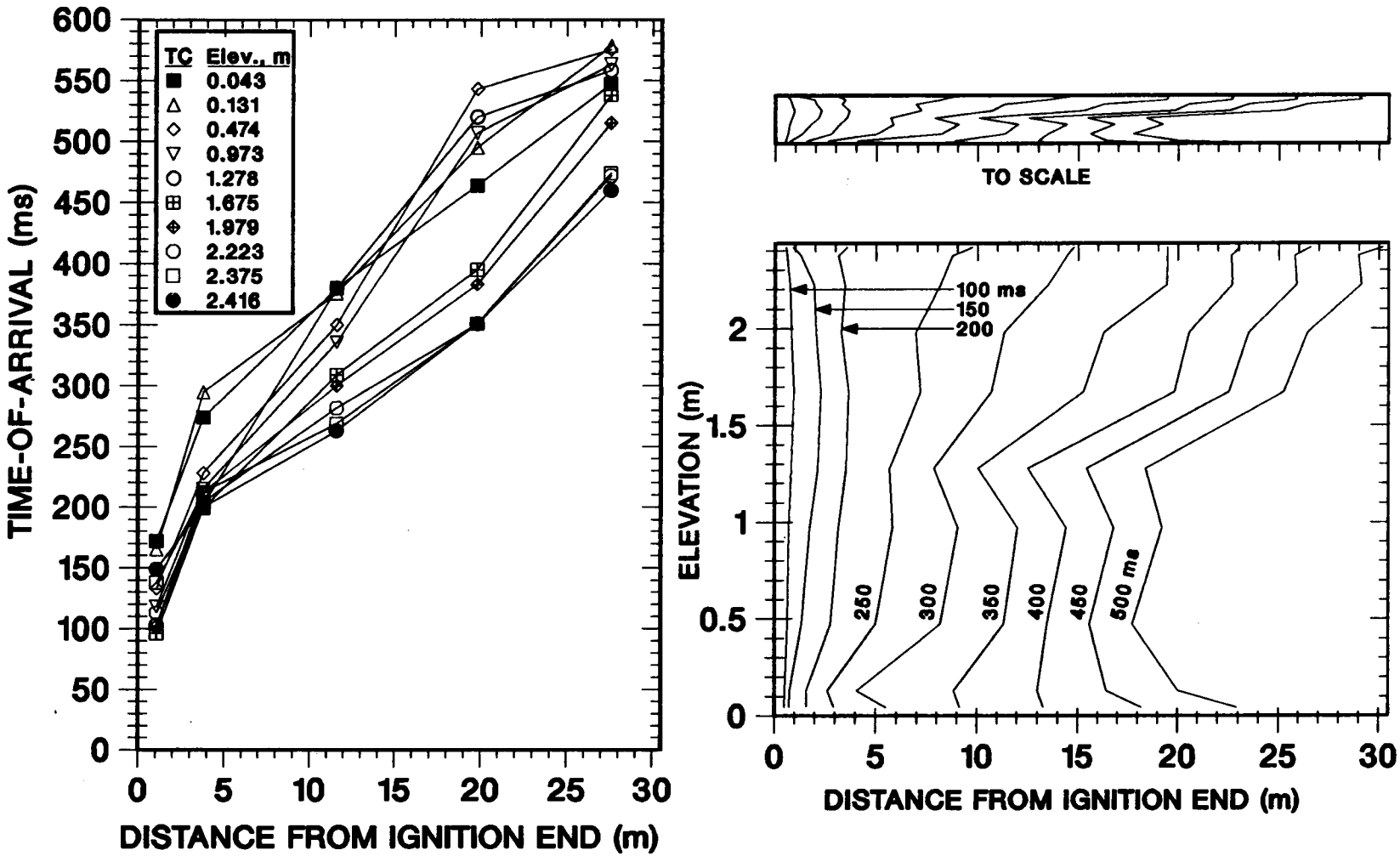

Figure 6.33. Test F-16, 17.6% H_2. 13% top venting. No obstacles. Combustion front trajectories and profiles.

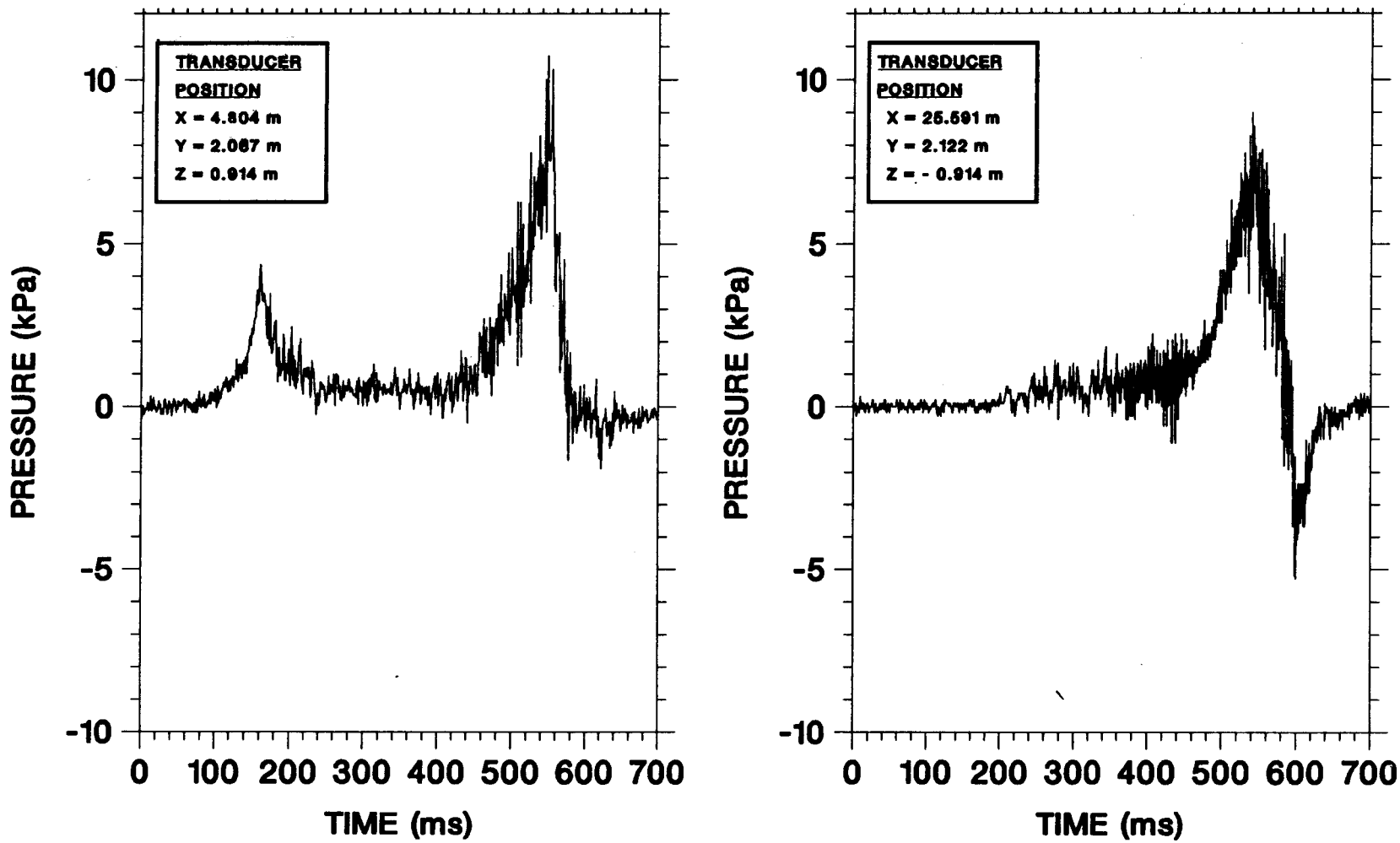

Figure 6.34. Test F-16, 17.6% H_2. 13% top venting. No obstacles. Pressure histories.

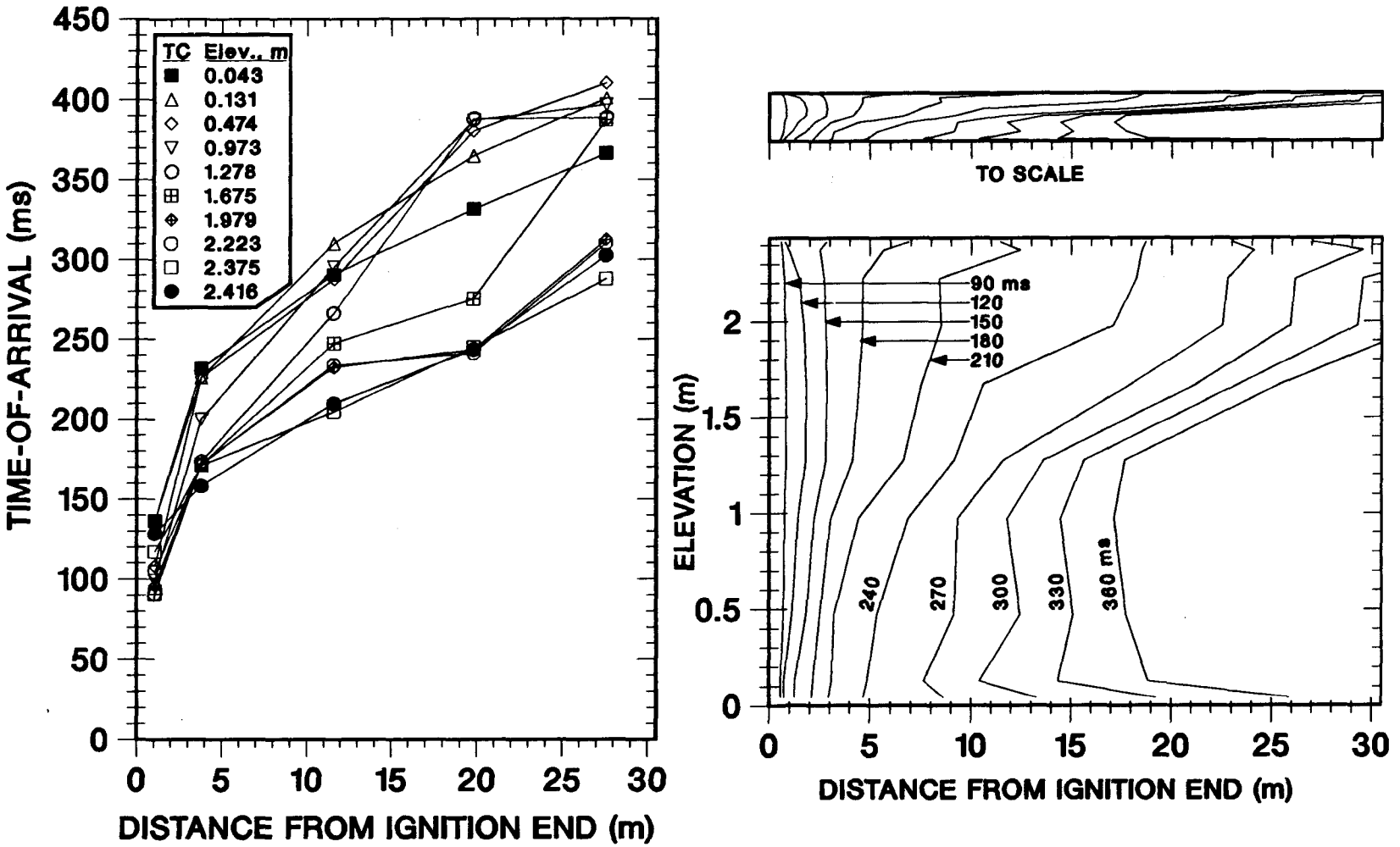

Figure 6.35. Test F-18, 18.1% H_2. 13% top venting. No obstacles. Combustion front trajectories and profiles.

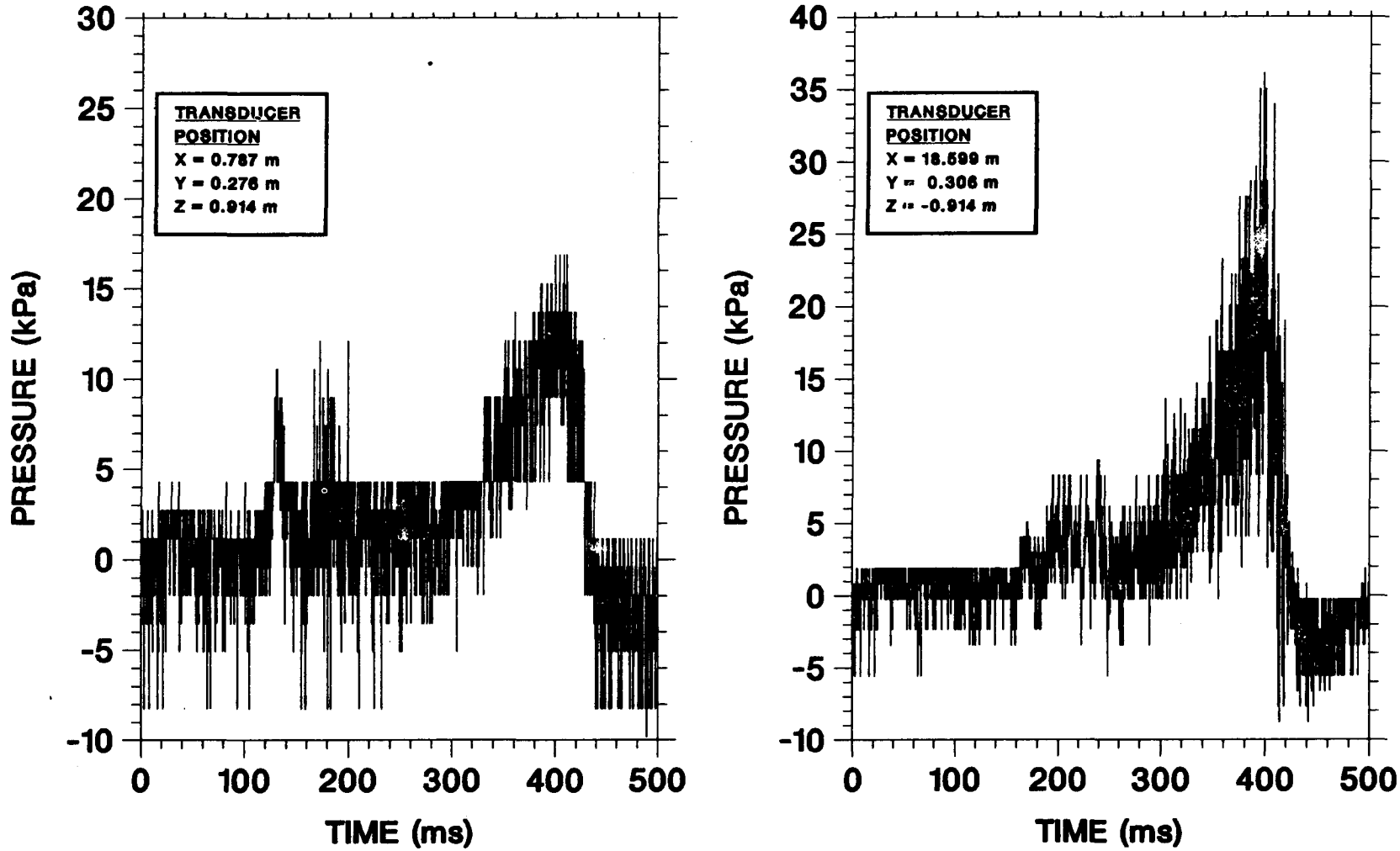

Figure 6.36. Test F-18, 18.1% H_2. 13% top venting. No obstacles. Pressure histories.

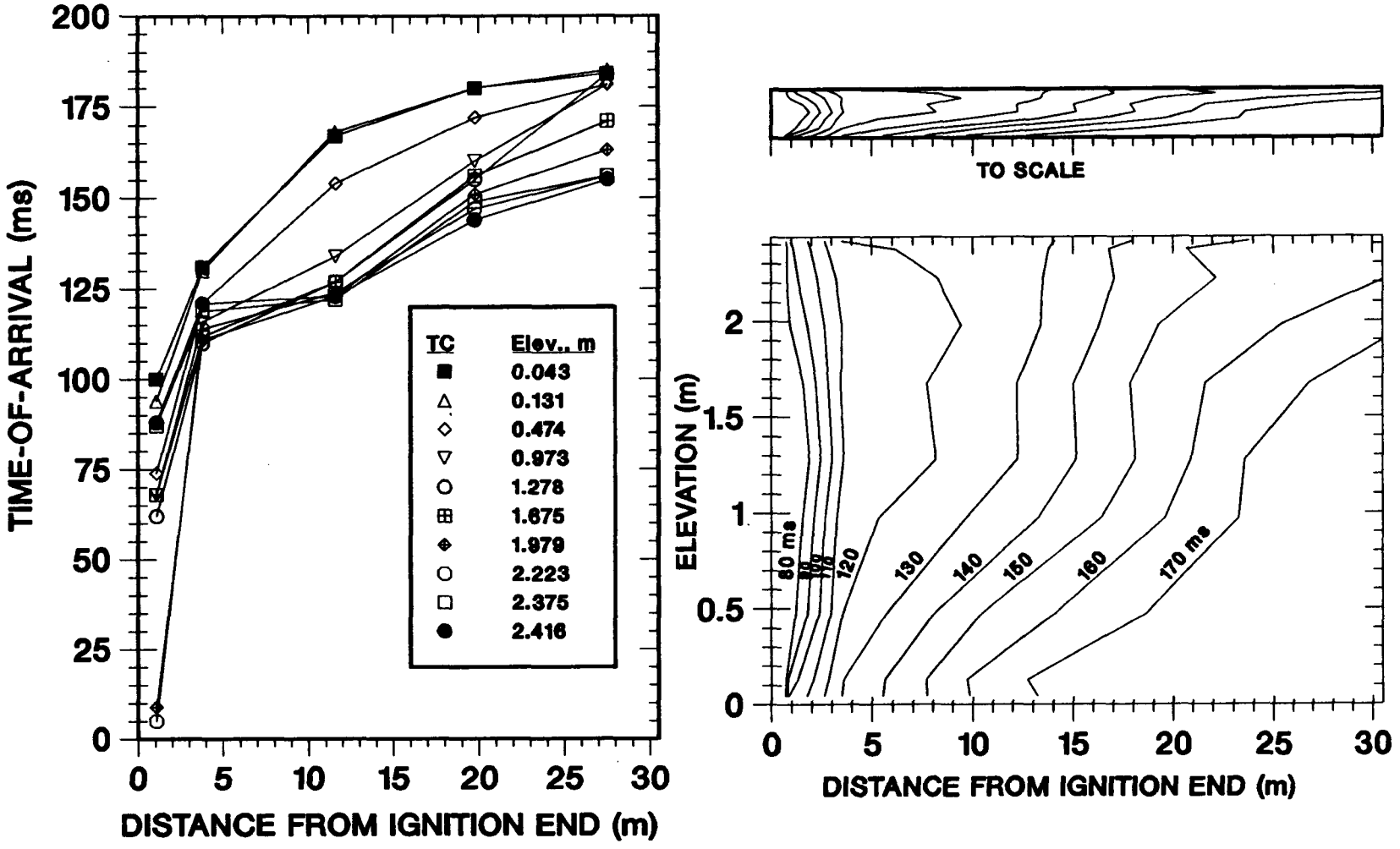

Figure 6.37. Test F-20, 20.7% H_2. 13% top venting. No obstacles. Combustion front trajectories and profiles.

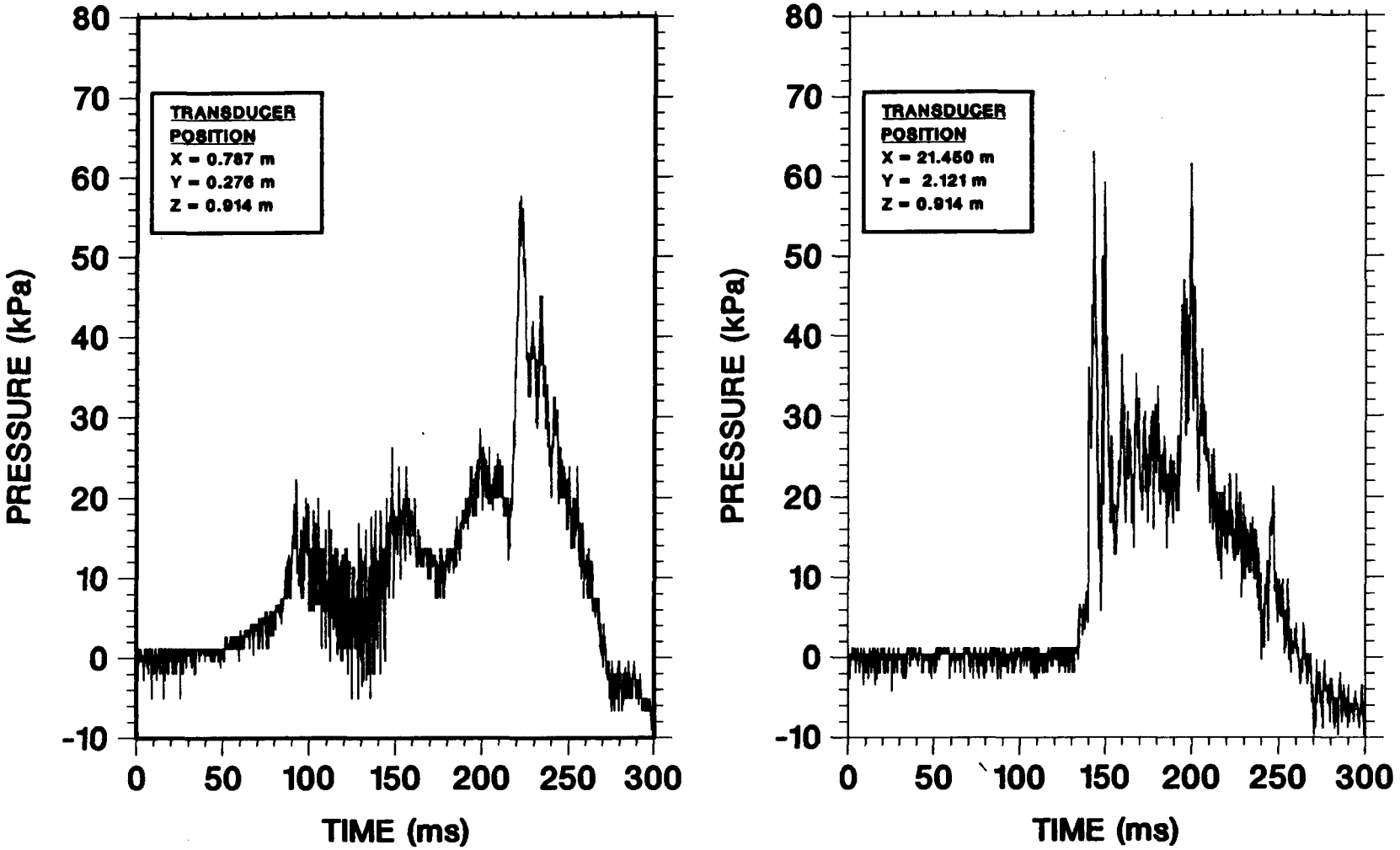

Figure 6.38. Test F-20, 20.7% H_2. 13% top venting. No obstacles. Pressure histories.

The results of test F-19 with 24.8% hydrogen are shown in Figures 6.39 and 6.40. A DDT was observed at roughly 11 meters from the ignition end. At the time, this result was so unexpected that all but two of the pressure transducers were set with too high an amplifier gain. The pressure peak was clipped for these transducers, although their results are still useful for determining detonation/retonation time-of-arrival. The response of the two transducers that did not saturate is shown in Figure 6.40. High speed cinematography taken along the channel axis from the exit end show that the detonation began at the top and progressed to cover the entire cross section. When the detonation left the channel exit it was essentially planar and perpendicular to the channel axis.

The variation of the equivalent planar flame speed versus axial position is shown in Figure 6.41 for the tests with 13% venting and no obstacles. DDT occurred so rapidly in test F-19, that there were too little data to accurately determine the deflagration speed prior to transition. Consequently, the curve for F-19 is suspect. The results for tests F-20, F-18, and F-16, show a flame acceleration leading to a first velocity peak followed by a small decline in velocity and then a second velocity increase. If we had carried out test F-20 prior to test F-19, we would not have been so surprised that a DDT was observed, and that it occurred about 11 meters from the ignition end.

The conclusion that 13% top venting results are more severe than no top venting results for sensitive mixtures and that both are more severe than 50% top venting results is clearly seen in Figure 6.42. We compare the time-of-arrival of the combustion front midway between the floor and the ceiling for a test with no top venting, F-12, a test with 50% top venting, F-4, and a test with 13% top venting, F-19. The hydrogen mole fractions are roughly comparable, 24.7%, 28.0%, and 24.8%, respectively. With 50% top venting the flame speed is slowest and there is no DDT, even though the hydrogen mole fraction was higher than in the other two tests. With no top venting, the flame speeds were higher, and DDT occurred near the exit. With 13% top venting, the DDT occurred much near the ignition end. The flame speeds for 13% top venting were as fast or faster than for no top venting.

6.7 Test F-9

The primary objectives of this research were to observe flame acceleration and DDT. Consequently, we planned on carrying out tests with hydrogen mole fractions no lower than 12%. However, due to a problem in carrying out test F-9, the expandable bag could not be fully inflated, and we were forced to test with only 6.9% hydrogen. This hydrogen mole fraction is below the

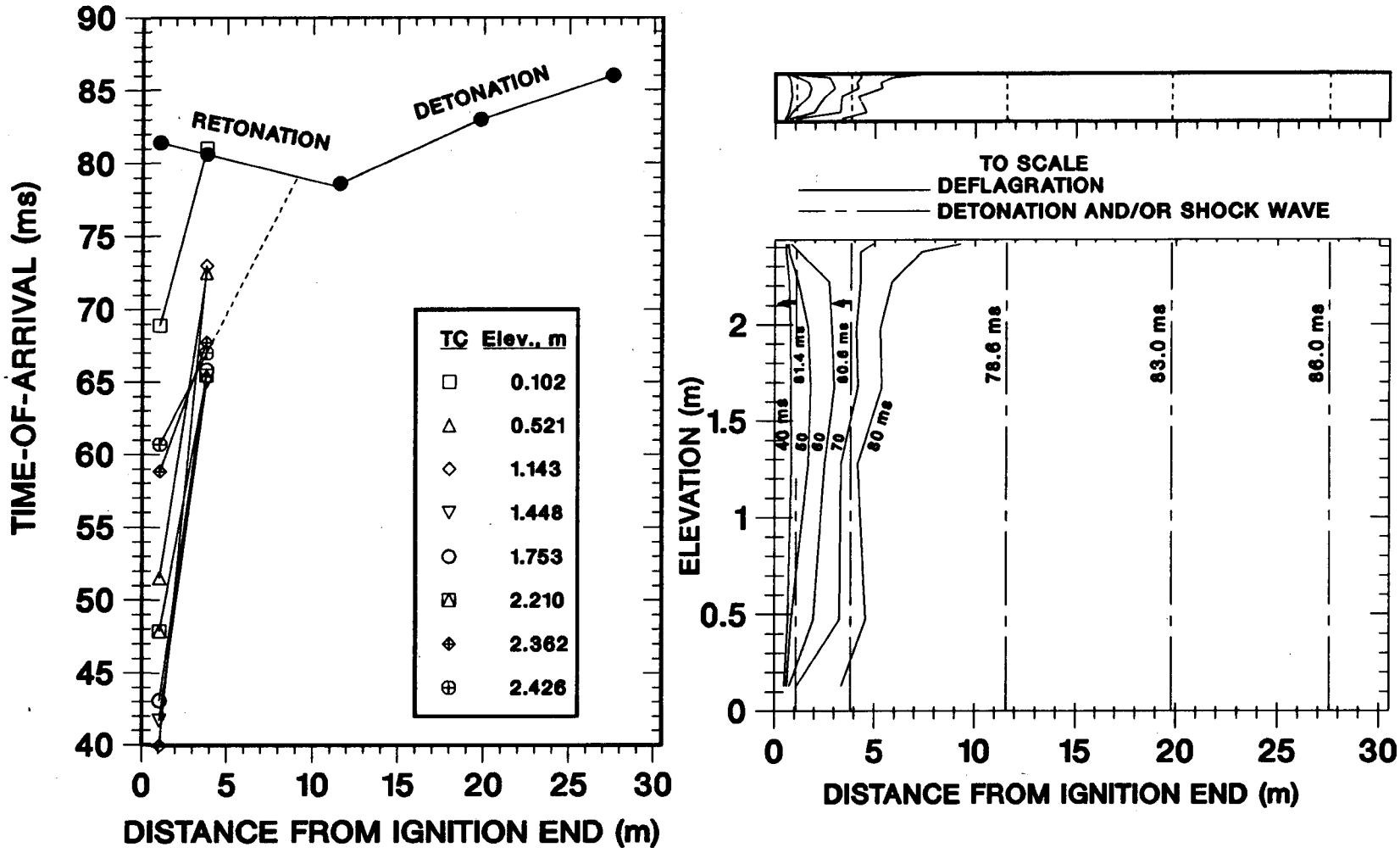

Figure 6.39. Test F-19, 24.8% H_2. 13% top venting. 33% blockage ratio. Combustion front trajectories and profiles.

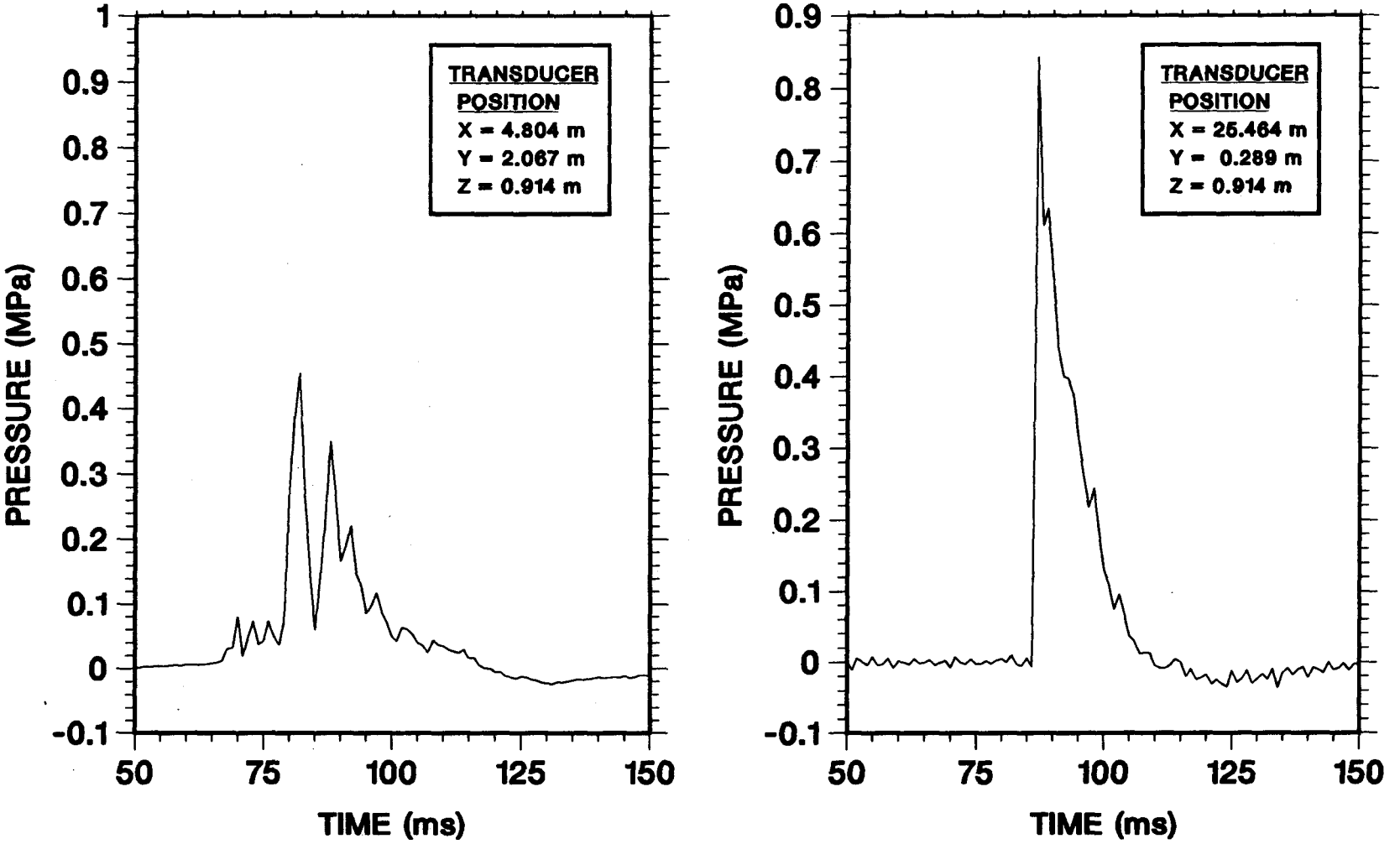

Figure 6.40. Test F-19, 24.8% H_2. 13% top venting. No obstacles. Pressure histories.

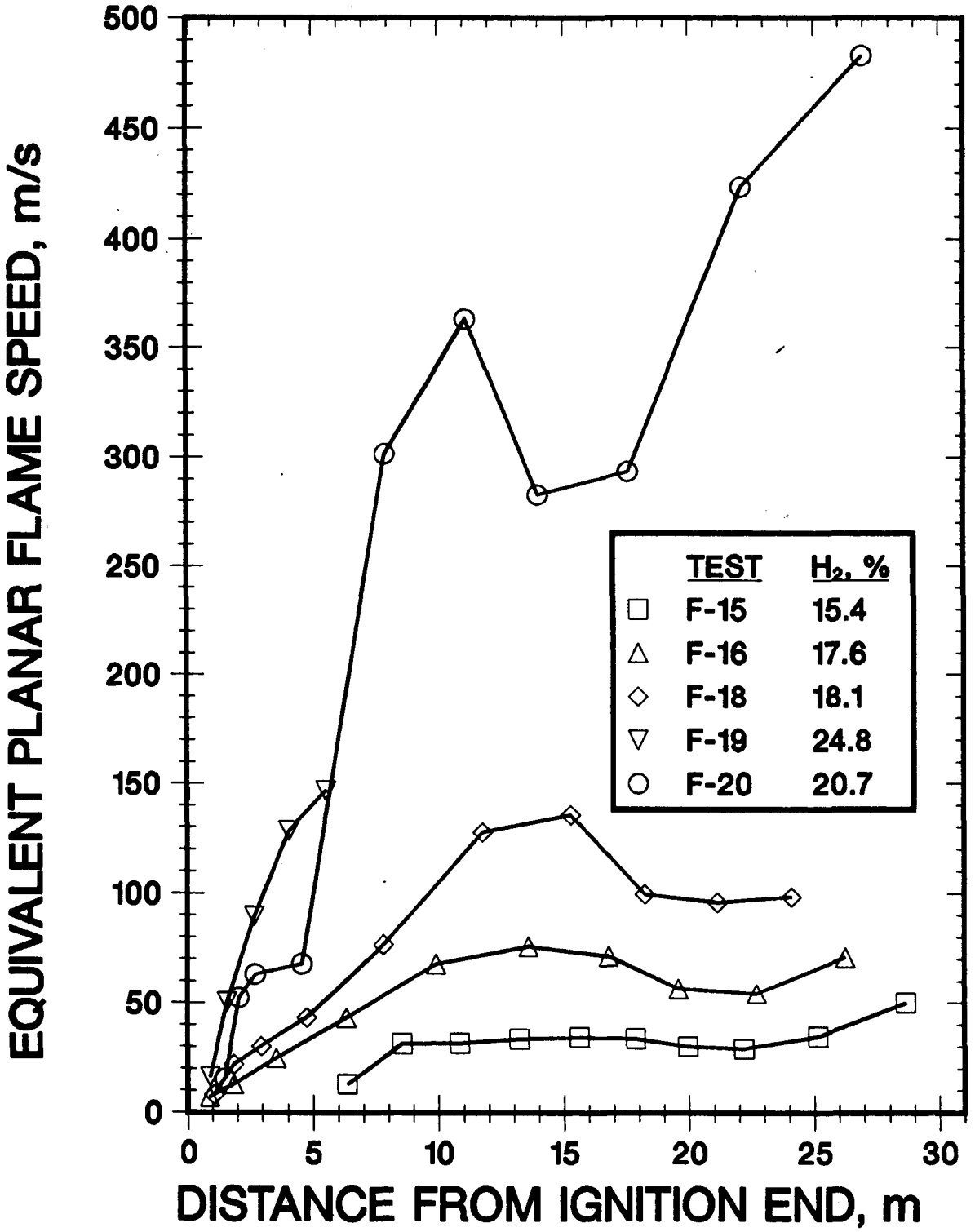

Figure 6.41. Comparison of Flame Speeds for Tests With 13% Top Venting and No Obstacles

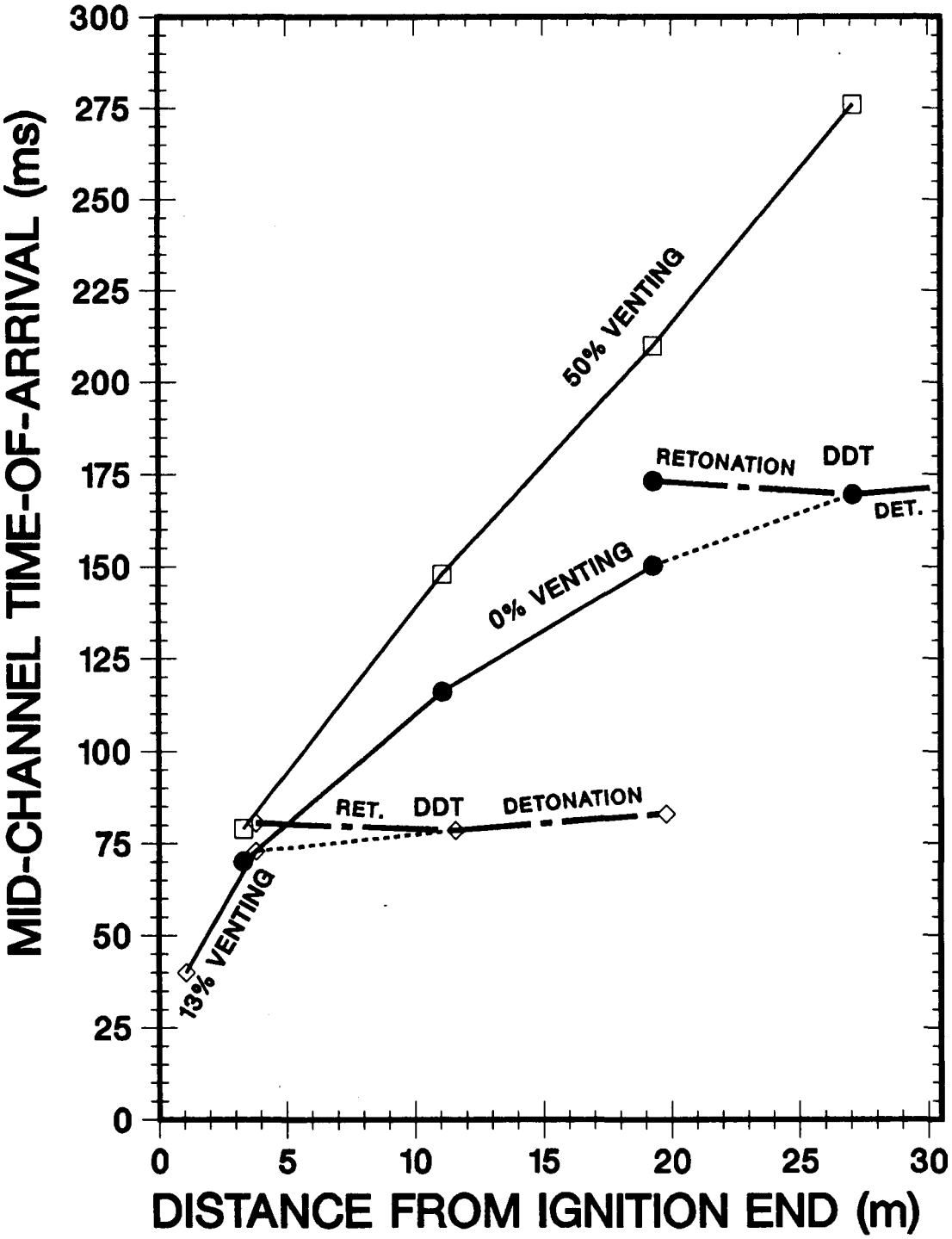

Figure 6.42. The Effect of Transverse Venting on Tests With ~25% H_2 and No Obstacles

downward flammability limit of 9.0%, above the upward flammability limit of 4.1%, and just above the horizontal flammability limit of 6.0%. The results were interesting enough to report, but they were different from the results of the other tests. For this test, the channel had no top venting and no obstacles.

After ignition, there were no observable effects seen on video or audible from the blockhouse. We thought we had a misfire. However, inspection of the data showed that there had been a flame. A clear flame time-of-arrival was indicated on the top two thermocouples for each rake. A faint indication of a slight temperature rise was seen on the third thermocouple from the top, presumably due to radiation from the flame. There was no response on the lower thermocouples. The results are shown in Figure 6.43. The near straightness of the line connecting the time-of-arrivals indicates that a flame front moved down the channel at a nearly constant speed of 1.2 m/s. The burned gas was confined to the region between the ceiling, 2.438 m above the floor, and a lower level that was above 2.050 m but below 2.354 meters above the floor. Hence the thickness of the burning layer was between 0.084 and 0.388 meters (3.3 to 15.3 inches). It appears there was a balance between buoyancy and burning giving quasi-steady conditions.

6.8 Summary

Figures 6.44 through 6.46 summarize the salient results of the FLAME tests. This section will be devoted to explaining these figures. Because these figures condense a great deal of information, they must be carefully scrutinized to be fully understood.

Figure 6.44 shows the region of deflagration-to-detonation transition as a function of the hydrogen concentration, top venting fraction, and the presence or absence of obstacles. The open circles indicate tests without obstacles in which DDT did not occur; the shaded circles indicate tests without obstacles in which DDT did occur. First considering the tests with no obstacles, we see that for 50% top venting DDT does not occur even near stoichiometric mixtures. For no top venting and 13% top venting, the data points on the figure indicate the borderline hydrogen concentration for DDT is below 25% hydrogen. It is seen that there are not enough tests in the hydrogen mole fraction range 20%-24% to indicate which of the two degrees of top venting has a lower borderline hydrogen concentration. Because the location of DDT in test F-19 with 13% top venting is nearer the ignition end than in test F-12 with no top venting, we believe low degrees of transverse venting promote DDT. The increase in flame speed and overpressure due to the turbulence created by flow out the vents, or possibly reignition of combustible gas in the channel from rapidly burning gases above

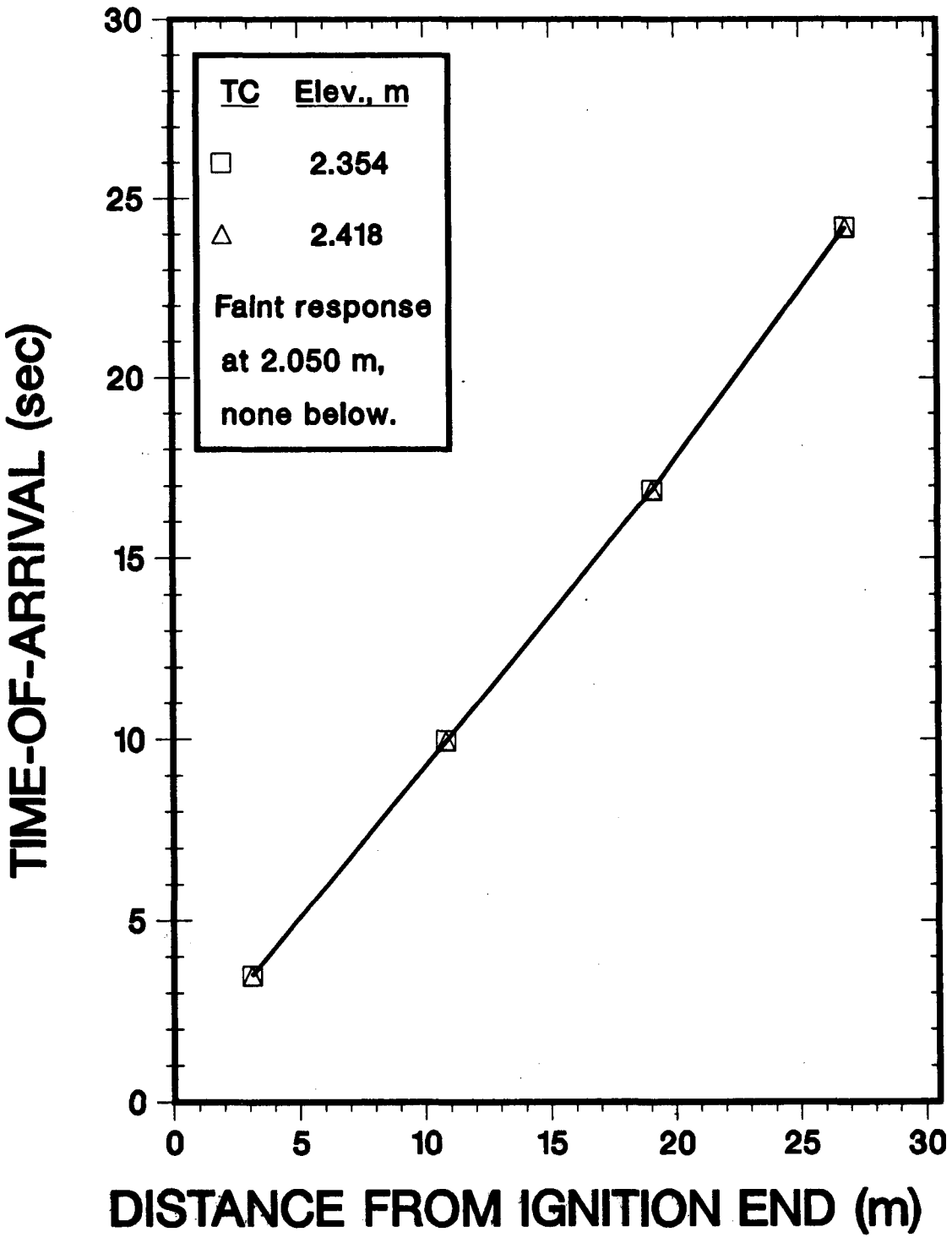

Figure 6.43. Test F-9, 6.9% H_2. No top venting. No obstacles. Deflagration trajectories.

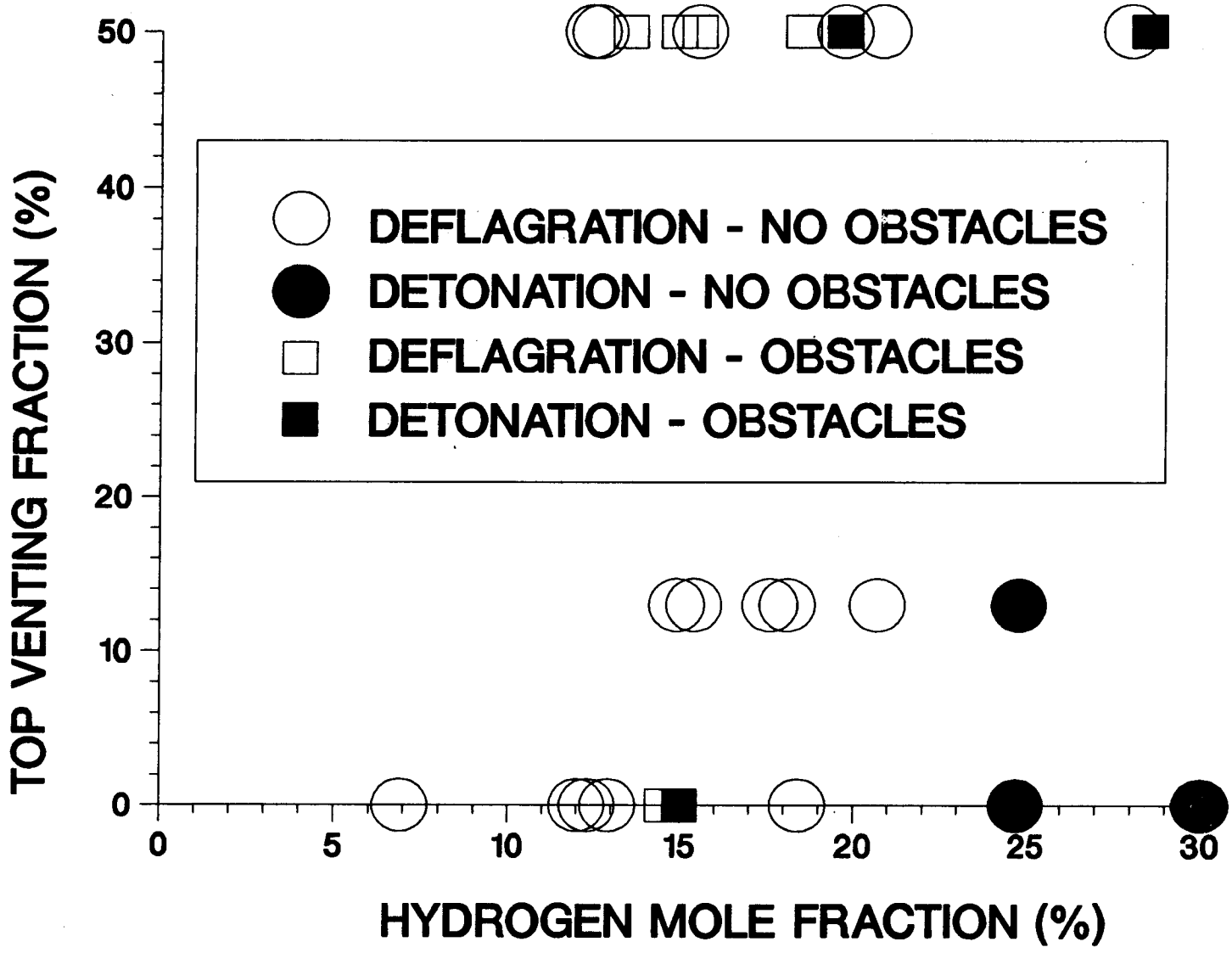

Figure 6.44. Flame DDT Results

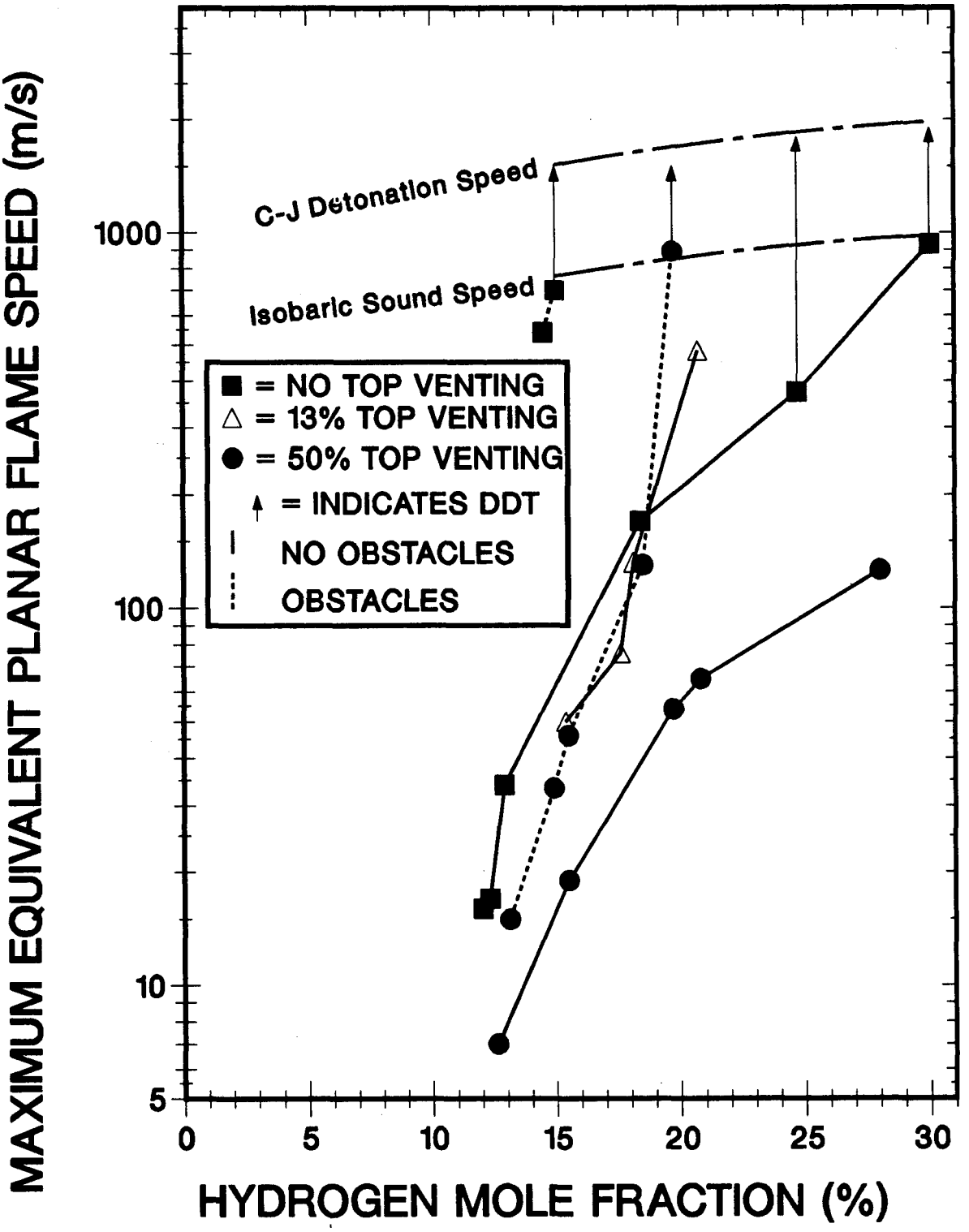

Figure 6.45. Flame Velocity Results

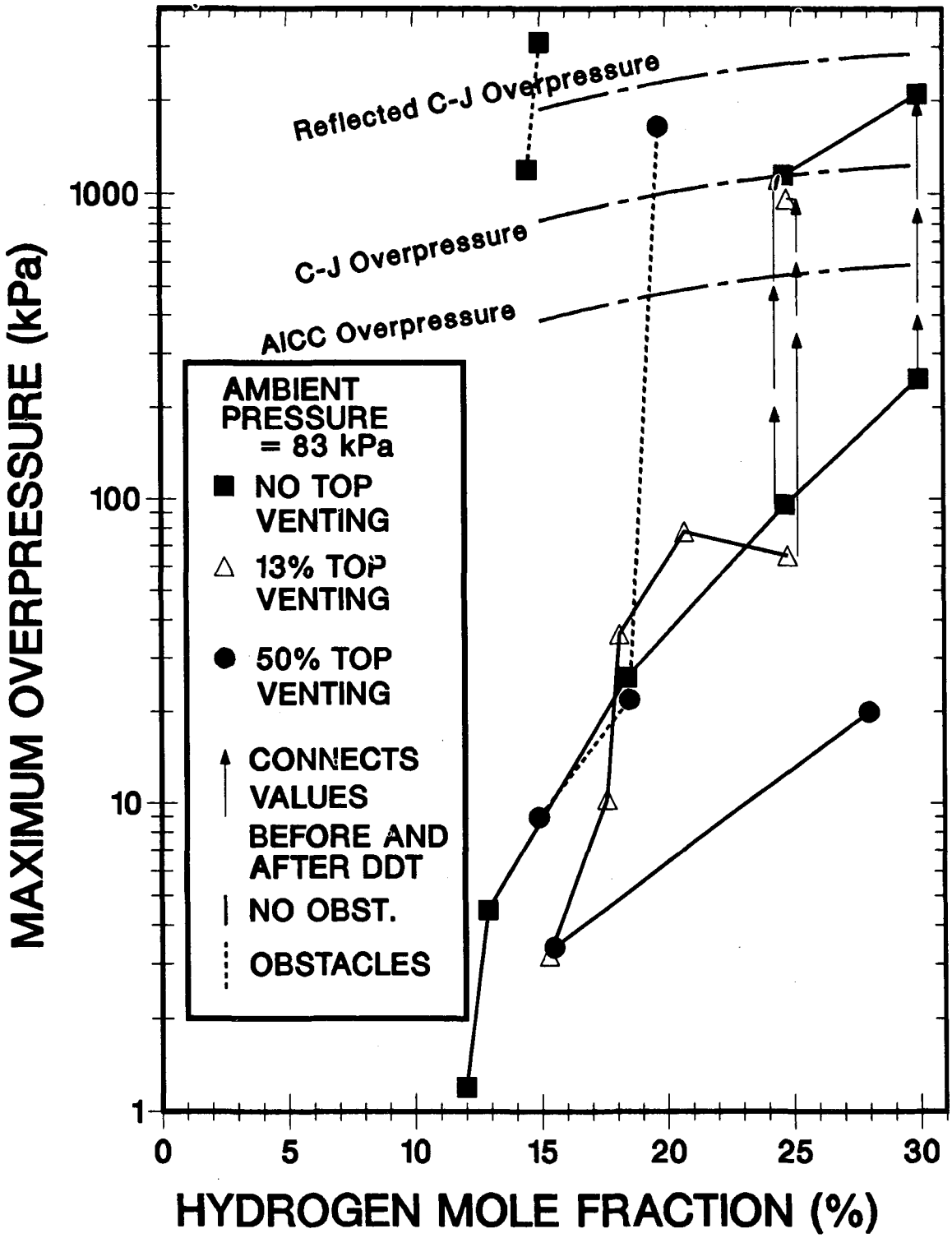

Figure 6.46. Flame Overpressure Results

the plates, overcomes the pressure relief due to flow of gas out of the channel. We expect that the borderline hydrogen concentrations for DDT with small degrees of transverse venting are lower than for no transverse venting, although there are not enough data to show this. With larger degrees of transverse venting, the data do show the increase in borderline hydrogen concentration for DDT.

The open squares in Figure 6.44 indicate tests with obstacles in which there was no DDT; the shaded squares indicate tests with obstacles in which there was DDT. The most striking result of the tests with obstacles is that the presence of obstacles greatly reduces the required hydrogen concentration for DDT. DDT is achieved with 50% top venting, but at a higher concentration than with no top venting. There were no tests carried out with obstacles and 13% top venting.

Figure 6.45 shows the maximum equivalent planar flame speed as a function of hydrogen mole fraction for the five series of tests, no top venting and no obstacles, no top venting and obstacles, 50% top venting and no obstacles, 50% top venting and obstacles, and 13% top venting with no obstacles. The legend box indicates that tests with no top venting are indicated with shaded squares; tests with 13% top venting are indicated with open triangles, and tests with 50% top venting are indicated with shaded circles. The tests with obstacles are distinguished from those without because the data points are connected with a dashed line instead of a solid line. Shown in chain-dashed lines at the top of the graph are the isobaric sound speed for the burned gas, and the Chapman-Jouguet detonation speed. For those tests in which DDT did occur, an upward pointing arrow from the maximum equivalent planar flame speed point indicates that the combustion accelerates and approaches detonation speeds. However, since detonation speeds were not accurately measured, no measured detonation speed is shown.

Figure 6.46 shows the maximum overpressure as a function of hydrogen concentration for the same five series of tests with the same graphical conventions as in Figure 6.45. Shown in chain-dash lines above are the adiabatic isochoric complete combustion (AICC) pressure and the C-J detonation pressure. Since pressures were measured near or after DDT, we do indicate separated points for the maximum overpressures of the deflagrations and detonations. Note that there were pressures measured above C-J values, but below normally reflected C-J values from rigid surfaces. The ratio of reflected C-J pressure to C-J pressure for hydrogen-air mixtures is close to 2.3.

The vertical scale of Figures 6.45 and 6.46 are logarithmic. This indicates that the flame speeds and overpresssures increase rapidly over orders of magnitude range as the hydrogen concentration is increased. The major effect of the presence of obstacles is shown by lower hydrogen concentration required to attain the same maximum equivalent flame speed or overpressure compared to a similar test without obstacles. Examining Figure 6.25, we see that no DDT occurred below 400 m/s. With 50% top venting and no obstacles present, this speed would not have been attained even for a stoichiometric mixture. The inhibiting effect of large degrees of transverse venting on the flame speed and overpressures is evident. The complex behavior of small degrees of transverse venting shows in the 13% top venting test series. For lean mixtures below approximately 18% hydrogen mole fraction, the flame speeds are lower and overpressures comparable to similar tests without transverse venting. Above this hydrogen concentration, the flame speeds and overpressures are higher than in tests without transverse venting.

7. CONCLUSIONS

7.1 Introduction

The purpose of this section is to draw some general conclusions from the results of the 29 tests discussed in Section 6. In particular, the results are summarized in Section 6.7 and Figures 6.44 through 6.46. The unique aspect of the data is the large scale of the FLAME channel. FLAME is a half-scale model of the upper plenum region of an ice condenser containment. These studies of flame acceleration and transition to detonation of hydrogen-air mixtures are applicable to nuclear reactor safety concerns (see Section 7.3), and also relevant to other safety problems.

The three variables in the tests were the hydrogen concentration, the degree of transverse venting, and the presence or absence of obstacles. The hydrogen mole fraction was varied between 12% and 30%. Leaner mixtures were excluded (except for test F-9) because they would not exhibit flame acceleration or deflagration-to-detonation transition (DDT) in this facility. Tests with mixtures on the rich side of stoichiometric would have been useful to determine if stoichiometric mixtures are the most dangerous, and how the decrease in reactivity on the rich side affects flame acceleration and DDT. Except for test F-26, only one obstacle configuration was used. More tests with other obstacle configurations would have been useful. One must keep in mind the limits of the testing program when considering the applicability of the conclusions to other geometries and mixtures.

7.2 Summary of Conclusions

The reactivity of the mixture is the most important variable in flame acceleration and DDT. This is in accord with the results of small-scale tests discussed in Section 1, and is expected. The maximum equivalent flame speeds in Figure 6.45 and the maximum overpressures in Figure 6.46 vary by over two orders-of-magnitude as a function of hydrogen concentration. Hence they are plotted logarithmically while the hydrogen mole fraction on the abscissa is plotted linearly. We found negligible flame acceleration and consequently no DDT at the lean limit of testing, 12% hydrogen. We did obtain DDT at 15% hydrogen with obstacles present and no transverse venting. Peraldi, Knystautas and Lee [67] found flame acceleration in hydrogen-air mixtures down to 10% hydrogen, and DDT down to 16% hydrogen, in a long 30-cm diameter tube with many

annular rings to promote flame acceleration. Although their geometry was of small scale compared to FLAME, their length/diameter ratio was much higher. Flame acceleration might have been observed at leaner mixtures if the FLAME channel were longer than 30.5 meters.

The presence of obstacles was the second most important variable. The presence of obstacles in the channel greatly increased the flame speeds, overpressures, and possibility of DDT. The boundary between deflagration and DDT occurred at a much lower hydrogen concentrations with obstacles present, as was shown in Figure 6.44. Again this is in accord with results found in small-scale tests.

In tests without obstacles and no transverse venting, the main mechanism of flame acceleration appears to have been hydrodynamic-combustion instabilities leading to a concave flame front. This "tulip-shaped" flame has been observed in small-scale tests [63,64] but not in large-scale tests. If there were no obstacles present in FLAME, it was easy to determine if there had been a DDT. The overpressures were much higher and a distinct wave (retonation) was seen moving back toward the ignition end. The retonation is a shock wave passing through burned gases, that promotes burning of any residual unburned gas pockets like a detonation.

It should be remembered that our tests with obstacles present mostly used a single obstacle configuration, simple baffles on the side walls with 33% blockage ratio. One test was done simulating the geometry in the ice condenser upper plenum region of PWRs with ice condenser containments. Hence, the conclusions reported in the following paragraphs for obstacle geometries were not verified over a range of obstacle configurations.

In contrast to the results without obstacles, with obstacles present it is difficult to tell if DDT has occurred when the tested mixtures are at borderline concentrations. The presence of "quasi-detonations", i.e., detonations whose structure is greatly perturbed by the presence of the obstacles and which move at speeds considerably below the detonation C-J speed, tends to blur the strict separation between highly-accelerated deflagrations and detonations. The peak overpressures can be high even without DDT. From a safety point of view, it may be unimportant to distinguish if a highly accelerated flame has undergone transition to detonation because the pressure loads be can similar in both cases. The flame speeds tended to accelerate to the range 500-700 m/s, the choked flow

condition in the burned gas. This is seen in all tests with obstacles except those with comparatively unreactive mixtures (~ 12% hydrogen). The choked-flow condition tended to be stable over roughly the latter half of the channel. If DDT is defined as the formation of a self sustaining detonation traveling at nearly C-J speed, then cinematography of the wave leaving the channel becomes a central means of verifying that DDT has occurred. However, for the lean mixtures in the borderline region, cinematographic analysis is complicated by the low luminosity of the burned gas. In addition, no retonation waves were seen. We hypothesize that this may be due to the breakup of the returning wave by the obstacles and debris in the channel. Of course, for mixtures which are much more reactive than borderline mixtures, there is no problem determining that DDT has occurred.

Peraldi, Knystautas, and Lee [67] found DDT possible if the ratio of the obstacle inner diameter to the detonation cell width was greater than one. In our tests DDT was observed if the ratio of the gap width between the obstacles to the detonation cell width was greater than about three, provided the flame speed had reached the choked-flow condition in the burned gas prior to the channel exit.

The third variable, transverse venting, also had a strong influence on the flame speeds, overpressures, and possibility of DDT. Large degrees of transverse venting reduce flame speeds and overpressures. The tests without obstacles and with a large degree of top venting (50%) show that it is possible to suppress flame acceleration and DDT even for highly reactive mixtures, i.e. nearly stoichiometric hydrogen-air mixtures. With obstacles present, DDT does occur if the mixture is sufficiently reactive.

Venting has two opposing effects. The loss of gas out the vents tends to lower the overpressure and slow the flame speed. However, the venting tends to create turbulence and increase the burning rate; i.e., the vents act as obstacles. For small degrees of venting the second effect can dominate, i.e., small degrees of venting can increase the possibility of DDT. The flames speeds, overpressures, and tendency toward DDT is increased by a small degree of transverse venting for hydrogen-air mixtures with hydrogen mole fractions above about 18%.

FLAME was built to study violent combustion effects at larger scale than laboratory tests. These phenomena are scale dependent, and get worse at larger scale. Our results

do show leaner hydrogen limits for DDT than at small scale. Subsequent to this work, we have built small-scale models of FLAME to observe scale effects on flame acceleration and DDT. This work will be reported in the future.

7.3 Application to Nuclear Reactor Safety

The results of the FLAME experimental program combined with other relevant work was used to create a methodology to predict the possibility of DDT in severe accident conditions, particularly for treating hydrogen-air-steam mixtures. [57] A brief summary of the methodology is presented in Appendix B. The two input variables in the methodology are the reactivity of a mixture and the flame-acceleration potential of volume through which the deflagration propagates. The output of the methodology is a qualitative estimate of the likelihood of DDT.

The methodology was used in a study of the Bellefonte nuclear power plant. [57] For the large dry PWR containment at Bellefonte, the methodology predicted little danger of detonation for the accidents considered. The methodology was also used by the first author in the Containment Loads Expert Panel of NUREG-1150 studies of the Sequoyah and Grand Gulf plants. For the Sequoyah ice condenser containment, in an analysis of many accident scenarios in which the large mixing fans are inoperative, mixtures with 18-22% hydrogen and little steam were predicted to occur in the ice condenser. For these mixtures and in that geometry, the formalism predicts that a flame is highly likely to undergo DDT.

8. REFERENCES

1. Reactor Safety Study, An Assessment of Accident Risks in U.S. Commercial Nuclear Power Plants, WASH 1400 U.S. Nuclear Regulatory Commission, Washington, D.C., NUREG 75-014, October 1975.

2. A.A. Heckes, "Hydrogen Explosions," Core-Meltdown Experimental Review, Sandia National Laboratories, Albuquerque, NM, NUREG-0205, SAND74-0382, March 1977.

3. J.O. Henrie and A.K. Postma, "Analysis of the Three Mile Island (TMI-2) Hydrogen Burn," Presented at the joint ANS/ASME/AIChE meeting, The Second International Topical Meeting on Nuclear Reactor Thermal-Hydraulics, Santa Barbara, CA., January 1983, Published as Thermal-Hydraulics of Nuclear Reactors, Vol. 2, ANS Order No. 700081, 1983

4. T.A., Butler and J.G. Bennett, "Nonlinear Response of a Post-Tensioned Structure to Static and Dynamics Internal Pressure Loads," Computers and Structures, 13, 647-659 (1981).

5. Report of the Zion/Indian Point Study: Volume 1, Appendix 3B, Sandia National Laboratories, Albuquerque, NM, SAND80-0617/1, August 1980.

6. "Chernobyl: Where do we go from here," Proceedings of the Conference-by-Computer, September 29 -October 17, 1986, McGraw-Hill Nuclear Publications.

7. S. Gordon and B.J. McBride, Computer Program for Calculation of Complex Chemical Equilibrium Compositions, Rocket Performance, Incident and Reflected Shocks, and Chapman-Jouguet Detonations, NASA SP-273, 1971.

8. M.P. Sherman, "Hydrogen Combustion in Nuclear Plant Accidents and Associated Containment Loads," Nuclear Engineering and Design, 82, 13-24, (1984).

9. H.F. Coward and G.W. Jones, Limits of Flammability of Gases and Vapors, Bulletin 503, Bureau of Mines, U.S. Dept. of Interior, 1952.

10. L.A. Lovachev et al., "Flammability Limits: An Invited Review," Combustion and Flame, 70, 259-289, (1973).

11. M. Hertzberg, "The Flammability Limits of Gases, Vapours and Dusts: Theory and Experiment," in Fuel-Air Explosions, Ed. J.H.S. Lee and C.M. Guirao, (Univ. of Waterloo Press, Ontario, Canada, 1981).

12. J.S. Yeaw and L. Shnidman, "The Extinction of Gas Flames by Steam," Proceedings American Gas Assoc., 717-745, (1938).

13. M.G. Zabetakis, Research on the Combustion and Explosion Hazards of Hydrogen-Air-Steam Mixtures, Bureau of Mines, Pittsburgh, PA, AECU-3327, Sept. 1956.

14. D. Renfro et al., "Development and Testing of Hydrogen Ignition Devices," Proc. of the Second International Conference on the Impact of Hydrogen on Water Reactor Safety, M. Berman et al., eds., Sandia National Laboratories, Albuquerque, NM, NUREG/CP-0038, EPRI RP 1932-25, SAND82-2456, 1982.

15. "Tennessee Valley Authority, Sequoyah Nuclear Plant, Research Program on Hydrogen Combustion and Control," Quarterly Report No. 3, Appendix A.2, 1981.

16. W.E. Lowry, D.R. Bowman, and B.W. Davis, Final Results of the Hydrogen Igniter Experimental Program, Lawrence Livermore National Laboratory, Livermore, CA NUREG/CR-2486, UCRL-53036, 1982.

17. R.K. Kumar, "Flammability Limits of Hydrogen-Oxygen-Diluent Mixtures," Journal of Fire Sciences, 3, 245-262, August 1985).

18. R.K. Kumar, H. Tamm, and W.C. Harrison, "Combustion of Hydrogen-Steam-Air Mixtures Near Lower Flammability Limits," Combustion Science and Technology, 33, 167-178 (1983).

19. D.D.S. Liu et al., Canadian Hydrogen Combustion Studies Related to Nuclear Reactor Safety Assessment, Canadian Report AECL-6994, October 1980.

20. S.F. Roller and S.M. Falacy, "Medium-Scale Tests of H2:Air:Steam Systems," Proc. of the Second International Conference on the Impact of Hydrogen on Water Reactor Safety, M. Berman et al., eds., Sandia National Laboratories, Albuquerque, NM, NUREG/CP-0038, EPRI RP 1932-25, SAND82-2456, 1982.

21. B.W. Marshall, Jr., "Hydrogen:Air:Steam Flammability Limits and Combustion Characteristics in the FITS Vessel," Sandia National Laboratories, Albuquerque, NM, NUREG/CR-3468, SAND84-0383, December 1986.

22. J.E. Hustad, and O.K. Sønju, Experimental Studies of Lower Flammability Limits of Gases and Mixtures of Gases at Elevated Temperatures, Combustion and Flame, 71, 283-294, (1988).

23. G.G. De Soete, "The Flammability of Hydrogen-Oxygen-Nitrogen Mixtures at High Temperatures," La Rivista dei Combustibili, 29, 166-172, (May-June 1975).

24. L.T. Thompson et al., Large-Scale Hydrogen Combustion Experiments, Electric Power Research Institute, Palo Alto, CA, Report NP-3878, Research Project 1932-11.

25. A.C. Ratzel, Data Analyses for Nevada Test Site (NTS) Premixed Combustion Tests, Sandia National Laboratories, Albuquerque, NM, NUREG/CR-4138, SAND85-0135, May 1985.

26. Large-Scale Hydrogen Combustion Experiments Vol. 1: Methodology and Results, Electric Power Research Institute, Palo Alto, CA, EPRI NP-3878, October 1988.

27. C.C. Wong, HECTR Analyses of the Nevada Test Site (NTS) Premixed Combustion Experiments, Sandia National Laboratories, Albuquerque, NM, NUREG/CR-4916, SAND87-0956, November 1988.

28. C.C. Wong, A Standard Problem for HECTR-MAAP Comparison: Incomplete Burning, Sandia National Laboratories, Albuquerque, NM, NUREG/CR-4993, SAND87-1858, August 1988.

29. W.B. Benedick, J.C. Cummings, and P.G. Prassinos, "Experimental Results From Combustion of Hydrogen:Air Mixtures in an Intermediate-Scale Tank," Proc. of the Second International Conference on the Impact of Hydrogen on Water Reactor Safety, M. Berman et al., eds., Sandia National Laboratories, Albuquerque, NM, NUREG/CP-0038, EPRI RP 1932-25, SAND82-2456, 1982.

30. W.B. Benedick, J.C. Cummings, and P.G. Prassinos, Combustion of Hydrogen:Air Mixtures in the VGES Cylindrical Tank, Sandia National Laboratories, Albuquerque, NM, NUREG/CR-3273, SAND83-1022, May 1984.

31. R.K. Kumar, H. Tamm, and W.C. Harrison, Intermediate-Scale Combustion Studies of Hydrogen-Air-Steam Mixtures, Electric Power Research Institute, Palo Alto, CA, EPRI NP-2955, June 1984.

32. R. Torok et al., Hydrogen Combustion and Control Studies in Intermediate Scale, Electric Power Research Institute, Palo Alto, CA, EPRI NP-2953, June 1983.

33. A.L. Furno et al., "Some Observations on Near-Limit Flames," 13th Symposium (International) on Combustion, Combustion Institute, Pittsburg, PA, 593-599, 1971.

34. H. Edmondson and M.P. Heap, "The Burning Velocity of Hydrogen-Air Flames," Combustion and Flame, 16, 161-165, (1971).

35. G.E. Andrews and D. Bradley, "Determination of Burning Velocities: A Critical Review," Combustion and Flame, 18, 133-149, (1972).

36. J. Warnitz, "Calculation of the Structure of Laminar Flat Flames II. Flame Velocity and Structure of Freely Propagating Hydrogen-Oxygen and Hydrogen-Air-Flames," Ber. Bunsenges Phys. Chem., 82, 643-649, (1978).

37. D.D.S. Liu and R. MacFarlane, "Laminar Burning Velocities of Hydrogen-Air and Hydrogen-Air-Steam Flames," Combustion and Flame, 49, 59-71, (1983).

38. R.K. Kumar, H. Tamm, and W.C. Harrison, "Combustion of Hydrogen at High Concentration Including the Effect of Obstacles," Combustion Science and Technology, 35, 175-186, (1983).

39. R.G. Abdel-Gayed and D. Bradley, "The Influence of Turbulence Upon the Rate of Burning," Fuel-Air Explosions, Edited by J.H.S. Lee and C.M. Guirao, (University of Waterloo Press, Ontario, Canada, 1982).

40. R.G. Abdel-Gayed et al., "Lewis Number Effects on Turbulent Burning Velocity," Twentieth Symposium (International) on Combustion, Combustion Institute, Pittsburgh, PA, 505-512, 1984.

41. I.O. Moen et al., "Flame Acceleration Due to Turbulence Produced by Obstacles," Combustion and Flame, 39, 21-32, (1979).

42. C. Chan and J.H.S. Lee, "Influence of Confinement on Flame Acceleration Due to Repeated Obstacles," Combustion and Flame, 49, 27-39, (1983).

43. P.A. Urtiew, Flame Propagation in Gaseous Fuel Mixtures in Semiconfined Geometries, Lawrence Livermore Laboratory, Livermore, CA, UCID-19000, 1981.

44. R.A. Strehlow, T.W.G. Yip, and B. Ghaffarian, Flame Acceleration Mechanisms Under Conditions of Partial Confinement, Dept. Aeron. and Astron. Eng., Univ. of Illinois, Urbana, IL, 1982.

45. R.B. Edelman and P.T. Harsha, "On the Generation of Turbulence in Highly Transient Flows," Acta Astronautica, 6, 1005-1008, (1979).

46. J.H.S. Lee and I.O. Moen, "The Mechanism of Transition From Deflagration to Detonation in Vapor Cloud Explosions," Prog. Energy Comb. Sci., 6, 359-389, (1979).

47. A.K. Oppenheim, "Novel Insight into the structure and Development of Detonation," Astron. Acta, 11, 391-395, (1965).

48. J.H. Lee, R.I. Soloukhin, and A.K. Oppenheim, "Current Views on Gaseous Detonation," Astron. Acta, 14, 565-584, (1969).

49. D. Pawel, H. Vasatko, and H.G. Wagner, "Observations on the Initiation of Detonation," Astron. Acta, 14, 509-511, (1969).

50. J.H.S. Lee, "Initiation of Gaseous Detonation," Ann Review Phy. Chem., 28, 75-104, (1977).

51. P.A. Urtiew and A.K. Oppenheim, "Experimental Observations of the Transition to Detonation in an Explosive gas, Proc, Royal Soc., A295, 13-28, (1966).

52. M.A. Cook, D.H. Pack, and W.A. Gey, "Deflagration to Detonation Transition," 7th Sym. Int. on Combustion, 820-836, 1958.

53. J.H.S. Lee, R. Knystaustas, and A. Freiman, "High Speed Turbulent Deflagrations and Transition to Detonation in H_2-Air Mixtures," Comb. and Flame, 56, 227-239, (1984).

54. M. Berman, "A Critical Review of Recent Large-Scale Experiments on Hydrogen-Air Detonations," Nuclear Science and Engineering, 93, 321-347, (1986).

55. A.K. Oppenheim, "On the Inadequacy of the Gasdynamic Processes for Triggering the Transition to Detonation," Combustion and Flame, 14, 13-20, (1970).

56. S. Dingman and A. Camp, "Pressure-Temperature Response in an Ice Condenser Containment For Selected Accidents," Transactions of the Thirteenth Water Reactor Safety Research Information Meeting, U.S. Nuclear Regulatory Commission, Washington, D.C., NUREG/CP-0071, October 1985.

57. M.P. Sherman and M. Berman, "The Possibility of Local Detonations During Degraded-Core Accidents in the Bellefonte Nuclear Power Plant," Nuclear Technology, 321-347, (April 1988).

58. J.W. Fisk et al., "Experimental Facilities to Study Hydrogen Combustion and Detonation," Designing for Hydrogen in Nuclear Power Plants, Ed. K. K. Niyogi and M. Bernstein, pp. 25-30, ASME, NY, 1984.

59. M.P. Sherman, "Hydrogen Flame Acceleration and Detonation," Proceedings of the Twelfth Water Reactor Safety Meeting, U.S. Nuclear Regulatory Commission, Washington, D.C., NUREG/CP-0058, October 1984.

60. M.P. Sherman et al., "The Effect of Transverse Venting on Flame Acceleration and Transition to Detonation in a Large Channel," Dynamics of Explosions, Vol. 106, Ed. J.R. Bowen, J.C. Leyer, and R.I. Soloukhin, AIAA, NY, 1986.

61. T.G. Beckwith and N.L. Buck, Mechanical Measurements, 2nd Ed., Menlo Park, CA, (Addison-Wesley, 1969).

62. B.W. Marshall, Jr. and A.C. Ratzel, III, Pressure Measurements in a Hydrogen Combustion Environment: An Evaluation of Three Pressure Transducers, Sandia National Laboratories, Albuquerque, NM, NUREG/CR-3721/2 of 2, SAND83-2621/2 of 2, May 1984.

63. D. Dunn-Rankin, P.K. Barr, and R.F. Sawyer, "Numerical and Experimental Study of "Tulip" Flame Formation in a Closed Vessel," Twenty-First Symposium (International) on Combustion, Combustion Institute, Pittsburg, PA, 1291-1301, 1986.

64. D.A. Rotman and A.K. Oppenheim, "Aerothermodynamic Properties of Stretched Flames in Enclosures," Twenty-First Symposium (International) on Combustion, Combustion Institute, Pittsburg, PA, 1303-1312, 1986.

65. O. Peraldi, R. Knystautas, and J.H. Lee, "Criteria for Detonation in Tubes," Twenty-First Symposium (International) on Combustion, Combustion Institute, Pittsburg, PA, 1629-1637, 1986.

66. W.B. Benedick, R. Knystautas, and J.H. Lee, "Large-Scale Experiments on the Transmission of Fuel-Air Detonations From Two-Dimensional Channels," Dynamics of Shock Waves, Explosions and Detonations, Vol. 94, Ed. J.R. Bowen, N. Manson, A.K. Oppenheim, and R.I. Soloukhin, 546-555, AIAA, NY, 1985.

67. J.R. Travis and T.G. Theofanous, "Some Examples of Hydrogen Transport and Mixing," ANS Proceedings, National Heat Transfer Conference, 182-193, 1987.

APPENDIX A

POSITION OF STRUCTURES AND INSTRUMENTATION

The purpose of this appendix is to document the location of the transducers used in the FLAME experiments. The locations are given using a Cartesian coordinate system as shown in the diagram below. The X coordinate is the axial distance from the inside of the door at the ignition end; the Y coordinate is the elevation from the floor; the Z coordinate is the distance from the midplane of the channel. The near wall was selected as the direction of positive Z.

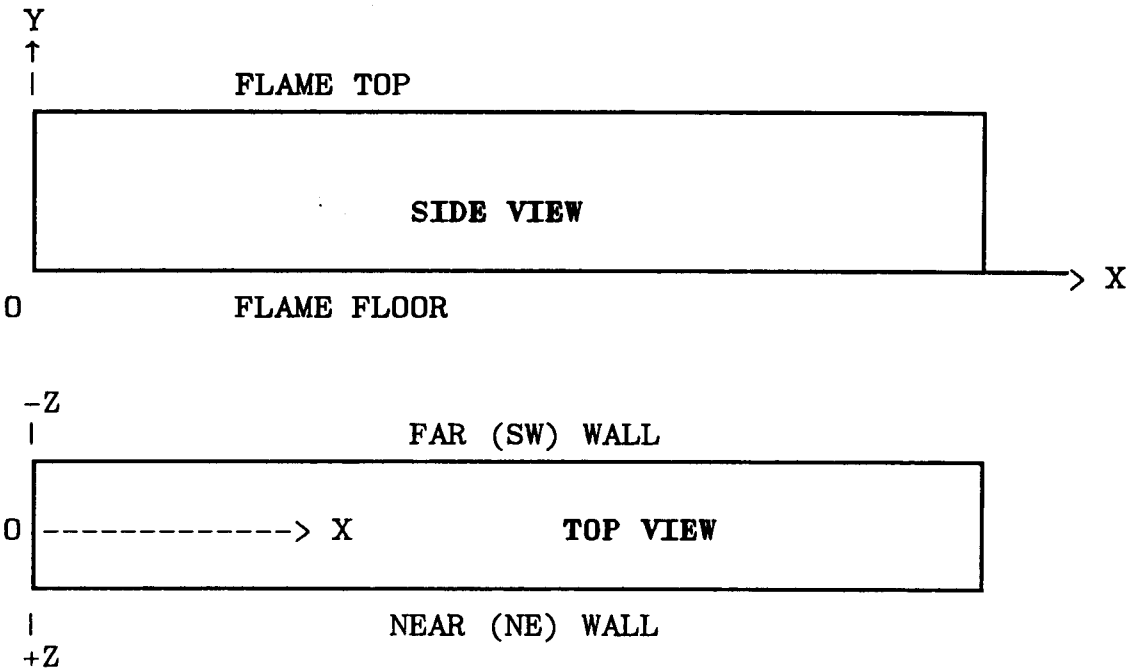

All dimensions are in meters, with a tolerance of $\pm$ 0.005 m. The coordinates of all devices in the walls are given at the inner surface of the wall, except for the strain gauges.

The pressure transducers, lithium-niobate gauges, two germanium photodiodes and the hydrogen inlets were each mounted in one of the 88 access pipes, and five of the germanium photodiodes were mounted in viewports. Their positions did not change during the test series. The coordinates to the center of the access pipes and viewports are quoted. In contrast, the number and position of thermocouples used to measure combustion front time-of-arrival changed several times during the test series.

Overall channel dimensions

Channel length = 30.5 m (100 ft)
Channel width = 1.83 m (6.0 ft)
Channel height = 2.44 m (8.0 ft)

ACCESS PIPE LOCATIONS

PIPE #	X (M)	Y (M)	Z (M)	
1	0.787	0.276	0.914	Near
2	2.143	0.297	0.914	Wall
3	3.569	0.283	0.914	
4	4.890	0.305	0.914	Lower
5	6.299	0.279	0.914	
6	7.683	0.270	0.914	
7	9.052	0.279	0.914	
8	10.500	0.292	0.914	
9	11.824	0.288	0.914	
10	13.167	0.267	0.914	
11	14.465	0.270	0.914	
12	15.951	0.264	0.914	
13	17.399	0.279	0.914	
14	18.701	0.210	0.914	
15	19.942	0.203	0.914	
16	21.441	0.292	0.914	
17	22.812	0.273	0.914	
18	24.181	0.264	0.914	
19	25.464	0.289	0.914	
20	27.000	0.286	0.914	
21	28.321	0.286	0.914	
22	29.816	0.311	0.914	
23	0.678	2.064	0.914	Near
24	2.089	2.075	0.914	Wall
25	3.550	2.080	0.914	
26	4.804	2.067	0.914	Upper
27	6.236	2.111	0.914	
28	7.658	2.125	0.914	
29	9.027	2.130	0.914	
30	10.351	2.115	0.914	
31	11.773	2.102	0.914	
32	13.145	2.130	0.914	
33	14.516	2.100	0.914	
34	15.929	2.146	0.914	
35	17.304	2.134	0.914	
36	18.669	2.134	0.914	
37	20.063	2.134	0.914	
38	21.450	2.121	0.914	
39	22.790	2.111	0.914	
40	24.194	2.121	0.914	
41	25.432	2.151	0.914	
42	26.988	2.140	0.914	
43	28.343	2.137	0.914	
44	29.804	2.102	0.914	

45	0.827	0.262	-0.914	Far
46	2.188	0.260	-0.914	Wall
47	3.518	0.262	-0.914	
48	4.937	0.295	-0.914	Lower
49	6.360	0.316	-0.914	
50	7.690	0.318	-0.914	
51	9.138	0.344	-0.914	
52	10.554	0.291	-0.914	
53	11.728	0.295	-0.914	
54	13.252	0.289	-0.914	
55	14.586	0.297	-0.914	
56	15.977	0.283	-0.914	
57	17.215	0.283	-0.914	
58	18.599	0.306	-0.914	
59	20.047	0.287	-0.914	
60	21.501	0.264	-0.914	
61	22.746	0.284	-0.914	
62	24.149	0.273	-0.914	
63	25.622	0.313	-0.914	
64	27.007	0.292	-0.914	
65	28.308	0.271	-0.914	
66	29.718	0.264	-0.914	
67	0.708	2.172	-0.914	Far
68	2.102	2.164	-0.914	Wall
69	3.461	2.194	-0.914	
70	4.991	2.189	-0.914	
71	6.350	2.207	-0.914	Upper
72	7.677	2.122	-0.914	
73	9.125	2.116	-0.914	
74	10.478	2.135	-0.914	
75	11.773	2.105	-0.914	
76	13.145	2.113	-0.914	
77	14.649	2.097	-0.914	
78	15.970	2.165	-0.914	
79	17.183	2.161	-0.914	
80	18.644	2.153	-0.914	
81	20.060	2.146	-0.914	
82	21.412	2.108	-0.914	
83	22.777	2.129	-0.914	
84	24.124	2.124	-0.914	
85	25.591	2.122	-0.914	
86	26.994	2.130	-0.914	
87	28.378	2.137	-0.914	
88	29.686	2.132	-0.914	

VIEWPORT LOCATIONS

Port #	Near Wall (Z=0.914 m) X (m)	Y (m)	Port #	Far Wall (Z=-0.914 m) X (m)	Y (m)
1	3.124	1.213	6	3.153	1.199
2	9.500	1.213	7	9.500	1.203
3	14.961	1.210	8	14.980	1.197
4	20.485	1.219	9	20.498	1.210
5	26.911	1.222	10	26.911	1.213

PRESSURE TRANSDUCER LOCATIONS

Transducer	X(m)	Y(m)	Z(m)	Access Pipe
PKU1	0.787	0.276	0.914	1
PKU2	4.804	2.067	0.914	26
PKU3	9.052	0.279	0.914	7
PKU4	14.586	0.297	-0.914	55
PKU5	18.599	0.306	-0.914	58
PKU6	21.450	2.121	0.914	38
PKU7	25.464	0.289	0.914	19
PKU8	25.464	2.122	-0.914	85
PKU9	21.412	2.108	-0.914	82
PKU10	18.701	0.210	0.914	14
PDYK1	2.188	0.260	-0.914	46
PDYK2	22.746	0.284	-0.914	61
PDYK3	29.816	0.311	0.914	22

GERMANIUM PHOTODIODE LOCATIONS

GPD #	X(m)	Y(m)	Z(m)	Viewport or Access Pipe*
1	3.124	1.213	-0.914	6
2	9.500	1.213	-0.914	7
3	14.980	1.197	-0.914	8
4	20.498	1.123	-0.914	9
5	26.994	2.130	-0.915	88*
6	26.911	1.213	-0.914	10
7	27.007	0.294	-0.914	64*

LITHIUM-NIOBATE GAUGES

Gauge #	X(m)	Y(m)	Z(m)	Access Pip
1	11.773	2.102	0.914	
2	20.063	2.102	0.914	

Thermocouple Positions for test F-1

Rake S	TC #	X(m)	Y(m)	Z(m)
	1	9.747	0.064	0.000
	2	9.747	0.089	0.000
	3	9.747	0.140	0.000
	4	9.747	0.267	0.000
	5	9.747	0.546	0.000
	6	9.747	0.876	0.000
	7	9.747	1.181	0.000
	8	9.747	1.486	0.000
	9	9.747	1.791	0.000
	10	9.747	2.096	0.000
	11	9.747	2.400	0.000
	12	9.747	2.477	0.000
Rake N	1	20.714	0.064	0.000
	2	20.714	0.089	0.000
	3	20.714	0.140	0.000
	4	20.714	0.267	0.000
	5	20.714	0.546	0.000
	6	20.714	0.876	0.000
	7	20.714	1.181	0.000
	8	20.714	1.486	0.000
	9	20.714	1.791	0.000
	10	20.714	2.096	0.000
	11	20.714	2.400	0.000
	12	20.714	2.477	0.000
Wall	1	21.441	0.292	-0.914
	2	29.804	2.102	-0.914
	3	4.890	0.305	-0.914
	4	13.167	0.292	-0.914
	5	11.773	2.102	-0.914

Thermocouple Positions for Tests F-2 to F-12

Rake A	TC #	X(m)	Y(m)	Z(m)
	1	3.315	0.016	0.000
	2	3.315	0.041	0.000
	3	3.315	0.092	0.000
	4	3.315	0.219	0.000
	5	3.315	0.524	0.000
	6	3.315	0.829	0.000
	7	3.315	1.133	0.000
	8	3.315	1.438	0.000
	9	3.315	1.743	0.000
	10	3.315	2.048	0.000
	11	3.315	2.353	0.000
	12	3.315	2.416	0.000

Rake B	1	11.088	0.010	0.000
	2	11.088	0.035	0.000
	3	11.088	0.086	0.000
	4	11.088	0.213	0.000
	5	11.088	0.518	0.000
	6	11.088	0.822	0.000
	7	11.088	1.127	0.000
	8	11.088	1.432	0.000
	9	11.088	1.737	0.000
	10	11.088	2.042	0.000
	11	11.088	2.346	0.000
	12	11.088	2.410	0.000
Rake C	1	19.304	0.022	0.000
	2	19.304	0.048	0.000
	3	19.304	0.098	0.000
	4	19.304	0.225	0.000
	5	19.304	0.530	0.000
	6	19.304	0.835	0.000
	7	19.304	1.140	0.000
	8	19.304	1.445	0.000
	9	19.304	1.749	0.000
	10	19.304	2.054	0.000
	11	19.304	2.359	0.000
	12	19.304	2.423	0.000
Rake D	1	27.077	0.022	0.000
	2	27.077	0.048	0.000
	3	27.077	0.098	0.000
	4	27.077	0.225	0.000
	5	27.077	0.530	0.000
	6	27.077	0.835	0.000
	7	27.077	1.140	0.000
	8	27.077	1.445	0.000
	9	27.077	1.749	0.000
	10	27.077	2.054	0.000
	11	27.077	2.359	0.000
	12	27.077	2.423	0.000

Thermocouple Positions for tests F-18-F-21

Rake A	TC #	X(m)	Y(m)	Z(m)
	1	1.067	0.025	0.000
	2	1.067	0.051	0.000
	3	1.067	0.102	0.000
	4	1.067	0.229	0.000
	5	1.067	0.521	0.000
	6	1.067	0.838	0.000
	7	1.067	1.143	0.000
	8	1.067	1.448	0.000
	9	1.067	1.753	0.000
	10	1.067	2.210	0.000
	11	1.067	2.362	0.000
	12	1.067	2.426	0.000
Rake B	1	3.810	0.025	0.000
	2	3.810	0.070	0.000
	3	3.810	0.146	0.000
	4	3.810	0.298	0.000
	5	3.810	0.603	0.000
	6	3.810	1.060	0.000
	7	3.810	1.365	0.000
	8	3.810	1.829	0.000
	9	3.810	2.127	0.000
	10	3.810	2.280	0.000
	11	3.810	2.356	0.000
	12	3.810	2.407	0.000
Rake C	1	11.582	0.025	0.000
	2	11.582	0.051	0.000
	3	11.582	0.102	0.000
	4	11.582	0.229	0.000
	5	11.582	0.527	0.000
	6	11.582	0.832	0.000
	7	11.582	1.137	0.000
	8	11.582	1.441	0.000
	9	11.582	1.746	0.000
	10	11.582	2.051	0.000
	11	11.582	2.356	0.000
	12	11.582	2.419	0.000

	TC #	X(m)	Y(m)	Z(
Rake D	1	19.787	0.025	0.0
	2	19.787	0.076	0.0
	3	19.787	0.152	0.000
	4	19.787	0.305	0.000
	5	19.787	0.610	0.000
	6	19.787	1.067	0.000
	7	19.787	1.372	0.000
	8	19.787	1.829	0.000
	9	19.787	2.134	0.000
	10	19.787	2.286	0.000
	11	19.787	2.362	0.000
	12	19.787	2.413	0.000
Rake E	1	27.559	0.025	0.000
	2	27.559	0.076	0.000
	3	27.559	0.152	0.000
	4	27.559	0.305	0.000
	5	27.559	0.610	0.000
	6	27.559	1.067	0.000
	7	27.559	1.372	0.000
	8	27.559	1.829	0.000
	9	27.559	2.134	0.000
	10	27.559	2.286	0.000
	11	27.559	2.362	0.000
	12	27.559	2.413	0.000
Rake F	1	29.79	1.22	-0.69
	2	29.79	1.22	-0.48
	3	29.79	1.22	-0.23
	4	29.79	1.22	0.23
	5	29.79	1.22	0.48
	6	29.79	1.22	0.69

Thermocouple positions for Tests F-22 - F-29

Rake A	1	1.067	0.076	0.000
	2	1.067	0.381	0.000
	3	1.067	0.762	0.000
	4	1.067	1.143	0.000
	5	1.067	1.524	0.000
	6	1.067	1.905	0.000
	7	1.067	2.286	0.000
	8	1.905	1.219	-0.610
	9	1.930	1.219	-0.864
	10	2.819	1.219	-0.889
Rake B	1	3.810	0.076	0.000
	2	3.810	0.381	0.000
	3	3.810	0.762	0.000
	4	3.810	1.143	0.000
	5	3.810	1.524	0.000
	6	3.810	1.905	0.000
	7	3.810	2.286	0.000
	8	3.734	1.219	-0.610
	9	3.810	1.219	-0.864
	10	3.810	1.219	-0.889
Rake C	1	11.582	0.076	0.000
	2	11.582	0.381	0.000
	3	11.582	0.762	0.000
	4	11.582	1.143	0.000
	5	11.582	1.524	0.000
	6	11.582	1.905	0.000
	7	11.582	2.286	0.000
	8	11.049	1.219	-0.610
	9	11.074	1.219	-0.864
	10	12.040	1.219	-0.889
Rake D	1	19.787	0.076	0.000
	2	19.787	0.381	0.000
	3	19.787	0.762	0.000
	4	19.787	1.143	0.000
	5	19.787	1.524	0.000
	6	19.787	1.905	0.000
	7	19.787	2.286	0.000
	8	18.352	1.219	-0.610
	9	18.377	1.219	-0.864
	10	19.304	1.219	-0.889
Rake E	1	27.534	0.025	0.000
	2	27.534	0.076	0.000
	3	27.534	0.152	0.000
	4	27.534	0.305	0.000

5	27.534	0.610	0.000
6	27.534	1.067	0.000
7	27.534	1.372	0.000
8	27.496	1.219	-0.610
9	27.521	1.219	-0.864
10	28.423	1.219	-0.889

Strain Gauge Locations

DEFINE: Z'=Z-1.283 Z'=0 AT CENTERLINE OF NEAR WALL
TOLERANCES: X: (+/- 0.05 METERS)
Y: (+/- 0.01 METERS) Z: (+/- 0.01 METERS)

STATION A

GAUGE #	X (m)	Y (m)	Z' (m)
1	1.83	1.47	-0.33
2	1.83	1.47	-0.31
3	1.83	1.47	0.31
4	1.83	1.47	0.33
5	1.83	0.05	-0.33
6	1.83	0.05	-0.30
7	1.83	0.05	0.30
8	1.83	0.05	0.33

STATION B

GAUGE #	X (m)	Y (m)	Z' (m)
1	8.53	1.47	-0.33
2	8.53	1.47	-0.31
3	8.53	1.47	0.31
4	8.53	1.47	0.33
5	8.53	0.05	-0.33
6	8.53	0.05	-0.30
7	8.53	0.05	0.30
8	8.53	0.05	0.33

STATION C

GAUGE #	X (m)	Y (m)	Z' (m)
1	15.24	1.47	-0.33
2	15.24	1.47	-0.31
3	15.24	1.47	0.31
4	15.24	1.47	0.33
5	15.24	0.05	-0.33
6	15.24	0.05	-0.30
7	15.24	0.05	0.30
8	15.24	0.05	-0.33

STATION D

GAUGE #	X (m)	Y (m)	Z' (m)
1	21.95	1.47	-0.33
2	21.95	1.47	-0.31
3	21.95	1.47	0.31
4	21.95	1.47	0.33
5	21.95	0.05	-0.33
6	21.95	0.05	-0.30
7	21.95	0.05	0.30
8	21.95	0.05	0.33

STATION E

GAUGE #	X (m)	Y (m)	Z' (m)
1	28.65	1.47	-0.33
2	28.65	1.47	-0.31
3	28.65	1.47	0.31
4	28.65	1.47	0.33
5	28.65	0.05	-0.33
6	28.65	0.05	-0.30
7	28.65	0.05	0.30
8	28.65	0.05	0.33

APPENDIX B

APPLICATION TO HYDROGEN-AIR-STEAM MIXTURES

The research conducted in the FLAME facility on flame acceleration and deflagration-to-detonation (DDT) at large scale with hydrogen-air mixtures has a major limitation when considering application to nuclear reactor safety. Many of the containment atmospheres in postulated severe accidents contain hydrogen-air-steam mixtures at somewhat elevated pressures and temperatures. Consequently, there is a need to relate our work with hydrogen-air mixtures to these conditions. An approximate methodology to handle this task was carried out by Sherman and Berman. [57] In this appendix an abbreviated summary of this methodology is presented. For a discussion of methods other than DDT for initiating detonation, and of the limitations of the evidence for the validity of the methodology see the original paper.

The methodology is based on the following assumptions:

1. The likelihood of DDT can be expressed as a function of two variables, one based on the reactivity of the mixture, and a second based on the flame acceleration potential of the volume through which the deflagration propagates.

2. The reactivity of the mixture is represented by the detonation cell width, λ.

3. The qualitative flame acceleration potential of a volume can be estimated from knowledge of its geometric configuration and size by reference to simple guidelines.

The significance of the second assumption is that the detonability of a hydrogen-air-steam mixture, which has not been measured, is assumed equal to that of a hydrogen-air mixture at atmospheric pressure and room temperature having the same detonation cell size, which presumably has been measured or is believed known. The detonation cell width of hydrogen-air-steam mixtures at a temperature of 100°C and an air partial pressure corresponding to 1 atmosphere pressure and 20°C is shown in Figure B.1. The abscissa used is equivalence ratio, the ratio of hydrogen to oxygen concentration divided by that at stoichiometric conditions. An equivalence ratio of unity means two hydrogen molecules per oxygen molecule regardless of the steam concentration. Equivalence ratios less than 1 are lean mixtures; equivalence ratios greater than 1 are rich mixtures. In Table B.1, mixtures are divided into five classes, depending

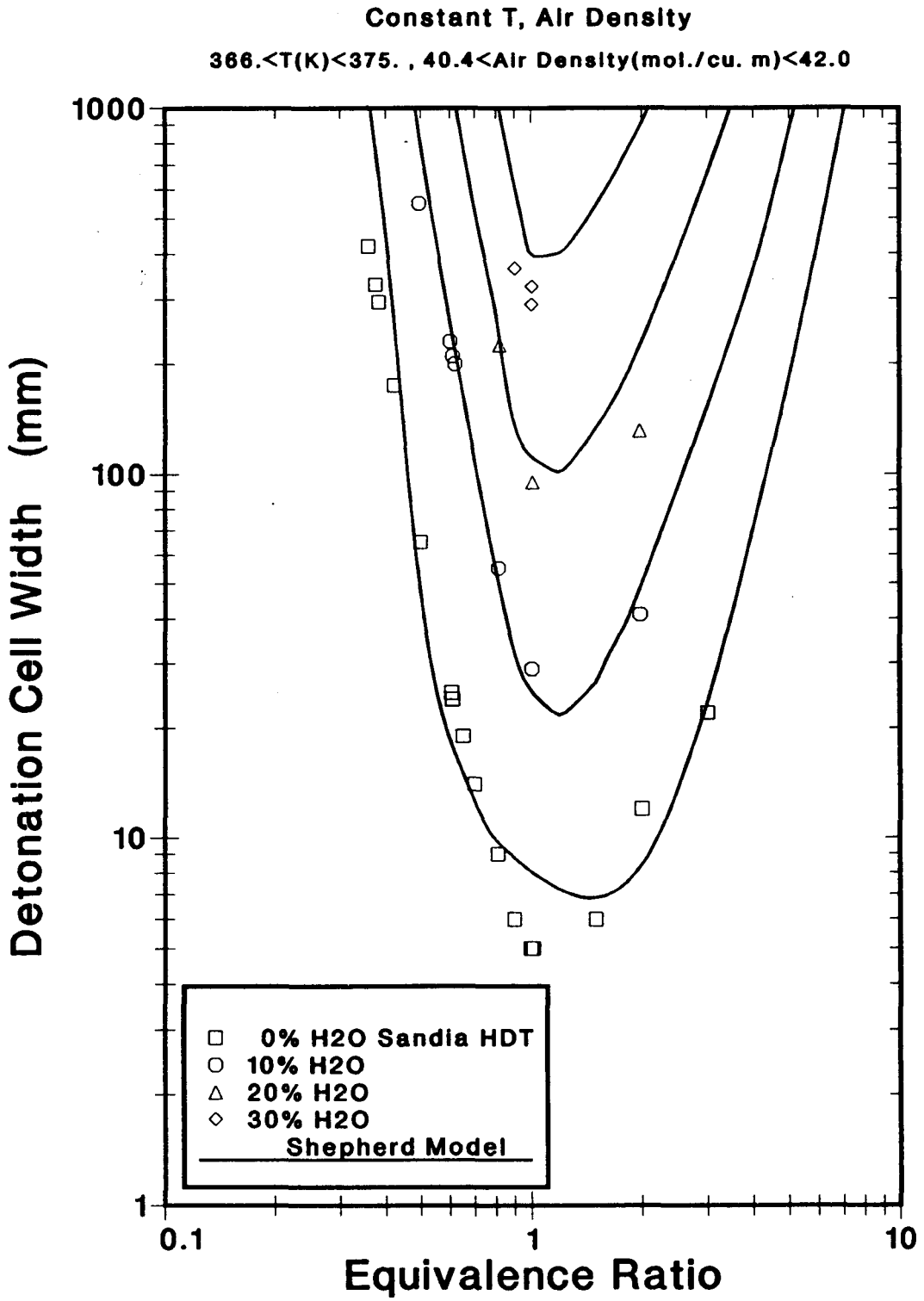

Figure B.1. Detonation Cell Width of Hydrogen-Air-Steam Mixtures

on their detonation cell width from very dangerous class 1 to difficult-to-detonate, class 5. Shown are the corresponding hydrogen mole fractions for H_2-air mixtures on the lean and rich sides.

Table B.1

Classification of Mixture Detonability
Example - Hydrogen-Air Mixtures At 20°C and 1-atm Pressure

Mixture Class	H_2 Mole Fraction (%)	Equivalence Ratio	Cell Width (mm)	H_2 Mole Fraction (%)	Equivalence Ratio
1	24 to 30	0.75 to 1.0	20 to 15	38 to 30	1.5 to 1
2	21 to 24	0.63 to 0.75	40 to 20	48 to 38	2.2 to 1.5
3	15 to 21	0.42 to 0.63	320 to 40	63 to 48	4.1 to 2.2
4	13.5 to 15	0.37 to 0.42	1200 to 320	70 to 63	5.6 to 4.1
5	<13.5	<0.37	> 1200	No data	>5.6

The flame acceleration potential of a given volume is classified into one of five geometric classes beginning with geometric class 1, being the most conducive to flame acceleration, to geometric class 5, being the least conducive. A description of these classes follows.

Geometric Class 1. Large geometries with obstacles in the path of the expanding unburned gases. Partial confinement favors gas expansion past the obstacles. A large tube with numerous obstacles, and with ignition going from a closed end to an open end, is an example. Class 1 geometries are the most favorable to large flame acceleration.

Geometric Class 2. Geometries similar to class 1 but with some feature which hinders flame acceleration. Examples would be a tube open on both ends or large amounts of transverse venting.

Geometric Class 3. Geometries that yield moderate flame acceleration but are neutral to DDT. Examples are large tubes without obstacles, and small tubes (several inch diameter) with obstacles.

Geometric Class 4. Geometries unfavorable to flame acceleration. Examples are large volumes with hardly any obstacles and large amounts of venting transverse to the flame path, and small volumes without obstacles. DDT will not usually occur in a class 4 geometry.

Geometric Class 5. Geometries so unfavorable to flame acceleration that not even large volumes of stoichiometric hydrogen-air mixtures are likely to detonate. The only examples are totally unconfined geometry at large scale and a small spherical geometry without obstacles and central ignition.

For a given mixture class and geometric class, the likelihood of DDT is given in Table 2 as a results class. The qualitative likelihood of DDT for the results classes is given below.

Result Class 1. DDT is highly likely.

Result Class $\frac{3}{2}$. DDT is likely.

Result Class 3. DDT may occur.

Result Class 4. DDT is possible but unlikely.

Result Class 5. DDT is highly unlikely to impossible.

Table B.2

Dependence of Result Class on Mixture and Geometric Class

Geometric Classes	Mixture Classes				
	1	2	3	4	5
1	1	1	2	3	4
2	1	2	3	4	5
3	2	3	3	4	5
4	3	4	4	5	5
5	4	5	5	5	5

The authors urge the users of this methodology to read the original reference.